Università degli Studi "ROMA TRE"

Scuola Dottorale in Biologia (XXI ciclo)
Sezione "Scienze biomolecolari e cellulari"

A Study on Flavin-containing Amine oxidases in *Arabidopsis thaliana*

Studio di Ammino Ossidasi Flaviniche in *Arabidopsis thaliana*

Candidata: Dott.ssa Valentina Spedaletti

Docente guida: Dott.ssa Paraskevi Tavladoraki

TABLE OF CONTENTS

ABSTRACT

Le poliammino ossidasi (PAO) sono enzimi FAD-dipendenti che ossidano le poliammine spermina (Spm) e spermidina (Spd) e/o i loro derivati acetilati a livello del gruppo amminico secondario. L'identità chimica dei prodotti di reazione delle PAO dipende dall'origine dell'enzima e riflette la modalità di ossidazione del substrato. In particolare, le PAO presenti nelle piante monocotiledoni, come la PAO di mais (ZmPAO), ossidano l'atomo di carbonio interno adiacente al gruppo amminico secondario della Spm e della Spd, con produzione di 1,3-diamminopropano (Dap), perossido di idrogeno e di un'amminoaldeide ed in tale maniera partecipano ad una via catabolica terminale delle poliammine. Le PAO animali e le spermina ossidasi (SMO) ossidano, invece, l'atomo di carbonio esterno adiacente al gruppo amminico secondario della Spd o della Spm (o dei loro derivati acetilati) producendo rispettivamente putrescina (Put) o Spd, un'amminoaldeide e perossido di idrogeno ed in tale maniera sono coinvolte in una via di interconversione delle poliammine.

In *Arabidopsis thaliana*, sono stati identificati cinque geni codificanti per PAO putative: l'*At5g13700* (*AtPAO1*), l'*At2g43020* (*AtPAO2*), l'*At3g59050* (*AtPAO3*), l'*At1g65840* (*AtPAO4*), e l'*At4g29720* (*AtPAO5*). L'AtPAO1 e l'AtPAO5 presentano un'omologia di sequenza con la ZmPAO (la PAO vegetale maggiormente caratterizzata ed avente una localizzazione apoplastica) rispettivamente del 23% e del 25% ed una probabile localizzazione citosolica. L'AtPAO2, l'AtPAO3 e l'AtPAO4 presentano un'omologia con la ZmPAO del 23%, un'omologia fra loro che varia tra il 58% e l'85% ed una localizzazione perossisomale. Recentemente, è stato dimostrato che l'AtPAO1 è in grado di ossidare la Spm, ma non la Spd e che è coinvolta in una via di interconversione delle poliammine in maniera simile a alle PAO animali e alle SMO.

Nel presente lavoro di tesi, è stato effettuato uno studio sulle proprietà biochimiche delle proteine ricombinanti AtPAO2 e AtPAO4 in seguito alla loro espressione eterologa in *Escherichia coli*. Tale studio ha dimostrato che le proteine ricombinanti AtPAO2 e AtPAO4 sono attive nei confronti della Spm e della Spd e che producono Spd dall'ossidazione della Spm e Put dall'ossidazione della Spd. Questi dati indicano quindi che queste due AtPAO hanno una modalità di ossidazione del substrato simile a quella dell'AtPAO1 e delle PAO e SMO animali e che sono coinvolte in una via di interconversione delle poliammine. L'esistenza di una via di interconversione delle poliammine in *A. thaliana* è stata dimostrata anche *in vivo*. Infatti, durante l'incubazione di protoplasti ottenuti da foglie di *A. thaliana* con Spd o Spm radioattiva è stato osservato un aumento della quantità di Put o Spd radioattiva. Tale aumento risulta fortemente inibito in presenza di guazatina, un inibitore specifico delle PAO.

Nel presente lavoro, è stato dimostrato anche che le proteine ricombinanti AtPAO1, AtPAO2 e AtPAO4 sono in grado di ossidare le poliammine non comuni termospermina (Termo-Spm) e norspermina (Nor-Spm), che sono state associate alla tolleranza agli stress. In particolare, è stato dimostrato queste poliammine non comuni sono per l'AtPAO1 dei substrati migliori rispetto alla Spm facendo ipotizzare che potrebbero essere i suoi substrati fisiologici. Questo dato è di fondamentale importanza se si considera che recentemente è stato identificato un gene (*ACAULIS5*) codificante per una proteina capace di sintetizzare la Termo-Spm dalla Spd e che piante di *A. thaliana* che presentano una mutazione in questo gene (*acaulis5)* mostrano dei difetti nell'allungamento dello stelo.

In *A. thaliana* sono presenti altri quattro geni: l'*At1g62830 (AtLSD1)*, l'*At3g13682 (AtLSD2)*, l'*At3g10390 (AtLSD3)* e l'*At4g16310 (AtLSD4*) che codificano per proteine aventi un dominio ammino ossidasico. Queste proteine presentano anche un dominio SWIRM, che è generalmente presente nei complessi coinvolti nelle modificazioni della cromatina, ed hanno un'omologia di sequenza con la proteina umana HsLSD1 (KIAA0601) che varia dal 26 al 30%. È stato dimostrato che l'HsLSD1, che ha gli stessi domini funzionali delle AtLSD, catalizza la demetilazione ossidativa dell'istone H3 mono o dimetilato sulla lisina 4 e fa parte di complessi multiproteici importanti nella regolazione dell'espressione genica.

Nel presente lavoro, in seguito ad espressione eterologa in *E. coli* è stata effettuata una parziale caratterizzazione biochimica della proteina AtLSD1, scelta come membro rappresentativo di questa famiglia genica, ed è stato dimostrato che questo enzima vegetale ha un'attività iston-demetilasica e presenta la stessa specificità di substrato della corrispondente proteina umana. Inoltre, dall'analisi del modello della struttura tridimensionale dell'AtLSD1, eseguito sulla base del cristallo dell'HsLSD1, è risultato un'elevato grado di conservazione delle strutture secondarie dell'HsLSD1 e dei residui facenti parte del sito catalitico e sono emerse alcune importanti differenze che suggeriscono che i *partners* molecolari dell'AtLSD1 possano essere differenti da quelli della proteina ortologa umana. Per effettuare un'analisi del profilo di espressione dei geni *AtLSD*, sono stati condotti degli esperimenti di RT-PCR dai quali è emerso che i livelli di espressione di tali geni risultano simili nei vari organi testati. Inoltre, allo scopo di approfondire l'analisi del profilo di espressione dell'*AtLSD1*, il promotore di tale gene è stato amplificato tramite PCR dal DNA totale estratto da foglie di *A. thaliana* ed è stato clonato in un vettore per l'espressione in pianta, mediata da *Agrobacterium tumefaciens*, a monte della sequenza codificante per la *green-fluorescent protein* (*GFP*) in fusione con la β-glucuronidasi (*GUS*). In questo modo è stato ottenuto un costrutto AtLSD1 prom::GFP-GUS. Per individuare i geni regolati dall'AtLSD1 tramite analisi microarray ed esperimenti di immunoprecipitazione della cromatina è stato preparato un costrutto per la sovraespressione dell'AtLSD1 in *A. thaliana*. In

particolare, la regione codificante per l'*AtLSD1* è stata amplificata tramite PCR utilizzando *primers* sequenza-specifici disegnati in modo tale da permetterne il clonaggio in un vettore che guidi la sovraespressione delle proteine in pianta e per aggiungere all'estremità 3' una coda di 6 istidine che faciliti l'individuazione della proteina. Per isolare i complessi nei quali la proteina AtLSD1 è eventualmente coinvolta attraverso cromatografia di affinità, è stato preparato anche un costrutto per la sovraespressione della proteina in fusione con una coda FLAG-HA. Tutti i plasmidi ricombinanti sono stati utilizzati per trasformare il ceppo GV301 di *A. tumefaciens* ed i batteri trasformati sono stati al loro volta utilizzati per trasformare piante di *A. thaliana*. Per determinare i ruoli fisiologici svolti dalle AtLSD, mutanti inserzionali per ognuno dei quattro geni (*Atlsd1*, *Atlsd2*, *Atlsd3* e *Atlsd4*) sono stati ottenuti da banche di semi di *A. thaliana* e sono stati analizzati. In particolare, per confermare la presenza dell'inserzione del T-DNA e per identificare le piante mutanti omozigoti per l'inserzione è stata effettuata un'analisi tramite PCR del DNA totale estratto dalle piante mutanti. In seguito, è stata eseguita un'analisi dettagliata del fenotipo dei mutanti *Atlsd* che ha evidenziato un fenotipo nel mutante *Atlsd3* caratterizzato da un ritardo nella fioritura.

Polyamine oxidases (PAOs) are FAD-dependent enzymes which oxidize the polyamines spermine (Spm) and spermidine (Spd) and/or their acetylated derivatives at the secondary amino group. The chemical identity of PAO reaction products depends on the enzyme source and reflects the mode of substrate oxidation. In particular, PAOs from monocotyledonous plants, such as maize PAO (ZmPAO), oxidize the carbon on the *endo*-side of the secondary amino group of Spm and Spd producing 1,3-diaminopropane (Dap), H_2O_2 and an aminoaldehyde, and are considered involved in a terminal catabolic pathway of polyamines. Conversely, animal PAOs and spermine oxidases (SMOs) oxidize the carbon on the *exo*-side of the secondary amino group of Spd or Spm (or their acetylated derivatives) producing putrescine (Put) or Spd, respectively, in addition to an aminoaldehyde and H_2O_2, and are considered involved in a polyamine back-conversion pathway.

In *Arabidopsis thaliana*, five putative PAO genes have been identified: *At5g13700* (*AtPAO1*), *At2g43020* (*AtPAO2*), *At3g59050* (*AtPAO3*), *At1g65840* (*AtPAO4*), *At4g29720* (*AtPAO5*). AtPAO1 and AtPAO5 have a sequence homology of 45% and 25%, respectively, with ZmPAO (the so far best characterized plant PAO which has an apoplastic localization) and a predicted cytosolic localization. AtPAO2, AtPAO3 and AtPAO4 display an homology of about 23% with ZmPAO, an homology of 58-85% to each other and a peroxisomal localization. Recently, AtPAO1 has been shown to oxidize only

Spm and not Spd and to be involved in a polyamine back-conversion pathway similarly to the animal PAOs/SMOs.

In the present work, a study on the biochemical properties of recombinant AtPAO2 and AtPAO4 expressed in *Escherichia coli* was performed. This study demonstrated that recombinant AtPAO2 and AtPAO4 are active towards both Spd and Spm and that produce Spd from Spm and Put from Spd. These data indicate that these two AtPAOs have a mode of substrate oxidation similar to that of AtPAO1 and animal PAOs/SMOs and thus that they are also involved in a polyamine back-conversion pathway. The existence of a polyamine back-conversion pathway in *A. thaliana* has been demonstrated also *in vivo*. Indeed, incubation of *A. thaliana* protoplasts with radiolabelled Spd or Spm resulted in the accumulation of radiolabelled Put or Spd, respectively, which was strongly reduced in the presence of the PAO-specific inhibitor guazatine.

In the present work, it was also shown that recombinant AtPAO1, AtPAO2 and AtPAO4 are able to oxidize the stress related uncommon polyamines thermospermine (Thermo-Spm) and norspermine (Nor-Spm). In particular, it was shown that these uncommon polyamines are better substrates than Spm for AtPAO1, suggesting that these polyamines may be the physiological substrates of this enzyme. This is of great importance considering that a gene (*ACAULIS5*) encoding for a protein able to synthesize Thermo-Spm from Spd has been recently characterized in *A. thaliana* and the *acaulis5* Arabidopsis mutant presents defects in stem elongation.

In *A. thaliana*, four more genes have been also identified: *At1g62830* (*AtLSD1*), *At3g13682* (*AtLSD2*), *At3g10390* (*AtLSD3*), *At4g16310* (*AtLSD4*) encoding for proteins with an amine oxidase domain. These proteins bear also a SWIRM domain, which is usually present in chromatin-modifying complexes, and display a 26-30% sequence homology with human HsLSD1 (KIAA0601). HsLSD1, which has the same functional domains as the four AtLSDs, has been shown to catalyse the oxidative demethylation of mono- or dimethylated lysine 4 of histone H3 and to participate in multiprotein complexes important in the regulation of gene expression.

In this work, partial biochemical characterization of AtLSD1, chosen as a representative member of this gene family, following expression in *E. coli* demonstrated that this plant enzyme has a demethylase activity with the same substrate specificity as the corresponding human protein. Modeling of the AtLSD1 three-dimensional structure, using the HsLSD1 crystal structure, evidenced a high degree of conservation of the HsLSD1 secondary structures and of the residues building up the catalytic site, but also some important differences which suggest that the AtLSD1 molecular partners are probably different from those of the human orthologue. To analyse the expression pattern of *AtLSDs*, RT-PCR experiments were performed which showed that the *AtLSD1*, *AtLSD2*, *AtLSD3* and *AtLSD4* transcripts are present at similar levels in all organs tested. With the aim to go deeper into the *AtLSD1*

expression pattern, the *AtLSD1* promoter was amplified by PCR from Arabidopsis total DNA and cloned in an *Agrobacterium tumefaciens*-based plant expression vector upstream of the sequence encoding green-fluorescent protein (*GFP*) in fusion with β-glucuronidase (*GUS*). In this way, an AtLSD1 prom::GFP-GUS construct was obtained. Furthermore, to identify the genes regulated by AtLSD1 through microarray analysis and chromatin immunoprecipitation experiments, a construct for AtLSD1 overexpression in *A. thaliana* was prepared. Indeed, the coding region of *AtLSD1* was amplified by PCR using sequence specific primers designed in a way to allow *AtLSD1* cDNA cloning through the Gateway technology in a vector which guides overexpression of proteins in plant and to add at the 3′ terminus of cDNA a sequence encoding for a 6-His tag to facilitate detection. To isolate the complexes in which AtLSD1 is eventually involved through a two-step affinity chromatography, a construct for AtLSD1 overexpression in *A. thaliana* in fusion with a FLAG-HA tag was also prepared. All the recombinant plasmids were used to transform the *A. tumefaciens* GV301 strain and the transformed bacteria were in turn used to transform *A. thaliana* plants. To determine the physiological roles of AtLSDs, insertional knock-out mutants for each one of the four *AtLSD* genes (*Atlsd1*, *Atlsd2*, *Atlsd3* and *Atlsd4* mutants) were obtained from *A. thaliana* seed banks and analyzed. In particular, PCR analysis of total DNA from mutant seedlings was performed to confirm the presence of T-DNA insertion and to identify the homozygous mutant plants for this insertion. Detailed phenotypic analysis of the *Atlsd* mutants was also performed which evidenced a delayed flowering phenotype for *Atlsd3* mutant.

1. INTRODUCTION

1.1 Polyamines and polyamine oxidases

1.1.1 General characteristics of polyamines

Polyamines are aliphatic polycations of low molecular mass that are found ubiquitously in all living organisms. The most common polyamines are the diamine putrescine (Put), the tri-amine spermidine (Spd), and the tetra-amine spermine (Spm) (Galston and Sawhney, 1990) (Fig. 1). In nature, there are also uncommon polyamines, such as 1,3-diaminopropane (Dap), cadaverine (Cad), norspermidine (Nor-Spd), norspermine (Nor-Spm) and thermospermine (Thermo-Spm) (Fig. 1). Nor-Spd, Nor-Spm and Thermo-Spm, which are abundant in the extreme thermophilic bacterium *Thermus thermophilus*, have also been detected in other bacteria, algae, fungi, animals and higher plants (Cohen, 1998). In particular, in the latter, Nor-Spd and Nor-Spm have been found in drought-tolerant cultivars of *Medicago sativa L.* and in heat-tolerant cotton species (Rodriguez-Garay *et al*., 1989; Kuehn *et al*., 1990).

Plant polyamines often occur in free soluble form. However, they can be also conjugated to low molecular mass molecules, such as hydroxycinnamic acid, by the formation of an amide linkage or bound to macromolecules such as proteins (Martin-Tanguy, 1997).

Common polyamines

NH_2-$(CH_2)_4$-NH_2	**Putrescine**
NH_2-$(CH_2)_3$-NH-$(CH_2)_4$-NH_2	**Spermidine**
NH_2-$(CH_2)_3$-NH-$(CH_2)_4$-NH-$(CH_2)_3$-NH_2	**Spermine**

Uncommon polyamines

NH_2-$(CH_2)_3$-NH_2	**1,3-diaminopropane**
NH_2-$(CH_2)_5$-NH_2	**Cadaverine**
NH_2-$(CH_2)_3$-NH-$(CH_2)_3$-NH_2	**Norspermidine**
NH_2-$(CH_2)_3$-NH-$(CH_2)_3$-NH-$(CH_2)_3$-NH_2	**Norspermine**
NH_2-$(CH_2)_4$-NH-$(CH_2)_3$-NH-$(CH_2)_3$-NH_2	**Thermospermine**

Fig. 1. **Structures of common and uncommon polyamines**

1.1.2 Physiological roles of polyamines

Polyamines are positively charged at physiological pH and this property allows them to interact with negatively charged macromolecules, such as DNA, RNA, proteins and phospholipids. In this way, polyamines are involved in the regulation of physical and chemical properties of membranes, stabilization of nucleic acid structure and modulation of enzyme activities (Galston and Sawhney, 1990). They are also known to protect DNA from damage caused by alkylating reagents, reactive oxygen species (ROS) and γ-rays (Ha *et al*., 1998; Mackintosh and Pegg, 2000).

Polyamines are also involved in cell cycle progression. Indeed, polyamine concentration vary during cell cycle. In particular, Put level increases during S e G2 phases, that of Spd during the entire cycle and that of Spm mainly during G1 and S phases (Thomas and Thomas, 2001). It has been suggested that Put is essential for the cell to enter S-phase, possibly driving the cell through the G1 restriction point prior to DNA synthesis and by the regulation of cyclin D1 (Wallace *et al*., 2003).

Polyamines are also considered to be essential for cell growth and differentiation (Cohen, 1998; Igarashi and Kashiwagi, 2000; Thomas and Thomas, 2001; Hanfrey *et al*., 2001). Inhibition of Spd synthesis, through deletion of enzymes involved in polyamine biosynthesis, is lethal at very early embryonic stages in mice (Wang *et al*., 2004a) and leads to lethal defect in embryo development in *Arabidopsis thaliana* plants (Imai *et al*., 2004; Urano *et al*., 2005). These data suggest an important role of Spd for viability of eukaryotic cells probably because it is a precursor of the unusual amino acid hypusine which in turn is involved in posttranslational modification of the eukaryotic translational initiation factor 5A (eIF5A) (Park, 2006).

On the other hand, polyamines are also involved in apoptotic cell death. Indeed, several studies suggest that higher or lower polyamine levels with respect to the physiological levels are implicated in apoptosis. Infact, it has been shown that an excessive production of polyamines can cause apoptosis, at least in some cell systems (Schipper *et al*., 2000). On the contrary, inhibitors of Spm biosynthetic enzymes have been shown to induce apoptosis in different cell lines. Data also exist suggesting a protective role of Spm against apoptosis (Kaneko *et al*., 1998; Hashimoto *et al*., 1999; Schipper *et al*., 2000; Seiler and Raul, 2005). In particular, it has been demonstrated that Spm prevents an increase in caspase 3 activity which generally precedes apoptosis. Other mechanisms that could be on the basis of the protective effect of Spm are inhibition of endonucleases, stabilization of DNA and protection of DNA against oxidative stresses (Schipper *et al*., 2000; Seiler and Raul, 2005).

In plants, polyamines have been suggested to play important roles in morphogenesis, growth, embryogenesis, organ development and leaf senescence (Kumar *et al*., 1997; Walden *et al*., 1997; Malmberg *et al*., 1998;

Liu *et al*., 2000; Kusano *et al*., 2007a). In general, cells undergoing division contain high levels of free polyamines while cells undergoing expansion and elongation contain low levels of free polyamines (Galston and Sawhney, 1995).

In higher plants, polyamines are also implicated in responses to various types of abiotic stress (Bouchereau *et al*., 1999; Alcázar *et al*., 2006; Kusano *et al*., 2007b; Groppa and Benavides, 2008). In Arabidopsis plants, K^+ deficiency induces an increase in Put accumulation and several studies have established a specific role of Put in maintaining a cation-anion balance in plant tissues (Boucherau *et al*., 1999). Furthermore, in *A. thaliana*, the expression levels of various enzymes involved in polyamine biosynthesis are increased following dehydration and cold stress (Pérez-Amador *et al*., 2002; Urano *et al*., 2003; Alcázar *et al*., 2006; Hummel *et al*., 2004; Vergnolle *et al*., 2005). In addition, different studies reported increase in Spd level in water-stressed and cold-tolerant tissues, indicating the stress-specific role of this polyamine (He *et al*., 2002; Nayyar *et al*., 2005). Salinity causes a significant increase in Spd and Spm levels and a decrease in Put level almost in all plant species studied. Furthermore, cellular alterations induced by sodium chloride treatment in wheat roots can be alleviated by exogenous Spd or Spm (Mansour and Al-Mutawa, 1999). These results would indicate a role for Spd and Spm in protecting plasma membrane under salinity and, thus, enhancing salt tolerance. The protective role of Spd and Spm in plant responses to abiotic stresses was also demonstrated using transgenic plants overexpressing polyamine biosynthetic genes (Kasukabe *et al*., 2004; Kasukabe *et al*., 2006) and loss-of-function mutant plants. In particular, enhancement of Spd synthesis in *A. thaliana* via a transgenic approach confers multi-stress tolerance and Arabidopsis *acl5/spms* mutant plants, which are unable to produce Spm, are hypersensitive to salt and drought stresses. Arabidopsis *acl5/spms* mutant plants are also Ca^{2+} deficient and lose more water compared to control plants, due to a failure of stomatal closure upon onset of drought (Yamaguchi *et al*., 2006; Yamaguchi *et al*., 2007). These results suggest that the absence of Spm may cause deregulation of Ca^{2+} trafficking, resulting in a lack of proper adaptation to high sodium chloride or drought stresses (Kusano *et al*. 2007a; Kusano *et al*., 2007b). It is plausible that one of the tasks of stress-induced polyamines is to modulate the activity of a certain set of ion channels to adapt ionic fluxes in response to environmental changes (Shabala *et al*., 2007; Zhao *et al*., 2007).

In plants, polyamines are also involved in plant-pathogen interactions, both incompatible and compatible ones (Walters, 2003). During the hypersensitive response (HR), which follows an incompatible plant-pathogen interaction and which consists in rapid H_2O_2 production and cell death at the site of pathogen entry, an enhanced polyamine synthesis and an apoplastic accumulation of Spm were reported (Torrigiani *et al*., 1997; Marini *et al*., 2001). Apolastic Spm may directly affect cation channel(s) and/or be catabolized to produce H_2O_2. Changes in K^+/Ca^{2+} trafficking and the generation of H_2O_2 can lead to

mithocondrial malfunction and cell death (Takahashi *et al*., 2003; Amirsadeghi *et al*., 2007; Kusano *et al*., 2007a).

Changes in polyamine metabolism were reported also during compatible plant-pathogen interactions. In particular, increased polyamine concentrations were found in green islands which are formed on cereal or barley leaves infected by biotrophic fungal pathogens, like rust and powdery mildew (Walters, 2000). Green islands surround the infection sites and are thought to represent regions in which a juvenile condition is maintained to ensure absorption of nutrients by the pathogen (Walters, 1989). It was suggested that the increased polyamine concentration in infected cereal or barley leaves might be related to green island formation (Walters, 2003).

1.1.3 Polyamine biosynthesis

Intracellular polyamines pools appear to be sensitively regulated by various homeostatic processes that include pathways for polyamine biosynthesis, catabolism, and transport across the cell membrane (Wallace *et al.*, 2003).

In plants, two alternative polyamine biosynthetic pathways are present (Bagni and Tassoni, 2001; Liu *et al*., 2007). In particular, the diamine Put can be synthesized, starting either from arginine (Arg) through the arginine decarboxylase (ADC) pathway or from ornithine through the ornithine decarboxylase (ODC) pathway (Fig. 2). In the ADC pathway, the Arg is first decarboxylated by ADC to form agmatine which is subsequently converted to Put by the combined action of agmatine iminohydrolase and N-carbamoylputrescine amidohydrolase. In the ODC pathway, Put is the direct product of ornithine decarboxylation by the action of ODC. Spd and Spm are formed by the subsequent addition of an aminopropyl group onto Put and Spd, respectively, in reactions catalysed by the enzymes spermidine synthase (SPDS) and spermine synthase (SPMS). The aminopropyl group is transferred from the decarboxylated *S*-adenosylmethionine (dcSAM), which in turn is synthesized from methionine in two sequential reactions catalyzed by methionine adenosyltransferase and *S*-adenosylmethionine decarboxylase (SAMDC), respectively (Fig. 2).

In *A. thaliana*, the ODC pathway seems to be absent since none ODC gene has been identified in the sequenced genome of this plant (Hanfrey *et al*., 2001), whereas all other polyamine biosynthetic genes have been assigned in *A. thaliana* genome. In detail, there are two *ADC* genes (*ADC1* and *ADC2*) (Watson and Malmberg, 1996; Watson *et al*., 1997), two *SPDS* genes (*SPDS1* and *SPDS2*) (Hanzawa *et al*., 2002), one *SPMS* gene (Panicot *et al*., 2002; Clay and Nelson, 2005) and at least four *SAMDC* genes (*SAMDC1*, *SAMDC2*, *SAMDC3* and *SAMDC4*) (Urano *et al*., 2003; Ge *et al*., 2006). Recently, a gene (*ACAULIS5* or *ACL5*) encoding for an enzyme able to produce Thermo-Spm from Spd has been reported (Knott *et al*., 2007). Furthermore, a loss-of-

function mutation on *ACL5* leads to defects in stem elongation (Hanzawa *et al*., 1997) and in vascular development (Clay and Nelson, 2005). Daily application of Thermo-Spm onto the shoot apex partially rescued the dwarf phenotype of *acl5* mutant (Kakehi *et al*., 2008).

In bacteria, both the ADC and the ODC pathways are present. However, in this case Put can be also synthesized directly from agmatine by agmatinase. Furthermore, in bacteria no *SPMS* gene is present thus Spm is not synthesized (Wortham *et al*., 2007) (Fig. 2). In animals, Put is prevalently synthesized by the ODC pathway, the ADC pathway being just a minor pathway in specific mammalian tissues (Gilad *et al*., 1996) (Fig. 2).

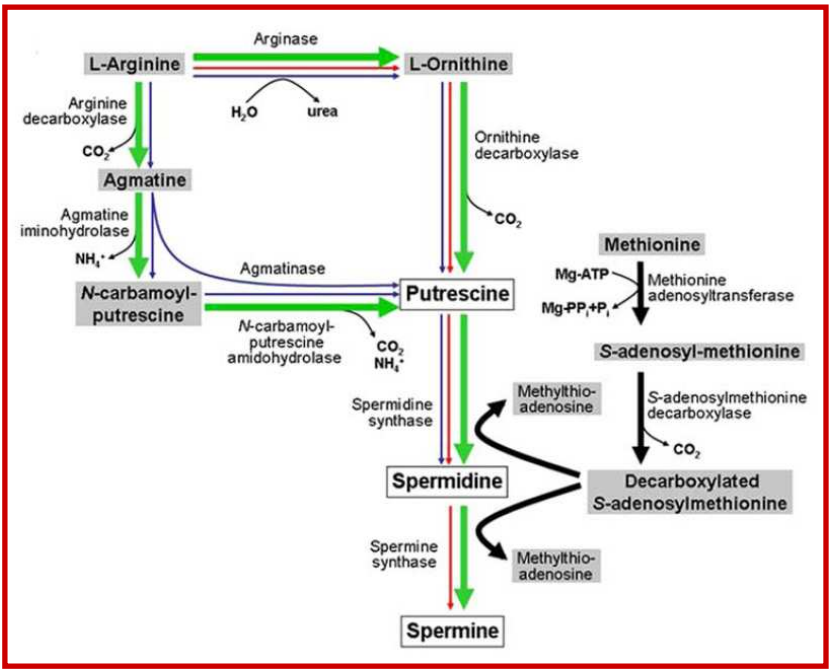

Fig. 2. **Polyamine biosynthetic pathways.** Plant pathway is indicated by green bold arrows. Blue and red arrows indicate bacterial and animal pathways, respectively. Figure taken from Kusano *et al*., 2008.

1.1.4 Polyamine catabolism

Polyamines are catabolized by the action of two classes of amine oxidases, the copper-containing amine oxidases (CuAOs) and the FAD-dependent amine oxidases (PAOs) (Cona *et al*., 2006).

CuAOs oxidize Put at the primary amino group producing 4-aminobutanal, H_2O_2 and ammonia (Cohen, 1998) (Fig. 3). 4-Aminobutanal cyclizes spontaneously to yield Δ^1-pyrroline that can be further oxidized to form γ-aminobutyric acid (GABA). GABA is subsequently transaminated and oxidized to succinic acid, which is incorporated into the Kreb's cycle, thus ensuring the recycling of carbon and nitrogen from Put (Cona *et al*., 2006) (Fig. 3).

PAOs catalyze the oxidation of Spm, Spd, and/or their acetylated derivatives at the secondary amino group (Federico and Angelini, 1991; Wang *et al*., 2001; Wu *et al*., 2003; Cona *et al*., 2006). The chemical identity of PAO reaction products depends on the enzyme source and reflects the mode of substrate oxidation. The until now characterized PAOs from monocotyledonous plants oxidize the carbon on the *endo*-side of the N^4-nitrogen of Spd and Spm, producing 4-aminobutanal and N-(3-aminopropyl)-4-aminobutanal, respectively, in addition to Dap and H_2O_2 (Cona *et al*., 2006) (Fig. 3). Animal PAOs and yeast (*Saccharomyces cerevisiae*) spermine oxidase (Fms1) oxidize the carbon on the *exo*-side of N^4-nitrogen of N^1-acetyl-Spm and N^1-acetyl-Spd to produce Spd and Put, respectively, in addition to 3-acetamidopropanal and H_2O_2 (Landry and Sternglanz, 2003; Vujcic *et al*., 2003; Wu *et al*., 2003) (Fig. 3). In this catabolic pathway, polyamine acetylation is catalyzed by the tightly regulated Spd/Spm N^1-acetyltransferase (SSAT), which is the rate-limiting factor (Wallace *et al*., 2003). Animal spermine oxidases (SMOs) and Fms1 also oxidize the carbon on the *exo*-side of N^4-nitrogen of Spm to produce Spd, 3-aminopropanal, and H_2O_2 (Wang *et al*., 2001; Vujcic *et al*., 2002; Cervelli *et al*., 2003; Landry and Sternglanz, 2003) (Fig. 3). 3-Aminopropanal and 3-acetamidopropanal, produced by polyamine catabolism, can be metabolized by an aldehyde dehydrogenase (ADH) to form β-alanine and N-acetyl-β-alanine, respectively, and N-acetyl-β-alanine in turn can be converted to β-alanine by the action of a selective hydrolase (HDL) (Fig. 3).

The animal PAOs and SMOs, as well as the yeast Fms1, are considered involved in a polyamine back-conversion pathway since they produce a common polyamine by the oxidation of another common polyamine (Seiler, 2004). On the contrary, the until now characterized PAOs from monocotyledonous plants are involved in the terminal catabolism of polyamines (Fig. 3). Only recently, a PAO from *A. thaliana* (AtPAO1) has been shown to be involved in a polyamine back-conversion pathway similarly to animal PAOs and SMOs (Tavladoraki *et al*., 2006).

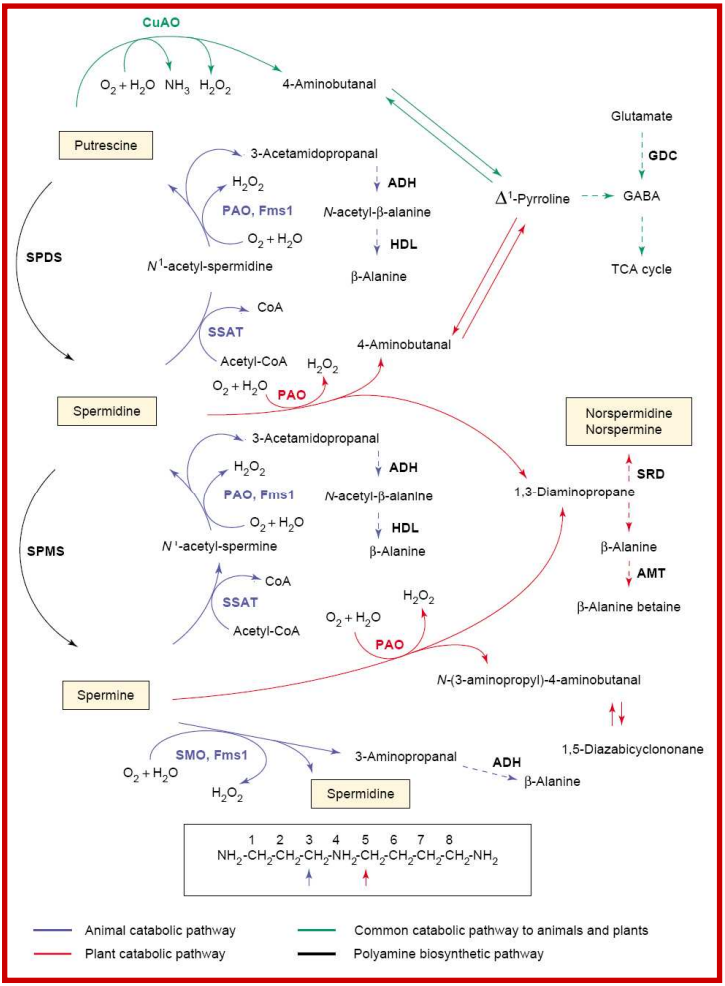

Fig. 3. **Schematic representation of the polyamine catabolic pathways in animals, yeasts and plants**. Catabolic reactions common to all organisms are indicated by green arrows, those specific to animal and yeast are indicated by blue arrows and those specific to plants are indicated by red arrows. The same colours are used for the corresponding catabolic enzymes. Broken arrows indicate metabolic pathways that involve polyamine oxidation products. Biosynthetic pathways are shown in black. In the insert, blue and red arrows indicate the Spd carbon atoms that are oxidized by animal and the until now characterized PAOs from monocotyledonous plants, respectively. Abbreviations: CuAO, copper-containing amine oxidase; PAO, polyamine oxidase; SMO, animal spermine oxidase; Fms1, yeast spermine oxidase; SSAT, spermidine-spermine N^1-acetyltransferase; ADH, aldehyde dehydrogenase; HDL, hydrolase; GDC, Glutamate decarboxylase; SPMS, Spm synthase; SPDS, Spd synthase; SRD, Schiff-base reductase/decarboxylase; AMT, β-alanine N-methyltransferase ; GABA, γ-aminobutyric acid. Figure modified from Cona *et al*., 2006.

Plant copper-containing amine oxidases

CuAOs are homodimers, each subunit of which contains a copper ion and a 2,4,5-trihydroxyphenylalanine quinone cofactor (TPQ) generated by a post-translational autocatalytic modification of a tyrosine residue in the active site (Medda *et al*., 1995). In plants, and in particular in *Pisum sativum*, *Lens culinaris* and *Cicer arietinum* seedlings, CuAOs represent the most abundant proteins of the extracellular fluids (Federico and Angelini, 1991).

The crystal structure of *Pisum sativum* CuAO (PSAO) (Kumar *et al*., 1996) showed that the copper ion, which was found close to the TPQ cofactor, is coordinated by three histidine residues and two water molecules present in the active site. An important characteristic of PSAO three-dimensional structure is the conformational flexibility of both the TPQ side chain and the enzyme surface, which seems to be essential for the catalytic reaction (Kumar *et al*., 1996).

In *A. thaliana*, 12 putative CuAO genes are present (*ATAOs*) (Alcázar *et al*. 2006). ATAO1, which shows 48% identity to PSAO, is the only until now biochemically characterized (Møller and McPherson, 1998). In particular, recombinant ATAO1 was expressed in insect cells and was shown to oxidize Put and, with a lower activity, Spd. Furthermore, the analysis of the *ATAO1* expression pattern in *A. thaliana* revealed that the highest expression level occurs in lateral root cap cells and in root differentiating vascular tissue.

Plant polyamine oxidases

The best characterized plant PAO is from *Zea mays* (ZmPAO). ZmPAO is a monomeric glycoprotein of 53 kDa, containing one molecule of FAD and having an apoplastic localization (Federico and Angelini, 1991). There are three genes encoding for ZmPAO (*ZmPAO1*, *ZmPAO2, ZmPAO3)*, which show a conserved gene organization and identical amino acid sequence (Tavladoraki *et al*., 1998; Cervelli *et al*., 2000). Its crystal structure has been solved to a resolution of 0.19 nm and contains two domains, the substrate-binding domain and the FAD-binding domain, which define a remarkable 30 Å long U-shaped catalytic tunnel at their interface (Fig. 4). The innermost part of the tunnel is positioned in front of the flavin isoalloxazine ring and forms the catalytic center (Binda *et al*., 1999; Binda *et al*., 2001).

ZmPAO shows a typical absorption spectrum of oxidised flavoprotein with absorption maxima at 280, 380 and 460 nm (Federico and Angelini, 1991). It catalyses the oxidation of Spm (K_m = 1.6 µM; k_{cat} = 32.9 s^{-1}) and Spd (K_m = 2.1 µM; k_{cat} = 50.2 s^{-1}) with an optimal pH of 6.5 (Polticelli *et al*., 2005). Another important biochemical characteristic of ZmPAO is the high value of K_m for oxygen (0.2 mM), which suggests that the oxygen concentration may be a relevant rate-limiting factor *in vivo* (Bellelli *et al*., 1997).

Fig. 4. **Crystal Structure of ZmPAO.** The FAD-binding domain is indicated in red, the substrate domain is indicated in green and the prosthetic group is shown in yellow ball-and-stick representation. Figure taken from Binda *et al*., 1999.

Furthermore, the aminoaldehydes, 4-aminobutanal and N-(3-aminopropyl)-4-aminobutanal, produced during the reaction for Spd and Spm respectively, are competitive inhibitor of the enzyme itself (with K_i values being 400 µM and 100 µM, respectively) (Federico *et al*., 1990).

In barley (*Hordeum vulgare*), two PAO genes (*HvPAO1* and *HvPAO2*) were isolated which encode for two proteins that display a high overall sequence homology with each other (73%) and with ZmPAO (84% and 73%, respectively) (Cervelli *et al*., 2001). HvPAO1 enzyme was purified from immature caryopsis and was also *in vitro* synthesized. It oxidizes both Spm and Spd with K_m values of 8.9 µM and of 5.0 µM respectively and a pH of optimum activity of 7.0 for both substrates similarly to ZmPAO (Cervelli *et al*., 2006). The similar catalytic properties shown for HvPAO1 and ZmPAO could be ascribed to the close phylogenetic relationship existing between them. On the contrary, HvPAO2 enzymatic features differ from the ones of HvPAO1. Indeed, despite the elevated sequence homology between HvPAO1 and HvPAO2, HvPAO2 purified from barley seedlings has a pH of optimum activity (5.5 for Spm and 8.0 for Spd) which is different from that of HvPAO1. Furthermore, HvPAO2 has a higher affinity for Spm (K_m = 4.8 µM) than for Spd (K_m = 560 µM) (Cervelli *et al*., 2001). Recently, it has been demonstrated a symplastic localization for HvPAO2. In particular, it has been shown that a C-terminal extension of eight amino acid residues present in the HvPAO2 sequence is a signal for protein targeting into the plant vacuoles (Cervelli *et al*.,

2004). On the contrary, the presence in HvPAO1 of an N-terminal signal peptide specific for the secretory pathway and the lack of the C-terminal extension present in HvPAO2 could suggest an apoplastic localization for HvPAO1 similarly to ZmPAO. The differences between HvPAO1 and HvPAO2 in catalytic properties and localization suggest that, in barley, the two PAO genes evolved separately, after a duplication event, to encode for two distinct enzymes, and they are likely to play different physiological roles (Cervelli *et al*., 2006).

In *A. thaliana*, five putative PAO genes are present: *At5g13700* (*AtPAO1*), *At2g43020* (*AtPAO2*), *At3g59050* (*AtPAO3*), *At1g65840* (*AtPAO4*) and *At4g29720* (*AtPAO5*) (Tavladoraki *et al*., 2006). AtPAO1 and AtPAO5 have an amino acid sequence homology of 45% and 25%, respectively, with ZmPAO and a predicted cytosolic localization. AtPAO2, AtPAO3 and AtPAO4 display an homology of about 23% with ZmPAO, an homology of 58-85% to each other and a peroxisomal localization (Kamada-Nobusada *et al*., 2008; Moschou *et al*., 2008). Recently, AtPAO1 has been shown to oxidize only Spm (K_m = 110 µM; k_{cat} = 2.7 s^{-1}) and not Spd with a pH value of optimum activity of 8.0 (Tavladoraki *et al*., 2006). It has been also demonstrated that AtPAO1 has a mode of substrate oxidation similar to that of animal PAOs producing Spd from Spm and thus that it is involved in a polyamine back-conversion pathway. In this way, AtPAO1 represents the first plant PAO shown to be involved in a polyamine back-conversion pathway (Tavladoraki *et al*., 2006).

*Physiological roles of CuAOs and PAOs in plant*s

CuAOs and PAOs contribute to important physiological processes not only through regulation of cellular polyamine levels but also through their reaction products: aminoaldehydes, Dap and mainly H_2O_2 (Boucherau *et al*., 1999; Sebela *et al*., 2001; Walters, 2003; Cona *et al*., 2006). In particular, 4-aminobutanal can be further metabolized to GABA (Fig. 3), which is an important metabolite associated with various physiological processes (including the regulation of cytosolic pH, carbon fluxes into the citric acid cycle, insect deterrence, protection against oxidative stress and signalling) and is largely and rapidly produced in response to biotic and abiotic stresses (Bouchè and Fromm, 2004). Dap is a precursor of β-alanine and uncommon polyamines (Terano and Suzuki, 1978; Koc *et al*., 1998) (Fig. 3), which in plants are associated with stress tolerance. H_2O_2 has a key role in both development and defence and is produced in the apoplast and intracellular compartments by several enzymatic systems (Apel and Hirt, 2004; Mittler *et al*., 2004; Yesbergenova *et al*., 2005).

The abundant localization of plant CuAOs and ZmPAO in tissues undergoing lignification or extensive cell wall-stiffening events suggests that these enzymes could influence, through H_2O_2 production, plant growth and development by affecting cell wall strengthening and rigidity (Rea *et al*., 1998;

Angelini *et al*., 1990; Laurenzi *et al*., 2001; Cona *et al*., 2005; Paschalidis and Roubelakis-Angelakis, 2005). In this regard, a positive spatial correlation between lignin, POD and CuAO levels has been found in chick-pea and tobacco, supporting a functional correlation between the two enzymes (Angelini *et al*., 1990; Paschalidis and Roubelakis-Angelakis, 2005).

A lot of biochemical, histochemical and immunocytochemical evidence also indicates the involvement of PAO in light-induced inhibition of maize mesocotyl growth (Cona *et al*., 2005; Laurenzi *et al*., 1999; Cona *et al*., 2003). Interestingly, the time course of the light-induced increase in PAO level is strongly correlated to the inhibition of extension growth in the mesocotyl apex (Laurenzi *et al*., 1999). Exogenously supplied auxin, which is involved in mesocotyl growth, inhibited the light-induced increase in PAO expression level, whereas auxin polar transport inhibitors caused an increase in PAO expression level under the same stimulus (Cona *et al*., 2003).

Recently, a new role in programmed cell death (PCD) associated with developmental differentiation has been proposed for CuAOs and PAOs (Møller and McPherson, 1998). Indeed, the considerable presence of ZmPAO and ATAO1 proteins in developing tracheary elements and root cap cells suggests the possibility of their specific involvement in the PCD of both cell types (Møller and McPherson, 1998; Cona *et al*., 2005).

Several studies have shown that in plants, CuAOs and PAOs contribute to the preformed and inducible defence responses that occur in the apoplast following biotic stress, mainly through H_2O_2 production. In particular, studies of the interaction between *Cicer arietinum* and the necrotrophic fungus *Ascochyta rabiei* have identified different distribution patterns and expression level of CuAO between susceptible (*cv* Calia) and resistant (*cv* Sultano) cultivars, the expression level being higher in the resistant cultivar compared to the susceptible one (Angelini *et al*., 1993). Furthermore, it has been demonstrated that the defence capacity of *cv* Sultano during interaction with *A. rabiei* is strongly impaired by 2-bromoethylamine, a potent, selective, mechanism-based inhibitor of CuAOs (Rea *et al*., 2002). The involvement of CuAOs in the extra-cellular cross-linking of structural proteins or lignin precursors has also been shown in *A. thaliana* during interactions with nematode parasites (Møller *et al*., 1998).

H_2O_2 derived from polyamine catabolism has been also shown to contribute to HR cell death (Yoda *et al*., 2003). Indeed, it has been reported that in *Nicotiana tabacum* plants resistant to tobacco mosaic virus (TMV), PAO expression level increases in tissues exhibiting TMV-induced HR and that PAO inhibition by the specific inhibitor guazatine markedly reduces HR (Yoda *et al*., 2003).

Further evidence regarding the participation of polyamine catabolism in defence mechanisms came from the observation that CuAOs are part of the complex network leading to wound- or herbivore-induced systemic protection.

Indeed, in chickpea tissue damage elicits a local and systemic increase in CuAO expression level. Jasmonic acid, which is a mobile wound signal, induces a further increase in CuAO expression level, whereas salicylic acid, a crucial component of systemic acquired resistance, exerts an opposite effect. Furthermore, inhibition *in vivo* of CuAOs by 2-bromoethylamine strikingly reduces local and systemic wound-induced H_2O_2 accumulation (Rea *et al*., 2002).

In several cases, the plant response to abiotic stress, such as drought, salinity, osmotic stress and heat stress, is associated with a stimulation of polyamine oxidation. In tomato leaf discs treated with sodium chloride, polyamine catabolism has been shown to be closely related to proline accumulation, which is one of the most commonly induced metabolic responses to water stress or salinity in higher plants. Furthermore, treatment with aminoguanidine, an inhibitor of CuAOs, strongly inhibited the parallel accumulation of proline (Aziz *et al*., 1998).

In rape leaf discs, osmotic stress caused by polyethylene glycol has been associated with increases in Put, Cad and Dap levels as well as a decrease in Spd level. Inhibitor studies have indicated that the stress-induced reduction of Spd level is due to stimulation of Spd oxidation and not to a block in Spd biosynthesis (Aziz *et al*., 1997). These results support the idea that under osmotic stress, rape leaf cells are induced to produce Dap through activation of PAO. The specific effect of this end product of polyamine catabolism is not well understood, but it can involve biosynthesis of uncommon polyamines and/or β-alanine. Indeed, Dap can be converted to stress associated uncommon polyamines, such as Nor-Spm and Nor-Spd, by the action of a Schiff-base reductase/decarboxylase (Fig. 3). In addition, Dap can be also converted in β-alanine through the concerted action of both a Dap-aminotransferase, reported in bacteria but not yet characterized in plants, and an aldehyde dehydrogenase. The role of β-alanine in stress responses may be due to its involvement, through the action of a β-alanine N-methyltransferase, in the production of β-alanine betaine (Fig. 3), an osmoprotectant found in species of *Plumbaginaceae* adapted to a wide range of adverse stress environments including saline and hypoxic conditions (Hanson *et al*., 1994; Raman and Rathinasabapathi, 2003).

Polyamine catabolism in plants is also associated with heat stress. For example, heat stress caused an increase in the levels of PAO and ADC in rice callus (Roy and Ghosh, 1996). This increase was higher in calli raised from a heat-tolerant cultivar than in those from a heat-sensitive one and correlated well with the increased levels of free and conjugated polyamines. Interestingly, PAO and ADC levels were also well correlated with the accumulation of uncommon polyamines under non-stress and stress conditions (Roy and Ghosh, 1996).

1.2 Histones and histone demethylases

1.2.1 Epigenetic modifications of histones

In eukaryotic cells, the basic unit of chromatin is the nucleosome core particle, a repeating element consisting of an histone octamer with 146 bp of DNA wrapped around it. Two copies of each of four histones H3, H4, H2A and H2B form the core octamer by protein–protein interactions of their globular domains and crystallographic analysis has revealed that the N-terminal tails of these histones protrude from the octamer (Luger *et al*., 1997).

For many years it was believed that the role of histones is constraint to their packaging function and that non-histone proteins carry the instructions for the chromatin activity and regulate gene expression. However, in recent years it became clear that the nucleosome core particle contributes to the dynamic remodeling of chromatin during gene activation/repression and carries important epigenetic information. This information resides primarily in the histone tails, which are subject to various covalent modifications, including acetylation, methylation, phosphorylation, ubiquitination, sumoylation and ADP-ribosylation (Jenuwein and Allis, 2001; Berger, 2002). In particular, it has been suggested that the specific histone tail modifications and their combinations constitute a "histone code" which provides signals for recruitment of specific chromatin-associated proteins, which in turn alter chromatin state and affect transcriptional regulation (Junewein and Allis, 2001; Zhang and Reinberg, 2001).

Acetylation of the ε-amino group of Lys residues is one of the first histone modifications described to be correlated with transcriptional activity (Allfrey *et al*., 1964; Hebbes *et al*., 1988). Acetylation influences transcription by neutralizing the positive charge of the histone tails and thus decreasing their affinity for DNA. Histones residues found in acetylated form are Lys 9 of histone H3 (H3K9), H3K14, H3K18, H3K23, H4K5, H4K8, H4K12, H4K16 and H4K20 (Fig. 5). Histone acetylation is regulated by the opposing activities of histone acetyltransferase (HATs) and histone deacetylase (HDACs) (Brownell and Allis, 1996; Kuo and Allis, 1998; Roth *et al*., 2001). HATs are classified into two categories (type A and type B) based on their subcellular distribution. The type A HATs are nuclear proteins, whereas the type B HATs are cytoplasmic proteins. In *A. thaliana*, AtGCN5, a type A HAT, appears to interact with the Arabidopsis homologs of the yeast transcriptional adaptor proteins ADA2a and ADA2b. Mutations disrupting *ADA2b* and *AtGCN5* induce various pleiotropic defects in *A. thaliana*, including dwarfism, aberrant root development, short petals and stamens, and reduced expression of cold regulated genes in cold acclimation (Vlachonasios *et al*., 2003).

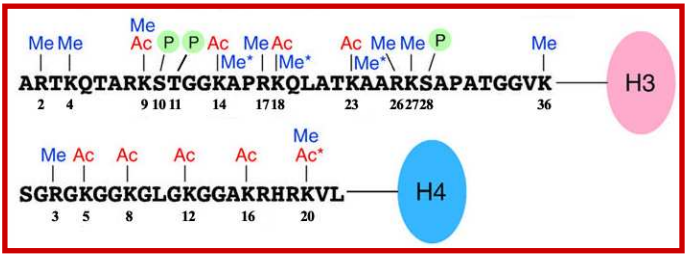

Fig. 5. **Epigenetic modifications of H3 and H4 histones tails.** Sites of histone acetylation (Ac, red), methylation (Me, blue) and phosphorylation (P in green circle) are indicated. Asterisks indicate plant-specific acetylation of H4K20 and plant-specific methylation of H3K14, H3K18, and H3K23. Figure modified from Chen and Tian, 2007.

Phylogenetic analysis subdivided HDACs into four classes (I - IV). Classes I, II, and IV enzymes utilize an active-site metal dependent catalytic mechanism, whereas class III HDACs utilize a NAD^+ dependent catalytic mechanism (Frye, 2000; Imai *et al*., 2000; Gregoretti *et al*., 2004). In *A. thaliana*, class I HDACs, such as AtHD1 and AtHDA6, are the best characterized HDACs. Down-regulation of *AtHD1* induces various developmental defects, including early senescence, serrated leaves, aerial rosettes, defects in floral organ identity and late flowering (Wu *et al*., 2000; Tian and Chen, 2001, Tian *et al*., 2005). AtHDA6 is mainly responsible for repression of repetitive transgenes and endogenous genes as well as maintenance of NORs (Nucleolus Organization Regions) (Probst *et al*., 2004; Chen and Tian, 2007). AtHD1 and AtHDA6 are also involved in plant responses to pathogens and environmental stresses (Zhou *et al*., 2005; Chen and Tian, 2007).

Specific histone residues can be also phosphorylated, such as H3S10 and H3S28 (Fig. 5). Recently, important progresses have been made toward understanding the role of histone phosphorylation in important cellular processes. Phosphorylation of H3S10 has been shown to correlate with chromosome condensation and segregation and with the activation of early response genes (including *c-fos* and *c-jun*) in mammalian cells (Nowak and Corces, 2004) as well as with the induction of transcription during heat-shock response in *Drosophila melanogaster* (Ivaldi *et al*., 2007; Hartzog and Tamkun, 2007). Furthermore, H3S10 phosphorylation modulates transcription by influencing other covalent modifications of the histone H3 tail. For example, the phosphorylation of H3S10 can activate transcription by promoting the H3K14 acetylation by specific type A HATs (Lo *et al*., 2001; Hartzog and Tamkun, 2007). In recent studies, an important role of H3S10 and H3S28 phosphorylation in DNA-damage response processes has been also suggested (Ozawa, 2008). Furthermore, it has been recently shown that Thr 11 of histone H3 (H3T11) is phosphorylated by protein-kinase-C-related kinase 1 (PRK1)

during androgen-receptor dependent transcription. Thus, phosphorylation of H3T11 can be considered as a novel chromatin mark for transcriptional regulation (Metzger *et al.*, 2008).

Histone methylation involves Lys and Arg residues such as H3K4, H3K9, H3K27, H3K36, H4K20, H3R2, H3R17, H3R26 and H4R3 (Fig. 5). Lys residues can be mono-, di-, or trimethylated, whereas Arg residues can be either mono- or dimethylated (Zhang and Reinberg, 2001). Methylation of H3K9 and H3K27 have been linked to epigenetic gene silencing. Indeed, methylated H3K9 is enriched in heterochromatin and has the potential to initiate chromatin condensation and silencing in animals (Peters *et al*., 2001). In *A. thaliana*, mono- and di-methylated H3K9 (H3K9me1 and H3K9me2) are enriched in centromeric and pericentromeric repeats (Gendrel *et al*., 2002; Jackson *et al*., 2004). Furthermore, in *A. thaliana* it has been demonstrated that, during vernalization, H3K9 and H3K27 dimethylation is increased in discrete domains within a negative regulator of flowering, the *FLOWERING LOCUS C* (*FLC*) (Bastow *et al*., 2004; Yan *et al*., 2004). In contrast to H3K9 and H3K27 methylation, which represses transcription, H3K4 methylation is linked to transcriptional activity. In particular, in *A. thaliana* H3K4 methylation is exclusively localized to euchromatin and is required for activation of *FLC* expression. Like H3K4 methylation, Arg methylation of H3 and H4 correlates with transcriptional activation; for instance, H4R3 methylation promotes gene expression facilitating acetylation of H4 (Zhang and Reinberg, 2001).

Ubiquitination is another posttranslational modification which can also involve histones residues. This process consists in the attachment of ubiquitin, a small globular protein of 76 amino acids, to a target substrate through a series of steps referred to as activation (E1), conjugation (E2) and ligation (E3) (Jason *et al.*, 2002). The major role identified thus far for ubiquitination of cellular proteins is their targeting to proteasome for degradation (Hochstrasser, 1996). However, histone ubiquitination has been recently associated to several processes other than degradation. For instance, H2A and H2B ubiquitination, which involves Lys residues (H2AK119 and H2BK120), varies during the cell cycle and its absence during G2/M transition is believed to be essential for cell cycle progression (Jason *et al.*, 2002). Furthermore, H3 ubiquitination, which has been recently reported *in vivo* in elongating spermatid of rat testes, could play a role in histone desplacement (Chen *et al*., 1998; Jason *et al.*, 2002; He and Lehming, 2003).

An additional histone modification is sumoylation, a process that conjugates small ubiquitin modifier peptides (SUMO) to Lys residues of histones and is catalyzed by an enzyme cascade similar to that for ubiquitination. It was reported that histone sumoylation mediates transcriptional repression and in plants trascriptional repression by histone sumoylation is involved in the regulation of flowering and development (Shiio and Eisenman, 2003; Jin *et al*., 2008).

Furthermore, histone residues can be also ADP-ribosylated. In particular, several studies have indicated that histones can be covalently modified by mono-ADP-ribose in response to DNA damage. In addition, it has been shown the existence of a cross-talk between mono-ADP-ribosylation and other posttranslational modifications of histones, such as acetylation or phosphorylation. Thus, it is possible that mono-ADP-ribosylation, along with other modifications of histone tails, may regulate subsequent steps in DNA damage response pathways (Hassa *et al*., 2006).

1.2.2 Histone methylation

Lysine and arginine methylation

Histone methylation is catalyzed by Lys-specific methyltransferases (PKMTs) and Arg-specific methyltransferases (PRMTs). PKMTs catalyze mono-, di-, and trimethylation of the Lys ε-amino group in a *S*-adenosylmethionine (SAM)-dependent manner (Zhang and Reinberg, 2001). PKMTs consist of two main classes, the SET domain containing family and the DOT1 family. The SET domain is a sequence comprising approximately 130 amino acids and its name is related to the three *D. melanogaster* genes involved in epigenetic processes in which it was originally identified: *Su(var)3–9*, *En(zeste)* and *Trithorax* (Jenuwein *et al*, 1998). In *A. thaliana* several proteins with homology to Su(var)3–9 have been identified, with KRYPTONITE (KYP) being the predominant PKMT (Jackson *et al*., 2002). KYP methylates H3K9 and the *kyp* mutant was isolated as a suppressor of gene silencing at the Arabidopsis SUPERMAN (SUP) locus, which is a regulator of floral homeotic genes (Jackson *et al*., 2002). DOT1-PKMTs do not contain a SET domain, methylate the H3K79 residue within the core domain and are involved in heterochromatin-mediated silencing (Feng *et al*., 2002; Ng *et al*., 2002).

PRMTs are separated into two main types. Whereas both types catalyze the formation of monomethyl-Arg, type I PRMTs continue to form asymmetric N,N′-dimethyl-Arg and type II PRMTs continue to form symmetric N,N-dimethyl-Arg (Zhang and Reinberg, 2001). Recently, it has been shown that AtPRMT5, a type II PRMT of *A. thaliana*, is involved in the vernalization-induced epigenetic silencing of *FLC* (Schmitz *et al*., 2008).

Lysine-specific histone demethylases

Although some histone modifications are highly dynamic, histone methylation had been initially regarded as irreversible. However, the recent discovery of several histone demethylases which can reverse methylation of Lys and Arg residues (Bannister *et al*., 2002; Shi *et al*., 2004) has changed this point of view.

Human Lys-specific histone demethylase 1 (HsLSD1 alias KIAA0601 and BHC110) is the first discovered histone demethylase. HsLSD1 acts on H3K4me1 and H3K4me2, respectively, through a FAD-dependent mechanism (Shi *et al*., 2004). The reaction involves two steps. First, the histone substrate is bound and its methylated K4 side chain is oxidized by the FAD with resultant reduction of oxygen. Then, the resulting imine intermediate is hydrolyzed to generate the demethylated H3 tail and formaldehyde (Forneris *et al*., 2006) (Fig. 6; Supplementary Fig. 1).

HsLSD1 was originally identified as a component of transcriptional repressor complexes. Indeed, HsLSD1 is typically associated with the transcriptional corepressor protein CoREST and with HDAC1 or HDAC2, to form a stable core subcomplex recruited by several chromatin-remodeling multiprotein complexes (Ballas *et al*., 2001, Shi *et al*., 2003). For instance, HsLSD1-CoREST–HDAC core was found in complex with the repressor element 1-silencing transcription factor (REST) to mediate long-term repression of neuronal genes in non-neuronal cells (Ballas *et al*., 2005; Ooi and Wood, 2007).

HsLSD1 is also involved in gene activation processes, thus highlighting its multifaceted function in chromatin regulation. In particular, activation of androgen receptor target genes requires HsLSD1-dependent histone H3K9 demethylation (Metzger *et al*., 2005).

The dual role of HsLSD1 in gene repression/activation is also demonstrated by its role in the fine regulation of growth hormone (Gh) production during pituitary development (Wang *et al*., 2007).

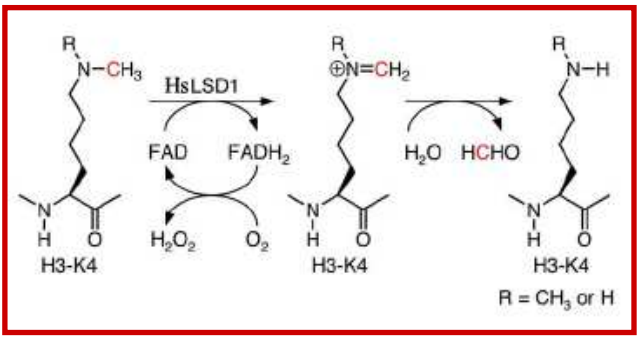

Fig. 6. **Mechanism of HsLSD1-catalyzed demethylation of H3K4.** The carbon atom that is oxidized to form formaldehyde is shown in red**.** Figure modified from Yang *et al*., 2006.

Activation of the *Gh* gene is regulated by the transcriptional activator pituitary transcription factor 1 (Pit1) during the early phases of development through recruitment of the HsLSD1-containing MLL1 (mixed lineage leukemia 1) coactivator complex. Pit1 and its associated complex is later replaced by the ZEB1 (zinc finger E-box binding homeobox 1) transcriptional repressor which recruits a corepressor complex containing CtBP (C-terminal Binding Protein), CoREST and HsLSD1, in this way switching off *Gh* gene expression. Thus, HsLSD1 is the key component of two opposing coactivator and corepressor complexes that fine-tune the temporal expression of a single target.

An important feature in the HsLSD1-mediated demethylation process is that, though HsLSD1 alone can demethylate H3K4 in peptides or bulk histones, the binding of HsLSD1 to the C-terminal SANT domain of CoREST renders HsLSD1 able to catalyze H3K4 demethylation on intact nucleosomal particles and also less prone to proteasomal degradation (Shi *et al*., 2005). Another important characteristic of HsLSD1 is the mechanism for substrate recognition. It has been demonstrated that HsLSD1 requires the first 20 N-terminal amino acids of the histone tail for productive binding (Forneris *et al*., 2005a). Such a specific recognition mechanism enables HsLSD1 to sense the epigenetic message encoded by the histone tail, as evidenced by the finding that the presence on H3 of other epigenetic markers affects HsLSD1 catalytic activity, decreasing or even completely hampering it (Shi *et al*., 2004; Shi *et al*., 2005; Forneris *et al*., 2005a; Forneris *et al*., 2006).

The crystal structures of HsLSD1 in free form and in complex with CoREST was recently solved (Stavropoulos *et al*., 2006; Chen *et al*., 2006; Yang *et al*., 2006). HsLSD1 is an asymmetric molecule consisting of three distinct structural domains. Two of them, the N-terminal SWIRM domain (named for its presence in the proteins Swi3, Rsc8, and Moira) and the C-terminal FAD-binding amine oxidase domain, closely pack against each other, forming a globular core structure from which the third domain, named Tower domain, protrudes as an elongated helix-turn-helix motif (Fig. 7).

Insight into substrate binding was obtained from recent crystallographic analyses of HsLSD1-CoREST in complex with an histone H3 peptide modified by the addition of a reactive chemical group (a propargyl unit) on the K4 side chain (Culhane *et al*., 2006; Yang *et al*., 2007). In this way, the peptide functions as an inhibitor through formation of a covalent adduct between its modified K4 and the flavin. The crystal structure of this complex revealed that the peptide binds to the amine oxidase domain, adopting a folded conformation that enables the substrate-binding site to accommodate the relatively long stretch of the N-terminal H3 tail. This binding mode positions the reactive H3K4 side chain in proximity to FAD. In general, the architecture of the substrate-binding site is characterized by the presence of various niches that accommodate the side chains of the histone peptide through formation of specific interactions (Yang *et al*., 2007). The addition of more epigenetic

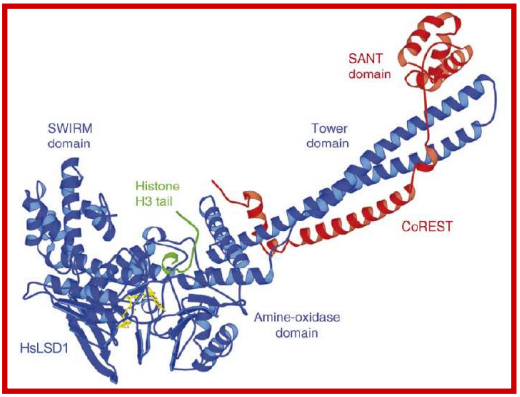

***Fig. 7*. Structural biology of HsLSD1 in complex with CoREST and a peptide substrate.** HsLSD1 (blue) consists of three domains: the amine oxidase domain, the SWIRM domain and the helical tower domain. HsLSD1 tightly associates with the CoREST C-terminal SANT domain (red)**.** The histone H3 N-terminal peptide (green) binds deeply in the HsLSD1 amine oxidase domain in proximity to the flavin cofactor (yellow). Figure modified from Forneris *et al*., 2008.

markers on the H3 N-terminal tail introduces steric and electrostatic perturbations which alter this network of interactions predictably, thus explaining the negative effect that nearly all epigenetic modifications have on HsLSD1–H3 binding (Forneris *et al.*, 2007; Forneris *et al*., 2008).

Recently, it has been reported that HsLSD1 is also active toward a non-histone protein such as the tumor suppressor p53 methylated at Lys 370 residue. Thus blocking its pro-apoptotic activity. This finding leaves open the question of which are the *in vivo* substrates of the enzyme (Huang *et al*., 2007).

In *A. thaliana*, four cDNAs: *At1g62830*, *At3g13682*, *At3g10390 (FLOWERING LOCUS D* o *FLD)*, *At4g16310* were identified encoding for proteins displaying 26-30% sequence homology with HsLSD1 and bearing, similarly to HsLSD1, both a flavin amine oxidase domain and a SWIRM domain (Shi *et al*., 2004). Recently, FLD has been shown to interact with a plant-specific C2H2 zinc finger-SET domain protein and to repress *FLC* expression (He *et al.*, 2003; Krichevsky *et al*., 2007).

Peptidyl-arginine deiminases

Arg methylation is prone to enzymatic conversion through a deimination reaction (Cuthbert *et al*., 2004; Kubicek and Jenuwein, 2004). The responsible enzymes, termed peptidyl-Arg deiminases or demethylases (PADs), are not very prominent in mammals and comprise only five members (PAD1–PAD4 and PAD6). The described reaction of monomethyl-Arg deimination is not a true reversion of the methyl mark since it generates an altered amino acid

(citrulline) and methyl-ammonium (Supplementary Fig. 1). PADs can deiminate unmodified Arg and monomethylated Arg residues of H3 and H4 histone tails (Cuthbert *et al*., 2004; Wang *et al*., 2004b). PAD4, the most characterized PAD, was reported to suppress the transcription of the estrogen-regulated genes by citrullination of methylated H3R17 and H4R3 (Cuthbert *et al*., 2004).

Jumonji C domain-containing histone demethylases

Recently, a new family of histone demethylases has been identified. Although the various members of this family contain numerous domains, such as PHD (Plant Homeodomain) and Tudor domains, they each feature a jumonjiC (JmjC, Japanese for 'cruciform') domain responsible for their demethylase activity, and for this reason they have been designated as jumonji C histone demethylases (JHDMs) (Tsukada *et al*., 2005).
JHDMs operate on methylated Lys and Arg residues via Fe(II)- and 2-oxoglutarate–dependent dioxygenation and proceed through a radical mechanism involving an iron-oxo intermediate (Supplementary Fig. 1). Overall, this reaction results in the demethylation of the methyl-Lys or methyl-Arg moiety to produce succinate and formaldehyde as the resulting byproducts (Anand and Marmorstein, 2007) (Supplementary Fig. 1). One important aspect of the JHDMs catalytic mechanism, in contrast to the mechanism employed by HsLSD1, is that it does not require a protonated nitrogen for activity and hence permits demethylation of trimethylated Lys residues.

There are 27 different JHDMs with varying substrate specificity within the human genome, whereas in *A. thaliana* 21 putative JHDMs were identified (Agger *et al*., 2008; Lu *et al*., 2008). Human JHDM1A, which is the first described JmjC domain-containing demethylase, specifically demethylates mono- and dimethylated H3K36 (H3K36me1 and H3K36me2; Tsukada *et al*., 2005). Interestingly, JHDM1B, a close homologue of JHDM1A involved in transcriptional repression of ribosomal RNA genes and *c-jun*, was recently reported to bear demethylase activity toward the H3K4me3 (Frescas *et al*., 2007; Koyama-Nasu *et al*., 2007).

In recent studies it has been shown that the various members (JMJD2A, JMJD2B, JMJD2C and JMJD2D) of JMJD2 family, a subfamily of JmjC domain containing proteins, prevalently catalyze the demethylation of H3K9me3 or H3K9me2 and H3K36me3 or H3K36me2 and are associated to prostate cancer (Cloos *et al*., 2006; Klose *et al*., 2006; Wissmann *et al*., 2007). In addition to the various members of the JMJD2 family, also JMJD1A can demethylate methylated H3K9. However, JMJD1A is specific for H3K9me1 and H3K9me2, in particular at androgen receptor target genes (Yamane *et al*., 2006). The jmjc-containing members of JARID1 family (JARID1A, JARID1B, JARID1C, JARID1D) specifically demethylate H3K4me3. Despite, the

similarity in substrate specificity, the various members of this family have very different physiological functions probably reflecting their presence in distinct protein complexes (Christensen *et al*., 2007; Yamane *et al*., 2007; Jensen *et al*., 2005). UTX and JMJD3, which have been recently identified as JHDMs, function as transcriptional activators and demethylate H3K27me2 and H3K27me3 (Agger *et al*., 2007). Furthermore, JMJD6, which is essential for the early embryogenesis, has been recently reported to bear demethylase activity toward H3R2me2 and H4R3me2 both *in vitro* and *in vivo* (Bose *et al*., 2004; Chang *et al*., 2007).

1.3 *Arabidopsis thaliana* as a model plant

A. thaliana is a small dicotyledonous species belonging to the *Brassicaceae* family, with low economical importance. However, *A. thaliana* has several traits that make it a useful model organism for understanding the genetic, cellular and molecular biology of flowering plants.

A. thaliana has a fast life cycle (the entire life cycle being completed in six weeks), has very limited space requirements for growth and maintainance and is a self-pollinated plant producing many seeds which can be dehydrated and stored at ambient temperature for long periods of time. With about 125 Mb on five chromosomes, *A. thaliana* has one of the smallest genomes among plants which has been completely sequenced by the Arabidopsis Genome Initiative. Another property that has made *A. thaliana* as the best model system for basic research in the biology of all multicellular eukaryotes is that it can be easily transformed by infection with genetically engineered *Agrobacterium tumefaciens*. This characteristic has permitted the development of mutagenesis methods based on random insertion of *Agrobacterium* T-DNA or transposons in the plant genome. Using these techniques, near-saturation libraries of insertional mutant alleles in *A. thaliana* have been created which can be screened by polymerase chain reaction for insertions in a gene of interest (Alonso *et al*., 2003; Muskett *et al*., 2003). Furthermore, the sequences of the insertion sites are available on internet (www.atidb.org/cgi-perl/index; http://signal.salk.edu/) and enable computer searches for mutants in a gene of interest and purchase of the corresponding seeds from the Arabidopsis stock center (www.arabidopsis.org/abrc/). The availability of *Agrobacterium*-mediated transformation techniques also enables to study gene function in *A. thaliana* by RNA interference-based gene silencing and overexpression strategies (Feng and Mundy, 2006).

1.4 Aims of the thesis

The main aim of the present work is the study of the physiological roles of plant PAOs and in particular of *A. thaliana* PAOs. This study of the PAOs of the dicotyledonous plant *A. thaliana* may result of great importance considering that until now only PAOs from monocotyledonous plants have been characterized and the substrate specificity and the nature of the reaction products of PAOs and thus the physiological roles depend on the enzyme source. On the other hand, the several genetic resources available for the model plant *A. thaliana* will be very useful instruments for this study.

In *A. thaliana* five putative PAO genes are present: *AtPAO1-5* (Tavladoraki *et al*., 2006). AtPAO1 has been recently shown to be involved in a polyamine back-conversion pathway similarly to the animal PAOs and SMOs and differently from ZmPAO, which is involved in a terminal catabolic pathway of polyamines. Furthermore, it was shown that AtPAO1 is able to oxidize the stress-related uncommon polyamine Nor-Spm, suggesting that this enzyme may be involved in plant responses to abiotic stresses.

An important goal of the present work is the heterologous expression and the biochemical characterization of the other members of the *AtPAO* gene family. The attention will be focalized to the substrate specificity and mode of catalysis of these enzymes to determine which are their physiological substrates and whether they are also involved in a polyamine back-conversion pathway similarly to AtPAO1. The results of this analysis will contribute greatly to elucidate the physiological role of each member of this gene family and to understand the physiological relevance of the two different catabolic pathways of polyamines.

In *A. thaliana*, four more genes have been also identified: *At1g62830*, *At3g13682*, *At3g10390*, *At4g16310* encoding for proteins with an amine oxidase domain. These proteins bear also a SWIRM domain, which is usually present in chromatin-modifying complexes, and have an elevated sequence homology with human HsLSD1. HsLSD1 has the same functional domains as the four identified Arabidopsis proteins, catalyses the oxidative demethylation of H3K4me1 and H3K4me2 and participates in multiprotein complexes important in the regulation of gene expression. It was hypothesized that *At1g62830*, *At3g13682*, *At3g10390* and *At4g16310* also encode for lysine-specific histone demethylases, and they were termed *AtLSD1* (*A. thaliana* lysine-specific demethylase 1), *AtLSD2*, *AtLSD3* and *AtLSD4*, respectively.

In this work, to verify whether AtLSDs indeed have a lysine-specific histone demethylase activity, the catalytic properties of AtLSD1, chosen as a representative member of this gene family, following expression in *E. coli* will be determined. The three-dimensional structure of AtLSD1 will be also modeled using the HsLSD1 crystal structure as a template to evidence differences and similarities in respect to the human orthologue. Furthermore, to

determine the physiological roles of this class of enzymes, insertional knock-out mutants for each one of the four *AtLSDs* will be isolated and characterized. Constructs will be prepared for AtLSD1 overexpression in *A. thaliana* plant, both to isolate the complexes in which AtLSD1 is eventually involved and to identify the genes it regulates through microarray analysis and chromatin immunoprecipitation experiments. Furthermore, to obtain detailed informations on the *AtLSDs* expression pattern RT-PCR experiments will be performed and an AtLSD1 prom::GFP-GUS construct will be prepared. *A. thaliana* plants will be transformed with the prepared costructs and characterized.

2. RESULTS

2.1 Polyamine oxidases of *A. thaliana*

2.1.1 Description of the PAO gene family in *A. thaliana*

A search of the Arabidopsis database with the amino acid sequence of ZmPAO revealed the presence of five cDNAs encoding for putative PAOs: *At5g13700* (*AtPAO1*), *At2g43020* (*AtPAO2*), *At3g59050* (*AtPAO3*), *At1g65840* (*AtPAO4*) and *At4g29720* (*AtPAO5*). AtPAO1 has a 45% identity at the amino acid level with ZmPAO and only a 19% to 24% identity with the other four putative AtPAOs. AtPAO2, AtPAO3, and AtPAO4 display low sequence identity (23% - 24% identity) with ZmPAO and elevated sequence identity to each other. In particular, the sequence identity between AtPAO2 and AtPAO3 is higher (85%) than that between AtPAO2 and AtPAO4 and between AtPAO3 and AtPAO4 (58% and 50%, respectively). On the contrary, AtPAO5 has low sequence identity not only with ZmPAO (22% sequence identity), but also with AtPAO2, AtPAO3 and AtPAO4 (23% identity) (Supplementary Fig. 2).

Gene structure analysis of *AtPAOs* revealed that while *AtPAO1* gene has a similar intron/exon organization to that of *ZmPAO* (Cervelli *et al.*, 2001), *AtPAO2*, *AtPAO3* and *AtPAO4* intron/exon organization is different from that of *AtPAO1* and *ZmPAO*. Furthermore it was shown that *AtPAO2*, *AtPAO3* and *AtPAO4* genes have a very similar intron/exon organization, all three genes containing eight introns with highly conserved positions (Fig. 8). This, together with the elevated sequence homology to each other, suggests that these three Arabidopsis genes are recent derivatives from a common ancestor and thus that they can be considered as members of the same subfamily. *AtPAO5* gene presents a very different gene organization from that of *ZmPAO* and the other *AtPAOs*, lacking any intron.

To determine the possible subcellular localization of AtPAO2-5, their amino acid sequences were analyzed by PSORT (www.psort.ims.u-tokyo.ac.jp). This analysis predicted the presence in AtPAO2, AtPAO3 and AtPAO4 of a sequence for peroxisomal targeting (Fig. 9) and indeed

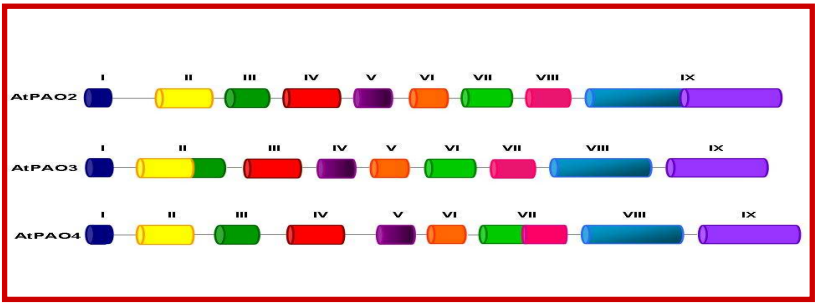

***Fig. 8*. Representation of AtPAO2, AtPAO3 and AtPAO4 intron/exon structure.** Exons are represented as colored boxes and are indicated by roman numbers, whereas introns are represented as black lines. Boxes with the same color represent common exons among genes.

peroxisomal targeting of all three enzymes has been very recently demonstrated (Kamada-Nobusada *et al*., 2008; Moschou *et al*., 2008). For AtPAO1 and AtPAO5, PSORT analysis did not reveal the presence of any signal for protein targeting to specific intracellular compartment, thus suggesting a cytosolic localization. However, AtPAO1 has a very high sequence identity (74%) with a PAO from *N. tabacum* (NtPAO), which has been shown to have an apoplastic localization (Yoda *et al*., 2006), thus leaving open the question of AtPAO1 subcellular localization.

2.1.2 Heterologous expression of AtPAO2, AtPAO4 and AtPAO5 in *Escherichia coli*

With the aim of completing the biochemical characterization of AtPAOs, the cDNAs encoding for AtPAO2 and AtPAO4, chosen as representative members of the subfamily in which they belong, and AtPAO5 were obtained from Arabidopsis leaves (Supplementary Fig. 3). In particular, the coding regions of *AtPAOs* were amplified by RT-PCR from leaves using sequence-specific primers (*AtPAO2-His for/AtPAO2-His rev; AtPAO4-His for/AtPAO4-His rev; AtPAO5-His for1/AtPAO5-His rev*). These primers were designed in such a way as to allow cDNA cloning in the pET 17b vector for inducible expression in the cytoplasm of *E. coli* cells [BL21(DE3) strain]. Furthermore, to facilitate purification of the recombinant proteins, a sequence encoding for a 6-His tag was added at the 3′ terminus of the cDNAs. In this way, the AtPAO2-pET 17b, AtPAO4-pET 17b and AtPAO5-pET 17b plasmids were constructed.

Soluble lysates obtained from *E. coli* cells transformed with AtPAO2-pET 17b and AtPAO4-pET 17b plasmids were tested for accumulation of the recombinant proteins through western blot analysis and enzyme activity

```
AtPAO1      RVEAQSDQETMKEAMSVL-----RDMF-GATIPYA-------------TDILVPRWWNNR 362
AtPAO2      DIEKMSDEAAANFAVLQL-----QRILPDALPP---------------VQYLVSRWGSDV 400
AtPAO3      DIEKKSDEAAANFAFSQL-----QKILPDASSP---------------INYLVSRWGSDI 401
AtPAO4      DLEKLSDEATANFVMLQL-----KKMFPDAPDP---------------AQYLVTRWGTDP 402
ATPAO5      ELEKLTDEEIKDAVMTTISCLTGKEVKNDTAKPLTNGSLNDDDEAMKITKVLKSKWGSDP 448
ZmPAO       RIEQQSDEQTKAEIMQVL-----RKMFPGKDVPDA-------------TDILVPRWWSDR 397
             :*  :*:         :     : :      *                  * :* :

AtPAO1      FQRGSYSNYPMISDNQLLQNIKAPVGRIFFTGEHTSEKFSGYVHGGYLAGIDTSKSLLEE 422
AtPAO2      NSMGSYSYDIVGKPHDLYERLRVPVDNLFFAGEATSSSFPGSVHGAYSTGLMAAEDCRMR 460
AtPAO3      NSLGSYSYDIVNKPHDLYERLRVPLDNLFFAGEATSSSYPGSVHGAYSTGVLAAEDCRMR 461
AtPAO4      NTLGCYAYDVVGMPEDLYPRLGEPVDNIFFGGEAVNVEHQGSAHGAFLAGVSASQNCQRY 462
ATPAO5      LFRGSYSYVAVGSSGDDLDAMAEPLPKINKKVGQVNGHDQAKVHELQVMFAGEATHRTHY 508
ZmPAO       FYKGTFSNWPVGVNRYEYDQLRAPVGRVYFTGEHTSEHYNGYVHGAYLSGIDSAEILINC 457
               * ::   :          :  *: :                 *         :

AtPAO1      MKQSLLLQPLLAFTESLTLTHQKPNNSQIYTNVKFISGTS 462
AtPAO2      VLERYGELDLF--QPVMGEE---GPASVPLLISRL----- 490
AtPAO3      VLERYGEL-----EHEMEEE---APASVPLLISRM----- 488
AtPAO4      IFERLGAWEKLKLVSLMGNSDILETATVPLQISRM----- 497
ATPAO5      STTHGAYYSGLREANRLLKHYKCNF--------------- 533
ZmPAO       AQKKMCKYHVQGKYD------------------------- 472
```

***Fig. 9*. Alignment of the amino acid sequence of AtPAOs and ZmPAO.** Multialignment was done using the program ClustalW sequence alignment (Altschul *et al*., 1990). Numbering of amino acid residues is shown at the right side. Residues present at an analogous position with respect to the Cys residue that is covalently linked to the FAD in MAOs are indicated by a yellow box. Peroxisomal targeting signals of recombinant AtPAO2, AtPAO3 and AtPAO4 are indicated in red. The identical residues and the conserved residues are labeled by the symbols * and :, respectively.

assay using Put, Spd and Spm (data not shown). This analysis showed high expression levels of recombinant AtPAO2 and AtPAO4 (about 2-4 mg per liter of culture) and catalytic activity toward Spd and Spm (V_{max} Spm /V_{max} Spd = 1 for AtPAO2 and V_{max} Spm/V_{max} Spd ~ 50 for AtPAO4).

On the contrary, recombinant AtPAO5 was not detectable by western blot analysis both in the soluble lysates and in the inclusion bodies of the bacteria transformed with AtPAO5-pET 17b plasmid. Furthermore, in the soluble lysates no PAO activity toward various polyamines was found although various conditions for expression and catalytic activity were used. In particular, induction of recombinant proteins was performed at various temperatures (25°C, 30°C and 37°C) and for various time periods (1h, 3h, 5h and 24h) and catalytic activity was tested at various pH values (pH 6.0 to pH 8.0). Recombinant AtPAO5 expression was also attempted using two more *E. coli* strains, the one [BL21(DE3)pLysS strain] permitting more stringent expression conditions and thus being useful for the expression of insoluble or toxic proteins and the other [BL21-CodonPlus(DE3)-RIPL strain] being characterized by an enriched tRNA pool. However, also in these cases AtPAO5 heterologous expression was not successful. To verify whether AtPAO5 can be produced in *Pichia Pastoris* the *AtPAO5* cDNA was amplified using AtPAO5-pET 17b plasmid as template and sequence-specific primers (*AtPAO5-His for2/AtPAO5-His rev*) and was cloned in the pGAPZαA vector for heterologous expression in the culture medium of *P. pastoris* (X33 strain). However, also using this expression system, expression of recombinant AtPAO5 wasn't achieved.

2.1.3 Purification and biochemical characterization of recombinant AtPAO2 and AtPAO4

To purify recombinant AtPAO2 and AtPAO4 from the bacterial lysates, affinity chromatography using a Ni^{2+}- charged resin was performed, which permitted to purify both recombinant proteins to electrophoretic homogeneity (Fig. 11). To this end, it was of particular importance the presence of 40% of glycerol in all the buffers used during the whole purification procedure to confer solubility and stability to the recombinant proteins.

Recombinant AtPAO2 and AtPAO4 displayed the characteristic UV-visible spectrum of the oxidized flavoproteins with three absorbance peaks at 280, 380, and 460 nm (data not shown) and had an apparent molecular mass of about 54 kDa, which well corresponds to the molecular mass expected from amino acid sequence analysis.

Precipitation of purified AtPAO2 and AtPAO4 with trichloroacetic acid resulted in the release of the FAD into the supernatant, suggesting a noncovalent linkage to both proteins. This is in agreement with the presence in AtPAO2 of a Ser residue at position 405, a position which in monoamine oxidase A (MAO-A) and MAO-B is involved in covalent binding to the isoalloxazine ring of the FAD through a Cys residue (Edmondson *et al*., 2004) (Fig. 9). Indeed, while Cys, His and Tyr residues have been shown to be involved in covalent binding to the flavin ring in some flavoenzymes (Edmonson and Newton-Vinson, 2001), until now such a covalent linkage has not been observed for Ser residues.

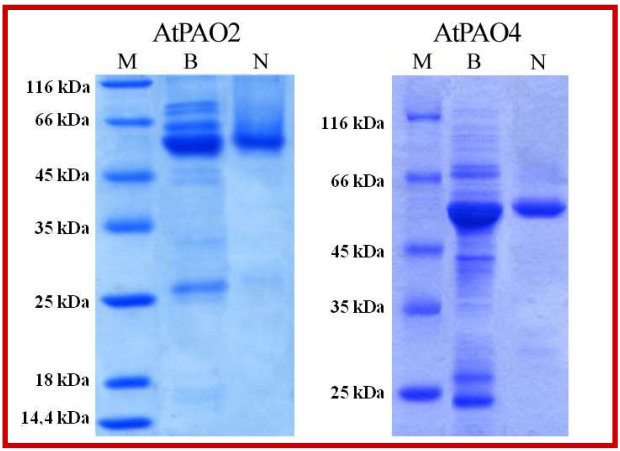

Fig. 11. **Analysis of purified recombinant AtPAO2 and AtPAO4.** Recombinant AtPAO2 and AtPAO4, purified from *E. coli* using a Ni^{2+}- charged resin, were analyzed by SDS-PAGE and stained by Coomassie Brilliant Blue. B: crude bacterial extract; N: pooled elution fractions from the Ni^{2+}-charged resin; M: molecular weight marker.

The noncovalent binding of the FAD molecule also in recombinant AtPAO4 was somehow unexpected since a Cys residue is present at position 407 (position 405 in AtPAO2) (Fig. 9). This probably reflects the fact that for covalent flavinylation some other amino acid residues play a crucial role to activate the process (Fraaije *et al.*, 2000).

Analysis of the catalytic constants of purified recombinant AtPAO2 and AtPAO4 indicated that these enzymes oxidize both Spm and Spd (Table I), in agreement with data from the analysis of the bacterial lysates. In particular, it was shown that AtPAO2 has similar k_{cat} values for the two substrates (4.2 s^{-1} for Spm and 4.6 s^{-1} for Spd), and that AtPAO4 has a k_{cat} for Spm (4.6 s^{-1}) which is about 50-fold higher than that for Spd (0.1 s^{-1}). K_m values for Spm and Spd of recombinant AtPAO2 and AtPAO4 were also determined. In detail, K_m values for Spm and Spd of AtPAO2 are 270 µM and 409 µM, respectively, whereas K_m values for Spm and Spd of AtPAO4 are 47 µM and 139 µM, respectively. These data suggest that recombinant AtPAO2 and AtPAO4 are less efficient enzymes (k_{cat}/K_m values for Spm being 15.5 s^{-1} mM^{-1} and 97.8 s^{-1} mM^{-1}, respectively) than recombinant ZmPAO (k_{cat}/K_m for Spm being 23.9 x 10^3 s^{-1} mM^{-1}; Polticelli *et al.*, 2005) and similarly efficient to murine SMO (mSMO; k_{cat}/K_m = 50.0 s^{-1} mM^{-1}; Cervelli *et al.*, 2003) and AtPAO1 (k_{cat}/K_m for Spm being 24.5 s^{-1} mM^{-1}; Tavladoraki *et al.*, 2006) in catalyzing Spm oxidation.

Since a peroxisomal localization has been recently demonstrated for AtPAO2 and AtPAO4 and considering that the until now characterized

	AtPAO1		AtPAO2		AtPAO4	
	k_{cat} (s^{-1})	K_m (µM)	k_{cat} (s^{-1})	K_m (µM)	k_{cat} (s^{-1})	K_m (µM)
Spm	2.7 ± 0.3 [a]	110 ± 20	4.2 ± 1.2	270 ± 30	4.6 ± 1.0	47 ± 5
Spd	-	-	4.6 ± 1.5	409 ± 40	0.10 ± 0.03	139 ± 18
N^1-acetyl-Spm	0.20 ± 0.04 [a]	470 ± 20	0.8 ± 0.2	233 ± 20	0.02 ± 0.01	ND
Nor-Spm	6.9 ± 1.3 [a]	90 ± 10	2.9 ± 0.8	ND	0.5 ± 0.1	ND
Thermo-Spm	5.7 ± 1.1	20.0 ± 3.0	0.4 ± 0.1	ND	0.10 ± 0.04	ND

Table I. Kinetic constants of substrate oxidation by recombinant AtPAOs. Data are mean ± SEM of at least three indipendent experiments**.** ND: not determined**.** [a] Data taken from Tavladoraki *et al.*, 2006. Enzymatic activity was determined in 100 mM Tris-HCl, at pH 7.5 for recombinant AtPAO2 and AtPAO4 and in 100 mM Tris-HCl, at pH 8.0 for AtPAO1.

mammalian PAOs with a peroxisomal localization prevalently oxidize N^1-acetyl derivatives of polyamines (Wang *et al*., 2003), the activity of recombinant AtPAO2 and AtPAO4 was also determined using N^1-acetyl-Spm as a substrate. It was shown that recombinant AtPAO2 and AtPAO4 oxidize N^1-acetyl-Spm (Table I) with k_{cat} values of 0.8 s^{-1} and 0.02 s^{-1}, respectively, which are much lower than that for Spm, suggesting that acetylated polyamines are not the physiological substrates of these enzymes.

In a recent work, it has been demonstrated that the stress-related uncommon polyamine Nor-Spm is a better substrate than Spm for recombinant AtPAO1 (Tavladoraki *et al*., 2006), suggesting that this polyamine may be its physiological substrate. For this reason, in the present study it was also determined the catalytic activity of recombinant AtPAO2 and AtPAO4 toward Nor-Spm and shown to be about 2-10 fold lower than that for Spm (Table I). In parallel, the catalytic properties of recombinant AtPAO2 and AtPAO4, as well as of recombinant AtPAO1, were determined toward another uncommon polyamine, Thermo-Spm, since an enzyme able to synthesize this polyamine has been recently identified in *A. thaliana* (Knott *et al*., 2007). Data obtained show that AtPAO1 has a higher k_{cat} value and a lower K_m value for Thermo-Spm than for Spm (Table I). On the contrary, AtPAO2 and AtPAO4 have lower k_{cat} values for Thermo-Spm than for Spm (Table I). Interestingly, recombinant mSMO was not active with Nor-Spm (Tavladoraki *et al*., 2006) and Thermo-Spm (present study), whereas recombinant ZmPAO has k_{cat} values for Nor-Spm and Thermo-Spm of 5.5 s^{-1} (Tavladoraki *et al*., 2006) and 1.0 s^{-1}, values which are much lower than that for Spm (k_{cat} = 32.9 s^{-1}; Polticelli *et al*., 2005)

The pH dependence of purified recombinant AtPAO2 and AtPAO4 catalytic activity was also examined using Spm and Spd as a substrate (data not shown). The results obtained show for both enzymes and for both substrates an increase in the catalytic activity with the increase of the pH reaching a maximum between pH 7.0 and pH 8.0. In detail, the optimum pH for AtPAO2 catalytic activity towards both Spd and Spm is 7.5, while that for AtPAO4 activity toward Spd is 8.0 and toward Spm is 7.0. At higher pH, the catalytic activity of recombinant enzymes diminishes.

2.1.4 Characterization of AtPAO2 and AtPAO4 reaction products

To determine the mode of substrate oxidation of recombinant AtPAO2 and AtPAO4, an analysis of the reaction products was performed. In particular, it was examined whether recombinant AtPAO2 and AtPAO4 oxidize Spm and Spd in a similar mode to that of ZmPAO, producing Dap among the other reaction products, or similar to that of AtPAO1 and animal PAOs, producing Spd from Spm and Put from Spd.

Analysis by HPLC of AtPAO2 polyamine reaction products using Spd as a substrate showed the production of an increasing amount of a compound with

the retention time of Put in parallel with a decrease in the amount of Spd (Fig.11A). Similarly, analysis of the reaction products using Spm as a substrate showed the formation of an increasing amount of a compound with the retention time of Spd and of a compound with the retention time of Put in parallel with a decrease in the amount of Spm (Fig.11B). In both cases, the formation of a product with the retention time of Dap was not observed (Fig. 11A and B). Similar results were obtained with recombinant AtPAO4 (data not shown).

These data demonstrate that AtPAO2 and AtPAO4 have a mode of substrate oxidation similar to that of animal PAOs and SMOs and are involved, together with AtPAO1, in a polyamine back-conversion pathway.

2.1.5 Determination of the polyamine back-conversion pathway *in vivo* in *A. thaliana*

To demonstrate the existence of a polyamine back-conversion pathway also *in vivo*, protoplasts isolated from Arabidopsis leaves were incubated with Spm or Spd radiolabelled at internal carbon atoms (Fig. 12). In the case of a polyamine back-conversion pathway, the radiolabelled Spm should be converted to radiolabelled Spd and the radiolabelled Spd to radiolabelled Put (Fig. 12). The Dap eventually produced by a terminal catabolic pathway of the polyamines is not radioactive (Fig. 12), while the radiolabelled aminoaldehydes produced can be easily distinguished from Spd and Spm during analysis of the polyamines by thin layer chromatography.

During incubation of *A. thaliana* protoplasts with radiolabelled Spd, the production of an increasing amount of radiolabelled Put was observed (Fig. 13). This production resulted diminished in the presence of guazatine, a specific PAO inhibitor. Similarly, during incubation of *A. thaliana* protoplasts with radiolabelled Spm, the production of an increasing amount of radiolabelled Spd and Put was observed (Fig. 13). These results confirm the existence of a polyamine back-conversion pathway *in vivo* in *A. thaliana.*

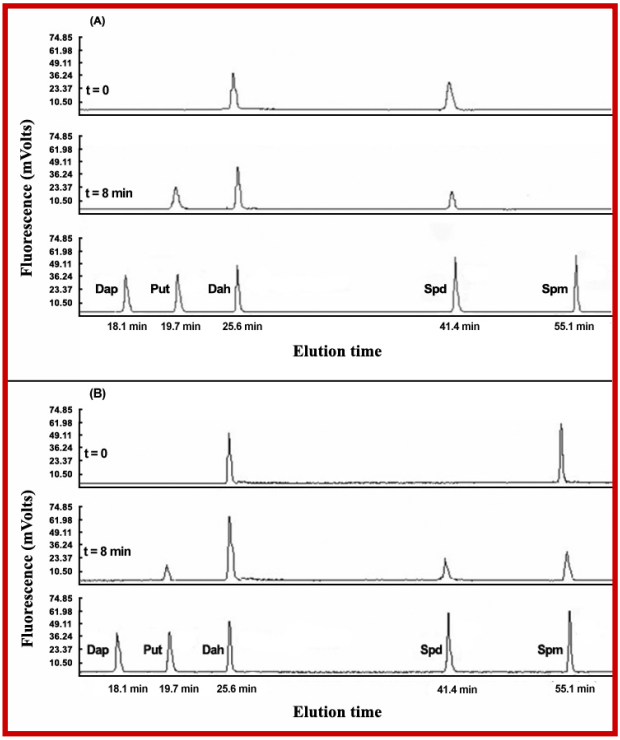

***Fig. 11*. HPLC analysis of the reaction products generated when Spm or Spd are oxidized by recombinant AtPAO2.** (A) Chromatograms show the analysis of the reaction products at t = 0 and t = 8 min, respectively, using 1 nM of purified recombinant AtPAO2 and 0.2 mM Spd as amine substrate. (B) Chromatograms show the analysis of the reaction products at t = 0 and t = 8 min, respectively, using 1 nM of purified recombinant AtPAO2 and 0.2 mM Spm as amine substrate. Aliquots of the reaction mixtures were analyzed for polyamine content after addition of an equal volume of 5% (w/v) perchloric acid containing 0.15 mM Diaminohexane (Dah; retention time = 25.6 min) as an internal standard. Data are from a single representative experiment, which was repeated twice. The retention times of the various polyamines are: Dap, 18.1 min; Put, 19.7 min; Spd, 41.4 min; Spm, 55.1 min.

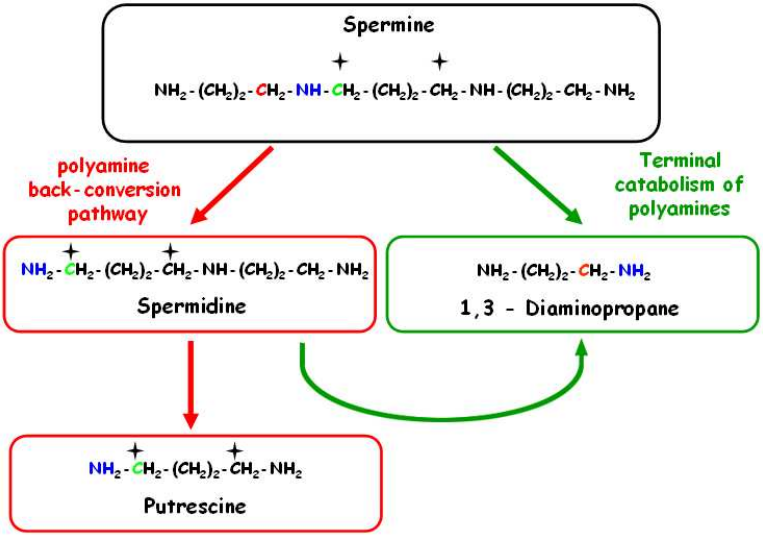

***Fig. 12*. Schematic representation of radiolabelled Spm and Spd oxidation through a polyamine back-conversion pathway and a terminal catabolic pathway.** In the figure, Spm, Spd and Put radiolabelled at internal carbon atoms (✦) are shown. In a polyamine back-conversion pathway, radiolabelled polyamines are produced, whereas in a terminal catabolic pathway not radioactive Dap is produced.

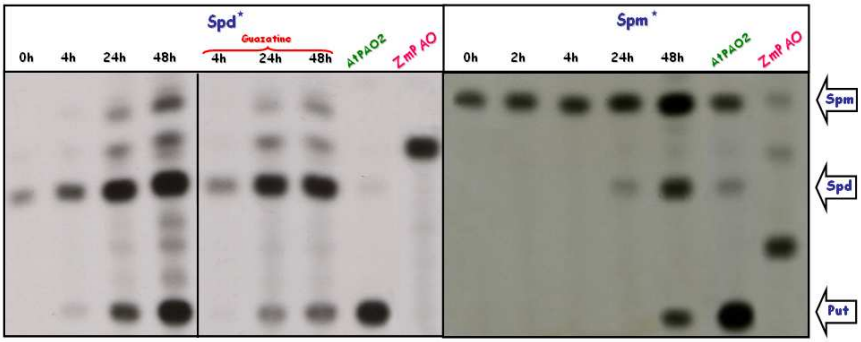

***Fig. 13*. Polyamine back-conversion *in vivo* in *A. thaliana*.** Thin layer chromatography followed by autoradiography was used to determine the polyamine content in protoplasts from *A. thaliana* leaves incubated with radiolabelled Spd or Spm. Aliquots of protoplasts were also pre-incubated with the PAO-specific inhibitor guazatine before addition of the radiolabelled polyamines. As a control, recombinant AtPAO2 and ZmPAO were incubated with radiolabelled Spd or Spm.

2.2 Histone demethylases of *A. thaliana*

2.2.1 Description of the lysine-specific histone demethylase gene family in *A. thaliana*

A search of the *A. thaliana* genome database using the amino acid sequence of ZmPAO revealed not only the presence of five cDNAs encoding for putative PAOs (Tavladoraki *et al*., 2006), but also that of four additional genes (*At1g62830*, *At3g13682*, *At3g10390*, *At4g16310*) encoding for proteins bearing both a flavin amine oxidase domain and a SWIRM domain (He *et al.*, 2003; Shi *et al*., 2004; Krichevsky *et al*., 2007), the latter domain being involved in chromatin-modifying complexes (Fig. 14). These proteins display 26-30% sequence homology with HsLSD1, which also possesses both a flavin amine oxidase domain and a SWIRM domain and which specifically acts on histone H3K4me1 and H3K4me2 in a FAD-dependent oxidative reaction. It was hypothesized that these four *A. thaliana* cDNAs also encode for lysine-specific histone demethylases, and they were termed *AtLSD1*, *AtLSD2*, *AtLSD3* and *AtLSD4*, respectively. Interestingly, despite the high sequence homology with HsLSD1, the amino acid sequence homology of the four AtLSDs with the two yeast demethylases (SWIRM1 and SWIRM2) (Nicolas *et al*., 2006), for which, however, histone demethylase activity has not yet been demonstrated, is very low (11–18%). AtLSD1, AtLSD2 and AtLSD3 display a fairly high overall sequence homology with each other (48–52%) and with AtLSD4 (25%–30%), which extends to both the amine oxidase and the SWIRM domains (Fig. 14).

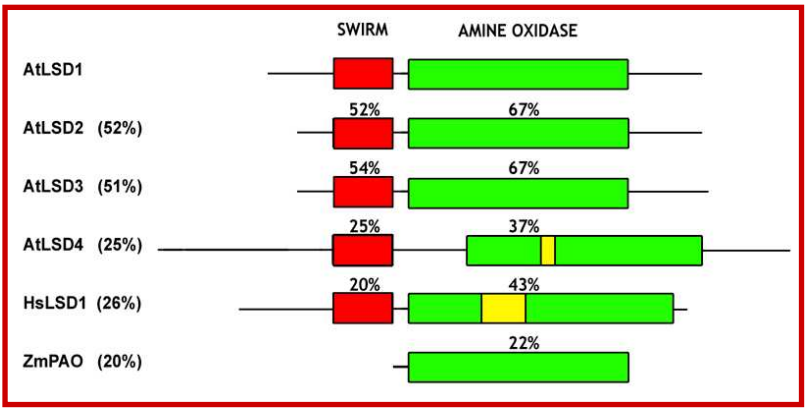

***Fig. 14*. AtLSDs, HsLSD1, and ZmPAO sequence comparison.** Schematic representation of the various domains of AtLSD1, AtLSD2, AtLSD3, AtLSD4 and ZmPAO. Red boxes indicate the SWIRM domains, green boxes indicate the amine oxidase domains and yellow boxes the Tower domain. Numbers indicate the percentage of amino acid sequence homology, as a whole or by domain, of the various proteins with respect to AtLSD1.

To determine the possible subcellular localization of the four putative Arabidopsis histone demethylases, the amino acid sequences were analyzed using PSORT (www.psort.ims.u-tokyo.ac.jp). This analysis predicted the presence of a nuclear localization signal at positions 517–534 of the AtLSD1 amino acid sequence, suggesting sorting to the nucleus similarly to HsLSD1 (Bradley *et al*., 2007). This has been recently confirmed by transient expression studies of AtLSD1 tagged with green fluorescent protein (Krichevsky *et al*., 2007). Nuclear localization was predicted also for AtLSD2 and AtLSD4, while mitochondrial/chloroplastic localization was predicted for AtLSD3. Furthermore, analysis of the amino acid sequence of the four AtLSDs for the presence of specific sequence motifs did not evidence the presence of HMG DNA-binding domains, as has been shown for the two yeast demethylases (Nicolas *et al*., 2006).

2.2.2 Expression pattern of the *AtLSD* gene family in different Arabidopsis organs

The expression pattern of the *AtLSD* gene family in different Arabidopsis organs (rosette and cauline leaves, stem, flowers, roots, and siliques) was analyzed by semiquantitative RT-PCR using gene-specific primers (*AtLSD1for/AtLSD1rev; AtLSD2for/AtLSD2rev; AtLSD3for/AtLSD3rev*; *AtLSD4for/AtLSD4rev*) (Fig. 15). This analysis showed that the *AtLSD1* transcript is present at similar levels in all tested organs, even though expression levels were expected to be higher in the flowers than in the other tissues considering the proposed role of chromatin remodeling enzymes in flowering control (He and Amasino, 2005). Similar results were obtained also for *AtLSD2*, *AtLSD3*, and *AtLSD4* transcripts (Fig. 15).

These data are in agreement with microarray data obtained from the *A. thaliana* database (Genevestigator expression analysis), which, however, demonstrate the differential expression pattern in specific parts or at specific developmental stages of the various organs, as, for example, in the shoot apex during transition from the vegetative to the inflorescence state.

2.2.3 Heterologous expression and biochemical characterization of AtLSD1 in *E. coli*

To verify whether the *AtLSD* gene family encodes for proteins with a lysine-specific histone demethylase activity, heterologous expression of AtLSD1, chosen as representative member of the family, in *E. coli* was attempted using the pET 17b vector. In particular, the coding region of *AtLSD1* was amplified by RT-PCR using the U21563 clone (Arabidopsis Biological Resource Center) as a template and sequence-specific primers (*AtLSD1-His for/AtLSD1-His rev*).

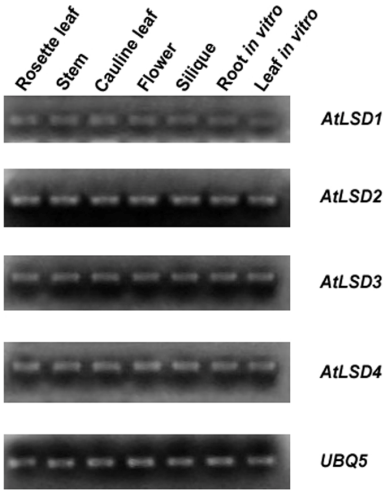

***Fig. 15*. Expression pattern of *AtLSD1*, *AtLSD2*, *AtLSD3*, and *AtLSD4* in various Arabidopsis organs.** The expression of the four *AtLSD* genes in various Arabidopsis organs (rosette and cauline leaves, stems, flowers, roots, and siliques) was analyzed by semiquantitative RT-PCR using gene-specific primers. *UBQ5* expression was used to confirm an equal amount of RNA among the various samples. Results at the exponential phase (at 28 cycles for *AtLSD1*, *AtLSD2*, and *AtLSD3*, at 30 cycles for *AtLSD4*, and at 25 cycles for *UBQ5*) are shown.

Furthermore, to facilitate purification of the recombinant protein, a sequence encoding for a 6-His tag was added at the 3′ terminus of the *AtLSD1* cDNA in the AtLSD1-pET 17b plasmid. Western blot analysis using an anti-6-His tag antibody of bacteria transformed with AtLSD1-pET 17b plasmid and treated with isopropyl β-D-thiogalactoside (IPTG) to induce expression of recombinant protein confirmed recombinant AtLSD1 accumulation in the soluble bacterial extracts (data not shown).

To purify the recombinant AtLSD1, affinity chromatography using a Ni^{2+}-charged resin was performed, which, however, was not sufficient to purify the recombinant protein to electrophoretic homogeneity (Fig. 16). Thus, the pooled elution fractions from the Ni^{2+}- charged resin were further chromatographed on a HiTrap heparin HP column from which the protein was recovered at a homogeneity greater than 95% (Fig. 16). The purified protein displayed the characteristic UV–visible spectrum of the oxidized flavoproteins with three absorbance peaks at 280, 380, and 460 nm (data not shown) and an apparent

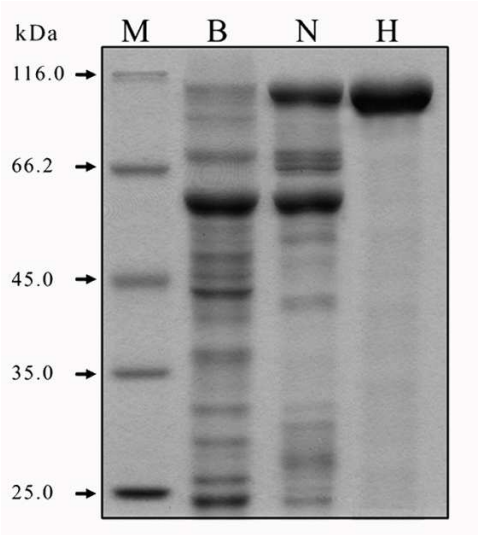

***Fig. 16*. Analysis of purified recombinant AtLSD1.** Analysis of representative protein samples from each stage of the purification protocol by SDS-PAGE (10% polyacrylamide). B: crude bacterial extract; N: pooled elution fractions from the Ni^{2+}-charged resin; H: pooled elution fractions from the HiTrap heparin HP column; M: molecular weight marker.

molecular mass of 94 kDa (Fig. 16), the molecular mass expected for the recombinant protein from amino acid sequence analysis.

Precipitation of purified AtLSD1 with trichloroacetic acid resulted in the release of the cofactor into the supernatant, indicating noncovalent binding to the protein.

Purified recombinant AtLSD1 was tested for its ability to oxidize various methylated H3 peptides and various polyamines using a peroxidase-coupled assay to quantify H_2O_2 levels (Forneris *et al*., 2005a; Forneris *et al*., 2005b; Holt and Baker, 1995). The results evidenced that, similarly to HsLSD1, the recombinant enzyme is able to demethylate H3K4me2 and H3K4me1 peptides, the specific activity with the H3K4me2 peptide being higher than that with the H3K4me1 peptide (Table II). Furthermore, the results also showed that, similarly to HsLSD1 (Shi *et al*., 2004), AtLSD1 is not able to oxidize either the H3K9me2 and H3K27me2 peptides or the common polyamines Spm, Spd and Put.

The ability of recombinant AtLSD1 to demethylate the H3K4me2 peptide was also analyzed by a Western blot based assay using an anti-H3K4me2 methylation-specific antibody to detect the dimethylation status of the peptide (Shi *et al.*, 2004). This analysis confirmed that the recombinant protein efficiently reduces the dimethylation level of the H3K4me2 peptide (Fig. 17).

	PEPTIDE	k_{cat} [a] (s^{-1})	K_m [a] (μM)
AtLSD1	H3K4me1	0.5 ± 0.06	8.9 ± 0.8
	H3K4me2	0.68 ± 0.08	10.7 ± 0.6
	H3K4me2 in 10% glycerol[b]	0.34 ± 0.08	12.8 ± 1.0
	H3K4me1-S10pho	no activity	no activity
HsLSD1-CoREST	H3K4me1	6.5 ± 0.60	6.1 ± 0.6

Table II. Kinetic Constants for the Demethylation of H3 Peptides by Recombinant AtLSD1 and HsLSD1 in complex with CoREST. [a] Enzymatic activity of recombinant AtLSD1 and recombinant HsLSD1 in complex with CoREST (HsLSD1-CoREST) was determined in 50 mM Tris-HCl, 30% glycerol, at pH 8.0, using a constant O_2 concentration at the air-saturated level and a peptide concentration either saturating (147 μM for apparent k_{cat} determination) or varying between 2 and 147 μM (for apparent K_m determination). Data are the mean ± SEM of at least three independent experiments. [b] The assay was performed in 50 mM Tris-HCl, 10% glycerol, at pH 8.0. Similar results were obtained in the absence of glycerol.

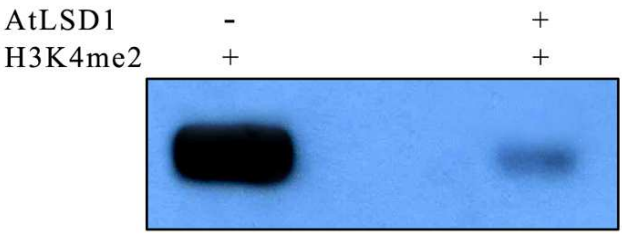

Fig. 17. **Demethylation of H3K4me2 peptide by recombinant AtLSD1.** H3K4me2 peptide was incubated for 2 h with recombinant AtLSD1 and analyzed by Western blot using an anti-H3K4me2 methylation-specific antibody.

The activity of the recombinant enzyme with the H3K4me2 and H3K4me1 peptides was shown to be higher at pH 8.0 than at pH 6.0 or at pH 9.0 (data not shown) and to increase at higher glycerol concentrations (50% increase in the

presence of 30% glycerol as compared to that in the presence of 0–10% glycerol) (Table II). Interestingly, k_{cat} values of AtLSD1 were shown to be about 10-fold lower than that of HsLSD1 in free form (Forneris *et al*., 2005a) or in complex with CoREST (present study and Forneris *et al*., 2007) (Table II). Misfolding of the recombinant protein can be excluded on the basis of circular dichroism spectroscopy analysis, which indicated a high secondary structure content, the α-helix/*β*-sheet percentage being 38-44% as calculated using CONTIN (Provencher, 1982), K2D (Andrade *et al*., 1993), or SELCON3 (Sreerama *et al.*, 1999) methods.

2.2.4 Characterization of the reaction products of AtLSD1 by mass spectrometry analysis

Demethylase activity of AtLSD1 was further confirmed by mass spectrometry analysis of its reaction products. Demethylation of the H3K4me1 and H3K4me2 peptides by AtLSD1 is expected to regenerate the unmodified peptide with the net loss of 14 and 28 Da, respectively, corresponding to the molecular mass of one or two CH_2 group(s). The H3K4me1, H3K4me2, H3K9me2, and H3K27me2 peptides were incubated with purified recombinant AtLSD1 or buffer, and the reaction mixtures were analyzed by mass spectrometry. In the absence of AtLSD1, the H3K4me1 and H3K4me2 peptides display molecular masses of 2268 and 2282, respectively, as expected for these peptides (Fig. 18A). In the presence of AtLSD1 for both peptides a new peak appeared at a molecular mass of 2254, which well corresponds to the molecular mass of the demethylated peptide (Fig. 18A). On the contrary, the peaks corresponding to the H3K9me2 and H3K27me2 peptides were found to be unaffected by incubation with recombinant AtLSD1 (Fig. 18B and C).

2.2.5 Analysis of the ability of AtLSD1 to interpret the histone code

The demethylase activity of AtLSD1 toward the H3K4me1 synthetic peptide was also tested in the presence of a second modification and in particular of phosphorylated H3S10 residue. As shown by the lack of any detectable activity of recombinant AtLSD1 toward the monomethylated Lys4 and phosphorylated Ser10 H3 peptide (H3K4me1-S10pho) (Table II), phosphorylation of the H3S10 residue totally abolished the AtLSD1 demethylase activity toward the H3K4me1 peptide. This result suggests that, similarly to the human demethylase (Forneris *et al*., 2005a), AtLSD1 is actually capable of “reading” the histone code, in that it discriminates between peptides bearing different covalent modifications on their side chains to the point that a single mark makes the difference between a reactive and a nonreactive peptide.

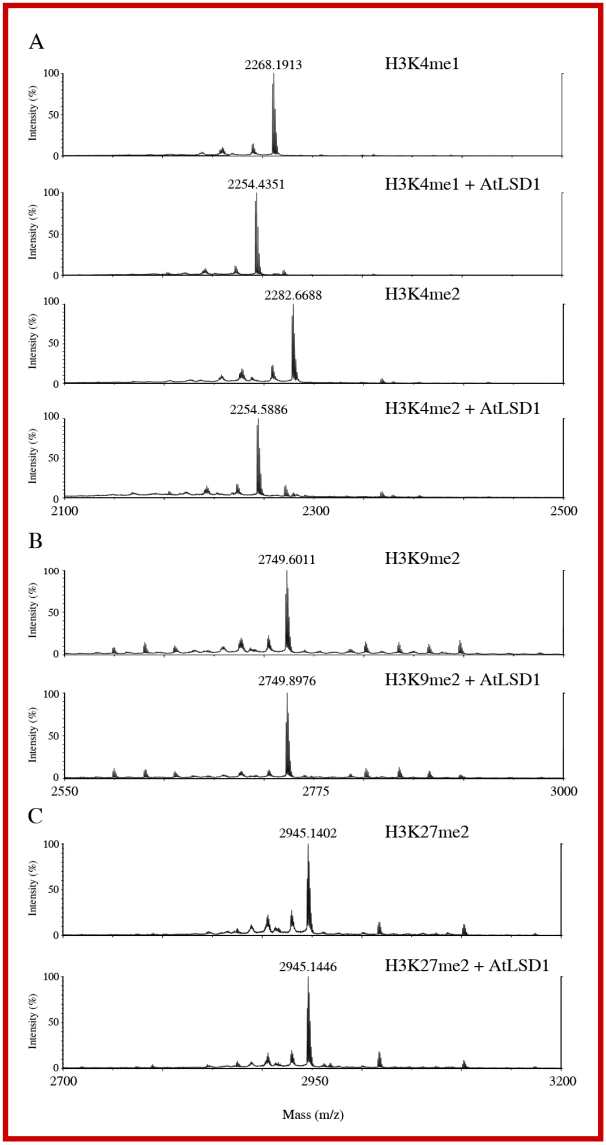

Fig. 18. **Mass spectrometry analysis of methylated H3 peptides after incubation with recombinant AtLSD1.** H3K4me1 and H3K4me2 (A), H3K9me2 (B), and H3K27me2 (C) peptides were incubated for 4 h with buffer or purified recombinant AtLSD1, and reaction mixtures were analysed by mass spectrometry. In collaboration with Prof. M. Eugenia Schininà, University of Rome "La Sapienza".

2.2.6 Comparative analysis of the three-dimensional structure of AtLSD1

It was also obtained the model of the AtLSD1 three-dimensional structure using the HsLSD1 crystal structure as a template (Yang *et al.*, 2006). As predicted on the basis of the amino acid sequence alignment, the most striking difference between the two proteins is the almost complete absence of the Tower domain in AtLSD1 (Fig. 19). On the other hand, a comparative analysis of the active site structures of AtLSD1 and HsLSD1 revealed a high degree of conservation of the residues building up the site, major substitutions in AtLSD1 being only Ser for Met332, Tyr for Trp695, and Tyr for Phe538 (Fig. 20). However, none of these residues are involved in direct contacts with the substrate-like pLys4Met peptide inhibitor in HsLSD1 (Forneris *et al.*, 2007). In addition, modeling of the complex formed between AtLSD1 and this substrate-like peptide inhibitor, made by superimposition of the three-dimensional model of AtLSD1 with the three-dimensional structure of the complex formed by HsLSD1 with the peptide inhibitor, highlighted the strict conservation of the complex network of interactions observed between the peptide inhibitor and HsLSD1 (Fig. 20). In particular, the acidic patch formed by Asp375, Glu379, and the carbonyl group of Cys360, which in HsLSD1 interacts with the peptide pArg8 residue, is strictly conserved in AtLSD1 (residues Asp367, Glu371, and Cys352). Strict conservation is also observed for residues Asp553 and Asp556 of HsLSD1 which bind the peptide pArg2 residue (Asp446 and Asp449 of AtLSD1). In addition, several hydrogen bonds which stabilize the HsLSD1 complex with the substrate-like peptide inhibitor are also conserved in the modeled AtLSD1 complex: (1) the hydrogen bond between Asn383 (Asn375 in AtLSD1) and the backbone nitrogen atoms of pThr11 and pGly12; (2) the hydrogen bond between His564 (His457 in AtLSD1) and the Oγ atom of pThr6; (3) the hydrogen bonds between the backbone nitrogen of pAla1 and Asn540 side chain carbonyl group and Ala539 backbone carbonyl group (Asn433 and Ala432 in AtLSD1). Finally, it is also conserved in the HsLSD1 Tyr761 residue (Tyr650 in AtLSD1) which interacts with the pMet4 residue of the substrate-like inhibitor, the latter residue mimicking the dimethylated Lys4 of the histone H3 tail (Fig. 20) (Forneris *et al.*, 2007).

Analysis of the surface electrostatic potential of AtLSD1 as compared to that of HsLSD1 evidenced a higher negative character of both the active site region and the SWIRM domain (Fig. 19). This feature, together with the absence of the HsLSD1 Tower domain, is probably related to the interaction of AtLSD1 with different molecular partners. As a matter of fact, a BLAST search using human CoREST as a bait did not retrieve any protein in the *A. thaliana* genome displaying significant similarity with CoREST.

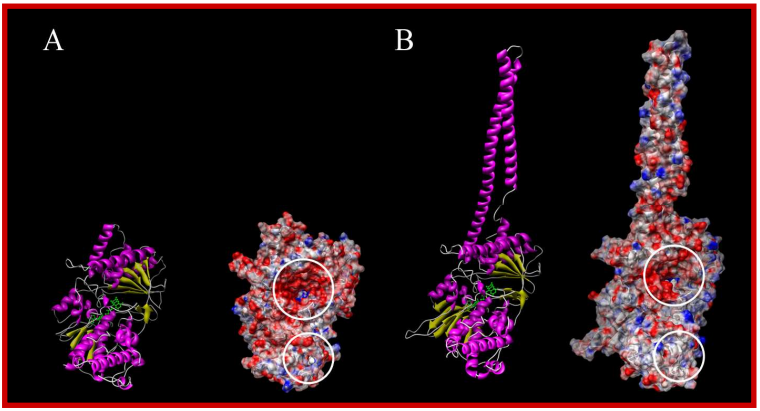

Fig. 19. **Schematic representation of the modeled three-dimensional structure of AtLSD1 (A) and of the crystal structure of HsLSD1 (Yang *et al.*, 2007) (B).** The FAD cofactor is shown in green to identify the active site region. Surface electrostatic potential contoured at +10 kT/e and –10 kT/e is shown in blue and red respectively. White circles highlight differences in the surface electrostatic potential between the two proteins. In collaboration with Dr. Fabio Polticelli, University "RomaTre".

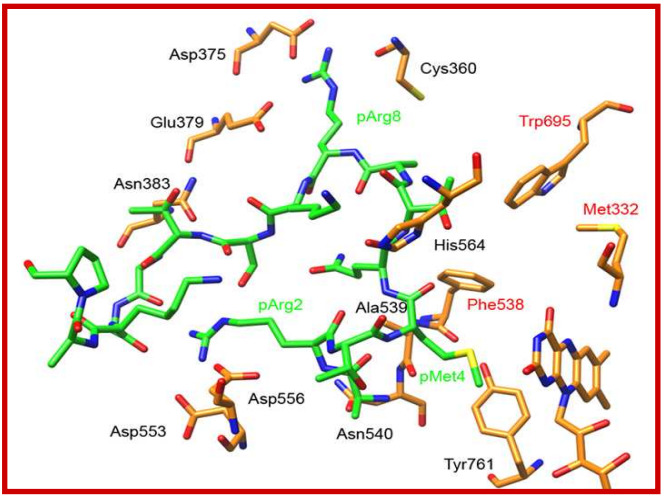

Fig. 20. **Schematic view of the complex formed by HsLSD1 with the substrate-like pLys4Met peptide inhibitor.** HsLSD1 and peptide inhibitor residues contributing to the complex formation are labeled in black and green, respectively. For reasons of clarity, carbon atoms of HsLSD1 are colored in orange and those of the peptide inhibitor in green. Active site HsLSD1 residues nonconserved in AtLSD1 (substitutions being Met332Ser, Phe538Tyr, and Trp695Tyr) are labeled in red. Note that none of the nonconserved residues interacts with the peptide inhibitor in the HsLSD1 complex. In collaboration with Dr. Fabio Polticelli, University "RomaTre".

2.2.7 Characterization of T-DNA insertional mutants for *AtLSD1, AtLSD2, AtLSD3* and *AtLSD4*

To study the physiological roles of AtLSDs, Arabidopsis insertional mutants for *AtLSD1*, *AtLSD2*, *AtLSD3* and *AtLSD4* genes were obtained from the collections of Arabidopsis seeds SALK (Salk Institute Genome Analysis Laboratory collection) and SAIL (Syngenta Arabidopsis Insertion Library). In detail, *Atlsd1* allele (SALK_142477.31.30.x) contains a T-DNA insertion in the gene coding sequence (about 1625 bp downstream of the translational start codon), *Atlsd2* allele (SALK_135831.43.30.x) contains a T-DNA insertion in the second exon (about 1931 bp downstream of the translational start codon), *Atlsd3* allele (SALK_015053.35.80.x) contains a T-DNA insertion in the first exon (about 783 bp downstream of the translational start codon) and *Atlsd4* allele (SAIL_640_B10) contains a T-DNA insertion in the first exon (about 325 bp downstream of the translational start codon) (Fig. 21).

To confirm the presence of the T-DNA insertion and to identify the homozygous mutant plants for the T-DNA insertion, PCR analyses using total DNA extracted from *Atlsd1*, *Atlsd2*, *Atlsd3* and *Atlsd4* seedlings were performed. In detail, to confirm the presence of the T-DNA insertion, a PCR analysis was performed using a T-DNA left border-specific primer and a gene-specific primer (*LBb1/AtLSD1-RP; Lba1/AtLSD2-RP; LBb1/ AtLSD3for*; *Lb3sail*/*AtLSD4-RP*). To select the homozygous mutant plants for the T-DNA insertion, a PCR analysis was performed using two gene-specific primers designed outside of the 5' and 3' ends of the T-DNA insertion (*AtLSD1-LP/AtLSD1-RP*, *AtLSD2-LP/AtLSD2-RP*, *AtLSD3for/AtLSD3-LP*, *AtLSD4-LP/AtLSD4-RP*). Indeed, a T-DNA insertion between these primer sites suppresses PCR amplification due to its elevated length and thus in the presence of a T-DNA insertion the fragment indicative of each WT allele is absent (Fig. 21; Fig. 22). This PCR analysis revealed the presence of homozygous *Atlsd1*, *Atlsd2* and *Atlsd3* plants, whereas no homozygous *Atlsd4* plants were found despite the fact that a large number of mutants were analyzed. It is possible that homozygous *Atlsd4* plants are not viable.

RT-PCR analysis of total RNA from *Atlsd1*, *Atlsd2* and *Atlsd3* seedlings homozygous for the T-DNA insertion, using gene-specific primers (*AtLSD1-LP/AtLSD1-RP*, *AtLSD2for/AtLSD2rev*, *AtLSD3for/AtLSD3-LP*), confirmed the absence of the full-length gene transcripts (Fig. 23).

To elucidate the biological roles of AtLSDs, the phenotype of homozygous mutant plants was analyzed in detail under physiological growth conditions. In particular, germination percentage, stem length, leaf morphology, root length, inflorescence characteristics and flowering time were analyzed. Flowering time was measured by the developmental criterion of the number of leaves formed, prior to flowering. Homozygous *Atlsd1* and *Atlsd2* plants did not show phenotypical changes. On the contrary, for homozygous *Atlsd3* plants a delayed

flowering phenotype was observed (Table III), thus confirming data reported in other studies (Krichevsky *et al.*, 2007; Jiang *et al.*, 2007).

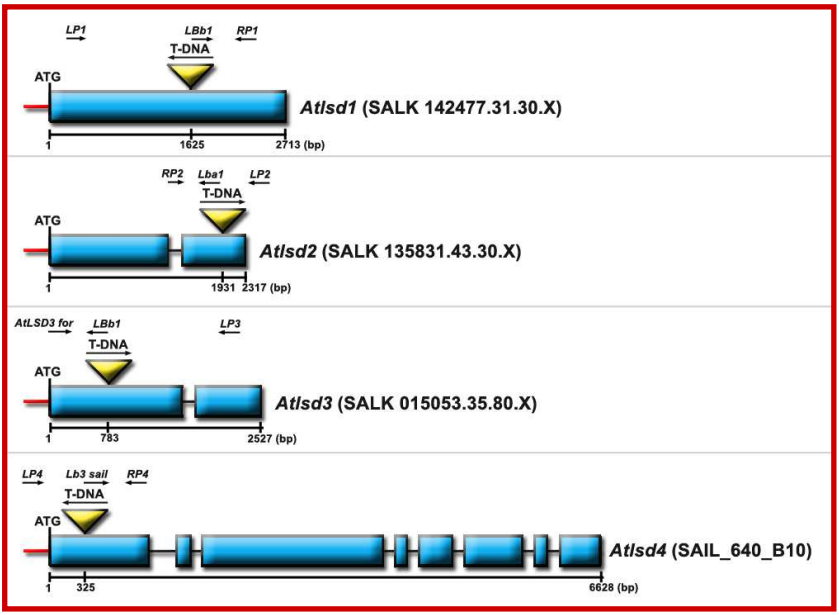

***Fig. 21*. Schematic rappresentation of the T-DNA insertion site in the *Atlsd1, Atlsd2, Atlsd3* and *Atlsd4* mutants.** Yellow triangles indicate the T-DNA insertion. Exons of *AtLSD1*, *AtLSD2*, *AtLSD3* and *AtLSD4* genes are represented as blue boxes, whereas introns are represented as black lines. Red lines represent the 5' nontranslated regions. *RP1 = AtLSD1-RP* primer*; LP1 = AtLSD1-LP* primer*; RP2 = AtLSD2-RP* primer*; LP2 = AtLSD2-LP* primer*; AtLSD3for = AtLSD3for* primer*: RP3 = AtLSD3-RP* primer; *RP4 = AtLSD4-RP* primer; *LP4 = AtLSD4-LP* primer. *Lba1* and *LBb1* are T-DNA left border-specific primers for SALK T-DNA insertion lines, whereas *Lb3 sail* is a T-DNA left border-specific primer for SAIL T-DNA insertion lines.

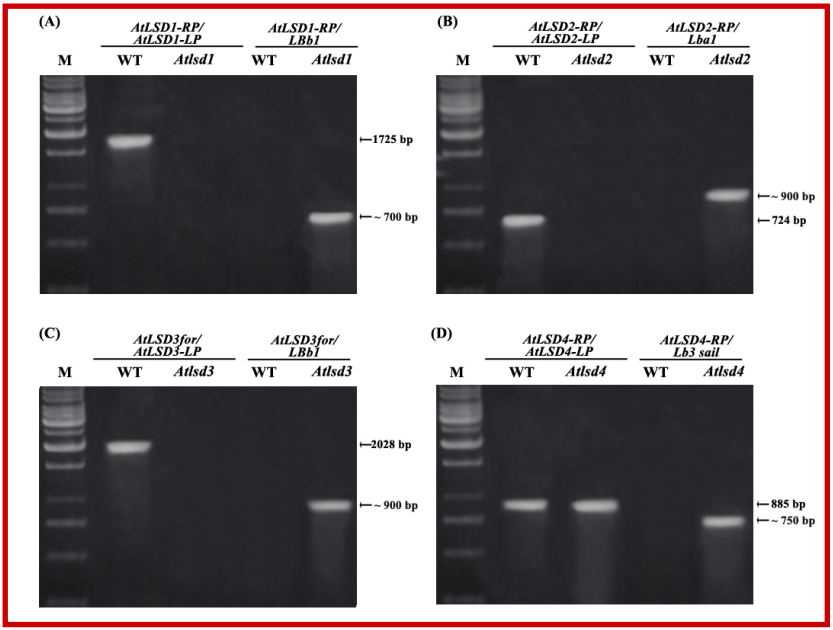

***Fig. 22*. Genotyping of *Atlsd1, Atlsd2, Atlsd3* and *Atlsd4* mutants.** The genotypes of *Atlsd1*, *Atlsd2*, *Atlsd3* and *Atlsd4* mutants were determined by two sets of PCR reactions. The presence of T-DNA insertion was determined using a T-DNA left border-specific primer and a gene-specific primer (*LBb1/AtLSD1-RP; Lba1/AtLSD2-RP; LBb1/ AtLSD3for*; *Lb3sail*/*AtLSD4-RP*). The absence of the fragment indicative of each WT allele was determined using two gene-specific primers designed outside of the 5' and 3' ends of each T-DNA insertion (*AtLSD1-LP/AtLSD1-RP*, *AtLSD2-LP/AtLSD2-RP*, *AtLSD3for/AtLSD3-LP*, *AtLSD4-LP/AtLSD4-RP*). Total DNA from wild-type plants (WT) was used as control. M: DNA Marker.

	Wild-type	*Atlsd1*	*Atlsd2*	*Atlsd3*
Leaf number	15.1 ± 1.8	16.4 ± 2.0	17.2 ± 2.5	70.1 ± 10.5

Table III. Total leaf number at bolting for wild-type and *Atlsd1, Atlsd2, Atlsd3* mutants. Values shown are means ± SD of total number of rosette and cauline leaves. Fifteen plants were scored for each mutant. The experiment was repeated three times with similar results.

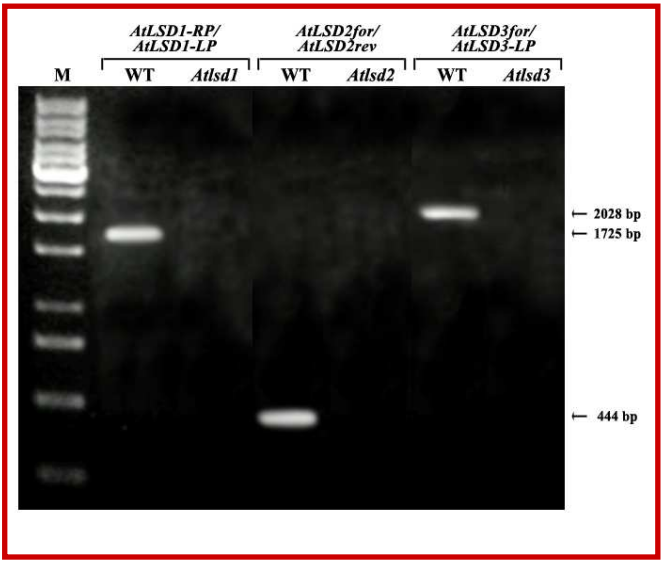

***Fig. 23*. RT-PCR analysis of total RNA from *Atlsd1*, *Atlsd2* and *Atlsd3* seedlings.** The absence of the full-length gene transcripts in homozygous *Atlsd1*, *Atlsd2* and *Atlsd3* plants was determined using gene-specific primers (*AtLSD1-LP*/*AtLSD1-RP*, *AtLSD2for*/*AtLSD2rev*, *AtLSD3for*/*AtLSD3-LP*). Total RNA from wild-type plants (WT) was used as control. The RT reaction was also performed in absence of reverse transcriptase as negative control (data not shown). M: DNA Marker.

2.2.8 Preparation of trangenic Arabidopsis plants transformed with an AtLSD1 prom::GFP-GUS construct and with constructs for AtLSD1 overexpression

To determine in detail the *AtLSD1* expression pattern, an AtLSD1 prom:GFP-GUS construct was prepared using the Gateway technology (Hartley *et al*., 2000). In particular, *AtLSD1* promoter was amplified by PCR from Arabidopsis total DNA using sequence-specific primers (*AtLSD1prom for/AtLSD1prom rev*). These primers were designed in such a way as to allow *AtLSD1* promoter cloning via pDONR 221 donor vector into pKGWFS7 vector (Karimi *et al*., 2002), a plant Gateway destination vector in which an in frame fusion between regions coding for enhanced green-fluorescent protein linked to the endoplasmic reticulum-targeting signal (*EgfpER*) and β-glucuronidase (*gus*) is present downstream of the promoter insertion site (Fig. 24). In this way, AtLSD1 prom-pKGWFS7 plasmid was obtained and characterization of *A. thaliana* plants transformed with this construct is in progress.

Furthermore, to study the AtLSD1 physiological roles, a construct was prepared for AtLSD1 overexpression in *A. thaliana* plants, using also in this

case the Gateway technology (Hartley *et al*., 2000). To obtain the AtLSD1 overexpression costruct, the *AtLSD1* coding region was amplified by PCR using the AtLSD1-pET 17b plasmid as substrate and sequence-specific primers (*overAtLSD1-His for/overAtLSD1-His rev*). These primers were designed in such a way as to allow *AtLSD1* cDNA cloning via pDONR 221 donor vector into pK2GW7 vector (Karimi *et al*., 2002), a plant Gateway destination vector which guides overexpression of proteins in plants under the control of the constitutive 35S cauliflower mosaic virus (CaMV) promoter (Fig. 25). Moreover, to facilitate detection of the protein, a sequence encoding for a 6-His tag was added at the 3′ terminus of cDNA. In this way, AtLSD1 His tag-pK2GW7 plasmid was obtained and characterization of *A. thaliana* plants transformed with this construct is in progress. The phenotype of these plants will be analyzed in detail under physiological conditions and following stress treatment. Microarray analysis and chromatin immunoprecipitation experiments will be also performed using these transgenic plants in parallel with the corresponding insertional mutant plants to determine the genes that are under the control of AtLSD1.

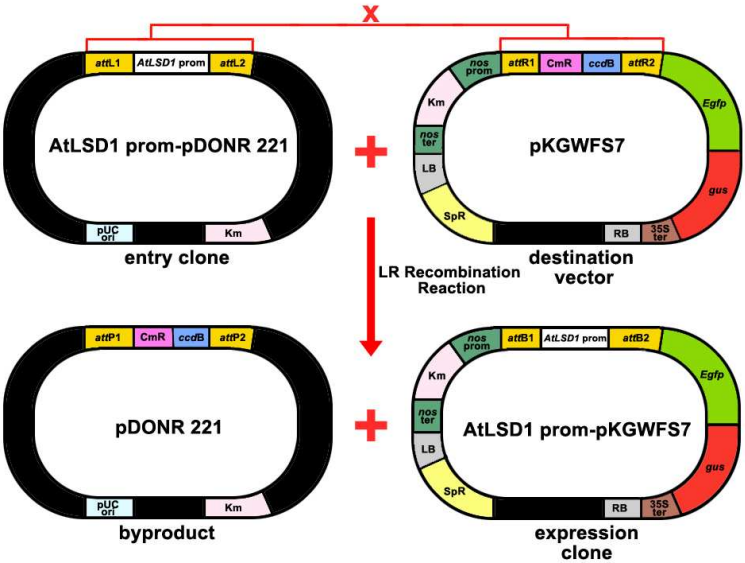

***Fig. 24*. Schematic rappresentation of the Gateway LR reaction performed to obtain the AtLSD1 prom::GFP-GUS construct.** pDONR221: pDONR 221 Gateway donor vector; pKGWFS7: pKGWFS7 plant Gateway destination vector; *att*L1, *att*L2, *att*R1, *att*R2, *att*P1, *att*P2, *att*B1 and *att*B2: site-specific *att*achment sites for recombination proteins; *AtLSD1* prom: *AtLSD1* promoter; pUC ori: pUC origin; Km: kanamycin resistance marker; CmR: chloramphenicol resistance marker; *ccd*B: *ccd*B gene; *Egfp*: *enhanced green-fluorescent protein* cDNA; *gus*: *β-glucuronidase* cDNA; *nos* prom: *nos* promoter; *nos* ter: *nos* terminator; LB and RB: left and right T-DNA borders; SpR: spectinomycin resistance marker; 35S ter: terminator of the cauliflower mosaic virus (CaMV) 35S transcript.

Considering that HsLSD1, the human hortologue of AtLSD1, participates in multiprotein complexes important in the regulation of gene expression (Forneris *et al*., 2008) and with the aim to isolate the complexes in which AtLSD1 is eventually involved another construct (FLAG HA AtLSD1-pK2GW7 plasmid) was prepared for AtLSD1 overexpression in *A. thaliana* plant in fusion with the FLAG and Hemoagglutinine (HA) tags. The two tags will allow isolation of protein complexes through a two-step affinity chromatography. To obtain this construct, the *AtLSD1* coding region was amplified by a three step-PCR using the AtLSD1-pET 17b plasmid as first template and sequence-specific primers (*overAtLSD1-HA FLAG for1/overAtLSD1-HA FLAG for2/overAtLSD1-HA FLAG for3* and *overAtLSD1-HA FLAG rev*) and cloned into pK2GW7 vector (Karimi *et al*., 2002) (Fig. 25). Characterization of *A. thaliana* plants transformed with FLAG HA AtLSD1-pK2GW7 plasmid is in progress.

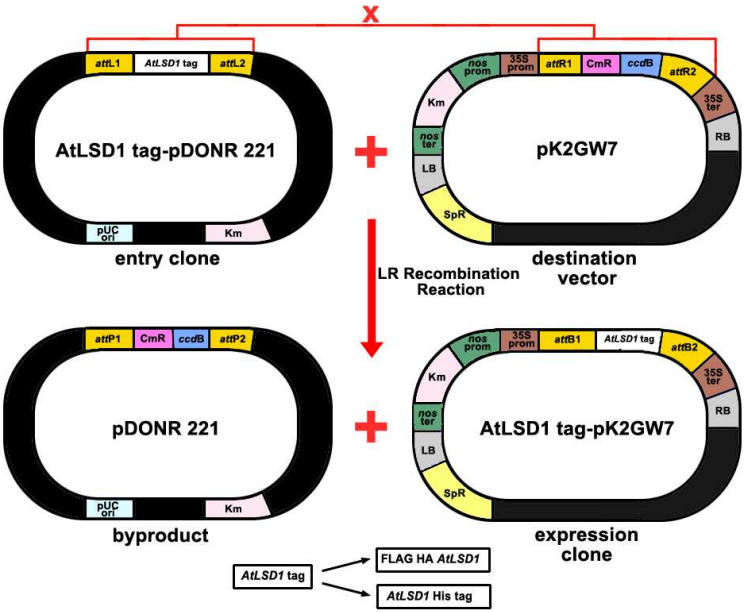

***Fig. 25*. Schematic rappresentation of the Gateway LR reaction performed to obtain the AtLSD1 overexpression constructs.** pDONR221: pDONR 221 Gateway donor vector; pK2GW7: pK2GW7 plant Gateway destination vector; *att*L1, *att*L2, *att*R1, *att*R2, *att*P1, *att*P2, *att*B1 and *att*B2: site-specific *att*achment sites for recombination proteins; *AtLSD1* His tag: *AtLSD1* cDNA linked to a sequence encoding for a 6-His tag; FLAG HA *AtLSD1*: *AtLSD1* cDNA linked to sequences encoding for the FLAG-HA tandem tags; pUC ori: pUC origin; Km: kanamycin resistance marker; CmR: chloramphenicol resistance marker; *ccd*B: *ccd*B gene; *nos* prom: *nos* promoter; *nos* ter: *nos* terminator; LB and RB: left and right T-DNA borders; SpR: spectinomycin resistance marker; 35S prom: promoter of the cauliflower mosaic virus (CaMV) 35S transcript; 35S ter: terminator of the cauliflower mosaic virus (CaMV) 35S transcript.

3. DISCUSSION

PAOs are involved in fundamental cellular processes, not only through their contribution to polyamine homeostasis but also through their reaction products (i.e. H_2O_2, Dap, and aminoaldehydes). The nature of reaction products and substrate specificity of PAOs depend on the source of the enzyme. The biological significance of such differences between the various PAOs and the specific role of each distinct PAO are not understood yet. To this end, the characterization of a major number of PAOs is fundamental. PAOs from monocotyledonous plants, such as ZmPAO, represent the until now best characterized plant PAOs and have been shown to be involved in the terminal catabolism of polyamines. Recently, AtPAO1 (Tavladoraki *et al*., 2006) has been shown to be the first plant PAO involved in a polyamine back-conversion pathway similarly to animal PAOs and SMOs. Thus, the characterization of the other *A. thaliana* PAOs results of great interest to determine whether these enzymes are also involved in a polyamine back-conversion pathway and to go deeper in the study of the physiological roles of polyamine catabolism in plants. In the present work, it was demonstrated that recombinant AtPAO2 and AtPAO4 catalyze the oxidative deamination of Spm and Spd to produce Spd and Put, respectively, and thus to be involved in a polyamine back-conversion pathway similarly to AtPAO1 and animal PAOs and SMOs.

Very recently, it has been demonstrated that AtPAO2 and AtPAO4 have a peroxisomal localization (Kamada-Nobusada *et al*., 2008; Moschou *et al*., 2008) conversely to ZmPAO which has an apoplastic localization. The differences between AtPAO2, AtPAO4 and ZmPAO in subcellular localization and mode of substrate oxidation probably reflect differences in the physiological roles of these enzymes. On the other hand, the peroxisomal localization of AtPAO2 and AtPAO4, analogous to that of the most known animal PAOs, gives direct evidence for peroxisome implication in polyamine oxidation and back-conversion also in plants. This compartmentalization could be of physiological importance considering the oxidative nature of PAOs, since the produced H_2O_2 could be efficiently scavenged through the abundant peroxisomal catalase. In AtPAO1, differently from AtPAO2 and AtPAO4, no signal for protein targeting to a specific intracellular compartment is present, thus suggesting a cytosolic localization. It is possible that, while AtPAO2 and AtPAO4 contribute to polyamine homeostasis, AtPAO1 is involved in other biological processes. However, the very high sequence identity (74%) of AtPAO1 with NtPAO, which has been shown to have an apoplastic localization (Yoda *et al*., 2006), leaves open the question of AtPAO1 subcellular localization and physiological roles.

Recombinant AtPAO2 and AtPAO4, similarly to AtPAO1, also oxidize N^1-acetyl-Spm, but much less efficiently than Spm suggesting that acetylated polyamines are not their physiological substrates. Thus, AtPAOs might be

involved in a polyamine back-conversion pathway in which the SSAT probably does not participate, this being contrary to animal PAOs, which mainly oxidize acetylated polyamines. In mammals, polyamines are acetylated in order to be excreted from the cells (Seiler, 1995; Wu *et al*., 2003) and PAOs may have the role to prevent this transport and to increase intracellular Spd and Put levels (Wu *et al*., 2003). On the contrary, both in mammals and plants the specific biological role of a SSAT-independent polyamine back-conversion pathway is not known yet, but the study of this pathway in *A. thaliana* may contribute greatly towards this end. The presence of a SSAT-dependent polyamine back-conversion pathway also in *A. thaliana* can not be excluded considering that small amounts of acetylated polyamines are present in this plant. Similarly, in *A. thaliana* the existence of a terminal polyamine catabolic pathway has not been yet demonstrated and can not be excluded. In this regards, it results of great importance the biochemical characterization of AtPAO5 to determine the pathway in which it is involved.

In the present work, it was also shown that recombinant AtPAO1, AtPAO2 and AtPAO4 are able to oxidize the stress related uncommon polyamines Thermo-Spm and Nor-Spm. In particular, it was shown that these uncommon polyamines are better substrates than Spm for AtPAO1 suggesting that they may be the physiological substrates of this enzyme. This is of great importance considering that a gene (*ACL5*) encoding for a protein able to synthesize Thermo-Spm from Spd has been recently characterized in *A. thaliana* (Knott *et al*., 2007) and the *acl5* Arabidopsis mutant presents defects in stem elongation (Hanzawa *et al*., 1997) and in vascular development (Clay and Nelson, 2005). In the future, the analysis of the expression pattern of *AtPAO* gene family will be of great importance to understand the role of each distinct AtPAO and to verify whether the *AtPAO1* expression pattern correlates well with Nor-Spm and Thermo-Spm accumulation *in vivo* under physiological or stress conditions.

In *A. thaliana*, four more genes have been also identified: *At1g62830* (*AtLSD1*), *At3g13682* (*AtLSD2*), *At3g10390* (*AtLSD3*), *At4g16310* (*AtLSD4*) encoding for proteins with an amine oxidase domain. These proteins bear also a SWIRM domain, which is usually present in chromatin-modifying complexes, and display a 26-30% sequence homology with human HsLSD1 (KIAA0601). HsLSD1, which has the same functional domains as the four AtLSDs, has been shown to catalyse the oxidative demethylation of H3K4me1 and H3K4me2 and to participate in multiprotein complexes important in the regulation of gene expression.

In the present work it was demonstrated that AtLSD1 is a lysine-specific histone demethylase with a substrate specificity similar to that of HsLSD1. In particular, it was shown that recombinant AtLSD1 specifically demethylates H3K4me2 and H3K4me1 peptides. On the contrary, no activity toward H3K9me2 and H3K27me2 peptides and polyamines was shown. Data presented in this work represent the first demonstration that also in plants

histone methylation is a reversible process. This is an important finding considering that in plants histone modifications are involved in key developmental processes, such as the transition from the vegetative to the reproductive stage (He and Amasino, 2005), and will probably contribute to get a better understanding of the underlying mechanism(s). In a recently published study (Krichevsky *et al*., 2007), the authors failed to detect demethylase activity of their recombinant AtLSD1. In the light of the results described in this work, it must be concluded that this may be due to instability and/or incorrect folding of the recombinant protein under their experimental conditions. Indeed, in this work it was observed that AtLSD1 catalytic activity resulted greatly enhanced in the presence of increasing amounts of glycerol.

A comparative analysis of the AtLSD1 and the HsLSD1 amino acid sequence and three-dimensional structure showed a high degree of conservation of the residues building up the active site and interacting with the pLys4Met peptide inhibitor, suggesting that electrostatic interactions are an important factor in the catalytic activity of both AtLSD1 and HsLSD1. Similarly, phosphorylation of the H3Ser10 residue, another important epigenetic mark, totally abolishes the demethylase activity toward the H3K4me1 peptide of both enzymes, probably due to unfavorable electrostatic interactions which make the peptide unable to bind the enzymes in a productive way (Forneris *et al.*, 2005a). These data suggest that, similarly to the human demethylase, AtLSD1 is able to "read" different epigenetic marks on the histone N-terminal tail, a finding which may have an important biological significance.

A prominent difference between AtLSD1 and HsLSD1 is the lack of the HsLSD1 Tower domain in the AtLSD1. This domain has been shown to be crucial for the histone demethylase activity of HsLSD1 (Stavropoulos *et al*., 2006; Chen *et al*., 2006) and to be involved in HsLSD1-CoREST complex formation (Chen *et al*., 2006; Yang *et al*., 2006), which in turn has been shown to stimulate the demethylase activity of HsLSD1 toward nucleosomes (Lee *et al*., 2005; Shi *et al*., 2005). In the case of AtLSD1, despite the lack of the Tower domain, a lysine specific histone demethylase activity has been demonstrated. However, AtLSD1 and HsLSD1 differ significantly from each other in catalytic efficiency. In particular, AtLSD1 displays a turnover rate 10-fold lower than that of HsLSD1. From this viewpoint it must be noted that a Towerless mutant of HsLSD1 has been shown to have a greatly reduced catalytic activity (approximately 0–10% as compared to the wild-type enzyme) (Stavropoulos *et al*., 2006; Chen *et al*., 2006), indicating that the Tower domain may be involved in the structural organization of the active site. These data suggest that small structural differences in the active site of AtLSD1 due to the lack of the Tower domain could explain the lower efficiency of this enzyme in respect to the human orthologue. However, it is also possible that AtLSD1 interacts *in vivo* with other proteins, as some recent data indicate (Krichevsky *et al*., 2007), which may affect its catalytic properties and increase its efficiency.

Functional partners of AtLSD1 seem to be different from those of HsLSD1. This is supported not only by the absence in the former protein of the Tower domain but also by a peculiar electrostatic potential distribution of the SWIRM molecular surface. In addition, the sequence similarity search using CoREST as a bait does not retrieve any protein in the *A. thaliana* genome which displays a significant sequence similarity with CoREST, ruling out the possibility that AtLSD1 interacts with CoREST-like macromolecules. The issue regarding functional roles/partners of proteins belonging to the LSD1 family is further complicated by recently published data (Huang *et al*., 2007) which demonstrate that HsLSD1 interacts with p53 to repress p53-mediated transcriptional activation and to inhibit the role of p53 in promoting apoptosis through demethylation of residue Lys370, a residue located in the C-terminal region of p53. However, p53 C-terminal tail does not display a significant sequence homology with the histone H3 N-terminal tail (data not shown), suggesting that proteins belonging to the LSD1 family are able to recognize various substrates, most likely through differential molecular interactions. This observation indicates that the *in vivo* functional role of this class of proteins is a very complex one, depending on the interaction with molecular partners which may differ significantly between animal and plant lysine-specific demethylases. Thus, characterization of the complexes in which AtLSD1 is eventually involved will contribute to define its molecular partners and its biological role. Furthermore, analysis of the expression pattern of *AtLSD* gene family will contribute to understand the role of each distinct AtLSD.

Very recently it has been reported that in Arabidopsis *AtLSD1*/*AtLSD2* or *AtLSD3* knockout increases H3K4 methylation level within the *FLC*, whereas it does not change H3K9 and H3K27 methylation levels (Jiang *et al*., 2007). These data are in agreement with the specific *in vitro* demethylase activity of AtLSD1 toward H3K4 demonstrated in the present work and suggest a similar substrate specificity *in vivo*. However, in another recent report, *AtLSD1* knockout has been shown not to change the H3K4 methylation level within the *FLC* but to reduce that at H3K9 and H3K27 (Krichevsky *et al*., 2007). The reason for such different results is not known, but it may reside in the fact that knockout of the various *AtLSDs* most probably interferes with the activity of other histone modifying enzymes, since these have been shown to participate in multiprotein complexes in which they function in a coordinated manner (Lee *et al*., 2006; Wissmann *et al*., 2007). This hypothesis could also explain the increase in the acetylation level of H4 within the FLC in the *AtLSD1* and *AtLSD3* knockout Arabidopsis mutants (Krichevsky *et al*., 2007; He *et al*., 2003).

4. REFERENCES

Agger K., Cloos P.A., Christensen J., Pasini D., Rose S., Rappsilber J., Issaeva I., Canaani E., Salcini A.E., Helin K. (2007) UTX and JMJD3 are histone H3K27 demethylases involved in HOX gene regulation and development. *Nature* **449**: 731-734.

Agger K., Christensen J., Cloos P.A., Helin K. (2008) The emerging functions of histone demethylases. *Curr. Opin. Genet. Dev.* **18**: 159-168.*

Alcázar R., Marco F., Cuevas J.C., Patron M., Ferrando A., Carrasco P., Tiburcio A.F., Altabella T. (2006) Involvement of polyamines in plant response to abiotic stress. *Biotechnol. Lett.* **28**: 1867-1876.*

Allfrey V.G., Faulkner R., Mirsky A.E. (1964) Acetylation and methylation of histones and their possible role in the regulation of RNA synthesis. *Proc. Natl. Acad. Sci. USA* **51**: 786-794.

Alonso J.M., Stepanova A.N., Leisse T.J., Kim C.J., Chen H., Shinn P., Stevenson D.K., Zimmerman J., Barajas P., Cheuk R., Gadrinab C., Heller C., Jeske A., Koesema E., Meyers C.C., Parker H., Prednis L., Ansari Y., Choy N., Deen H., Geralt M., Hazari N., Hom E., Karnes M., Mulholland C., Ndubaku R., Schmidt I., Guzman P., Aguilar-Henonin L., Schmid M., Weigel D., Carter D.E., Marchand T., Risseeuw E., Brogden D., Zeko A., Crosby W.L., Berry C.C., Ecker J.R. (2003) Genome-wide insertional mutagenesis of *Arabidopsis thaliana*. *Science* **301**: 653-657.*

Altschul S.F., Gish W., Miller W., Myers E.W., Lipman D.J. (1990) Basic local alignment search tool. *J. Mol. Biol.* **215**: 403-410.

Amirsadeghi S., Robson C.A., Vanlerberghe G.C. (2007) The role of the mitochondrion in plant responses to biotic stress. *Physiol. Plant.* **129**: 253-266.

Anand R. and Marmorstein R. (2007) Structure and mechanism of lysine-specific demethylase enzymes. *J. Biol. Chem.* **282**: 35425-35429.*

Andrade M.A., Chacon P., Merelo J.J., Moran F. (1993) Evaluation of secondary structure of proteins from UV circular dichroism spectra using an unsupervised learning neural network. *Protein Eng.* **6**: 383-390.

Angelini R., Manes F., Federico R. (1990) Spatial and functional correlation between diamine-oxidase and peroxidase activities and their dependence upon de-etiolation and wounding in chick-pea stems. *Planta* **182**: 89-96.*

Angelini R., Bragaloni M., Federico R., Infantino A., Porta-Puglia A. (1993) Involvement of polyamines, diamine oxidase and peroxidase in resistance of chick-pea to *Ascochyta rabiei*. *J. Plant Physiol.* **142**: 704-709.*

Apel K. and Hirt H. (2004) Reactive oxygen species: metabolism, oxidative stress, and signal transduction. *Annu. Rev. Plant Biol.* **55**: 373-399.

Aziz A., Martin-Tanguy J., Larher F. (1997) Plasticity of polyamine metabolism associated with high osmotic stress in rape leaf discs and with ethylene treatment. *Plant Growth Regul.* **21**: 153-163.

Aziz A., Martin-Tanguy J., Larher F. (1998) Stress-induced changes in polyamine and tyramine levels can regulate proline accumulation in tomato leaf discs treated with sodium chloride. *Physiol. Plant.* **104**: 195-202.

Bagni N. and Tassoni A. (2001) Biosynthesis, oxidation and conjugation of aliphatic polyamines in higher plants. *Amino Acids* **20**: 301-317.*

Ballas N., Battaglioli E., Atouf F., Andres M.E., Chenoweth J., Anderson M.E., Burger C., Moniwa M., Davie J.R., Bowers W.J., Federoff H.J., Rose D.W., Rosenfeld M.G., Brehm P., Mandel G. (2001) Regulation of neuronal traits by a novel transcriptional complex. *Neuron.* **31**: 353-365.

Ballas N., Grunseich C., Lu D.D., Speh J.C., Mandel G. (2005) REST and its corepressors mediate plasticity of neuronal gene chromatin throughout neurogenesis. *Cell* **121**: 645-657.

Bannister A.J., Schneider R., Kouzarides T. (2002) Histone methylation: dynamic or static? *Cell* **109**: 801-806.

Bastow R., Mylne J.S., Lister C., Lippman Z., Martienssen R.A., Dean C. (2004) Vernalization requires epigenetic silencing of *FLC* by histone methylation. *Nature* **427**:164-167.*

Bellelli A., Angelini R., Laurenzi M., Federico R. (1997) Transient kinetics of polyamine oxidase from *Zea mays* L. *Arch. Biochem. Biophys.* **343**: 146-148.

Berger S.L. (2002) Histone modifications in transcriptional regulation. *Curr. Opin. Genet. Dev.* **12**: 142-148.

Binda C., Coda A., Angelini R., Federico R., Ascenzi P., Mattevi A. (1999) A 30 Å long U-shaped catalytic tunnel in the crystal structure of polyamine oxidase. *Structure* **7**: 265-276.*

Binda C., Angelini R., Federico R., Ascenzi P., Mattevi A. (2001) Structural bases for inhibitor binding and catalysis in polyamine oxidase. *Biochemistry* **40**: 2766-2776.

Bose J., Gruber A.D., Helming L., Schiebe S., Wegener I., Hafner M., Beales M., Köntgen F., Lengeling A. (2004) The phosphatidylserine receptor has essential functions during embryogenesis but not in apoptotic cell removal. *J. Biol.* **3**: 15.

Bouchè N. and Fromm H. (2004) GABA in plants: just a metabolite? *Trends Plant Sci.* **9**: 110-115.

Bouchereau A., Aziz A., Larher F., Martin-Tanguy J. (1999) Polyamines and environmental challenges: recent development. *Plant Sci*. **140**: 103-125.*

Bradley C., van der Meer R., Roodi N., Yan H., Chandrasekharan M.B., Sun Z.W., Mernaugh R.L., Parl F.F. (2007) Carcinogen-induced histone alteration in normal human mammary epithelial cells. *Carcinogenesis* **28**: 2184-2192.*

Brownell J.E. and Allis C.D. (1996) Special HATs for special occasions: linking histone acetylation to chromatin assembly and gene activation. *Curr. Opin. Genet. Dev*. **6**: 176-184.

Cervelli M., Tavladoraki P., Di Agostino S., Angelini R., Federico R., Mariottini P. (2000) Isolation and characterization of three polyamine oxidase genes from *Zea mays. Plant Physiol. Biochem*. **38**: 667-677.*

Cervelli M., Cona A., Angelini R., Polticelli F., Federico R., Mariottini P. (2001) A barley polyamine oxidase isoform with distinct structural features and subcellular localization. *Eur. J. Biochem.* **268**: 3816-3830.*

Cervelli M., Polticelli F., Federico R., Mariottini P. (2003) Heterologous expression and characterization of mouse spermine oxidase. *J. Biol. Chem.* **278**: 5271-5276.*

Cervelli M., Di Caro O., Di Penta A., Angelini R., Federico R., Vitale A., Mariottini P. (2004) A novel C-terminal sequence from barley polyamine oxidase is a vacuolar sorting signal. *Plant J*. **40**: 410-418.*

Cervelli M., Bianchi M., Cona A., Crosatti C., Stanca M., Angelini R., Federico R., Mariottini P. (2006) Barley polyamine oxidase isoforms 1 and 2, a peculiar case of gene duplication. *FEBS J*. **273**: 3990-4002.*

Chang B., Chen Y., Zhao Y., Bruick R.K. (2007) JMJD6 is a histone arginine demethylase. *Science* **318**: 444-447.

Chen H.Y., Sun J.M., Zhang Y., Davie J.R., Meistrich M.L. (1998) Ubiquitination of Histone H3 in Elongating Spermatids of Rat Testes. *J. Biol. Chem.* **273**: 13165-13169.*

Chen Y., Yang Y., Wang F., Wan K., Yamane K., Zhang Y., Lei M. (2006) Crystal structure of human histone lysine-specific demethylase 1 (LSD1). *Proc. Natl. Acad. Sci. USA* **103**: 13956-13961.*

Chen Z.J. and Tian L. (2007) A Roles of dynamic and reversible histone acetylation in plant development and polyploidy. *Biochim. Biophys. Acta* **1769**: 295-307.*

Christensen J., Agger K., Cloos P.A., Pasini D., Rose S., Sennels L., Rappsilber J., Hansen K.H., Salcini A.E., Helin K. (2007) RBP2 belongs to a family of demethylases, specific for tri-and dimethylated lysine 4 on histone 3. *Cell* **128**: 1063-1076.

Clay N.K. and Nelson T. (2005) *Arabidopsis* thickvein mutation affects vein thickness and organ vascularization, and resides in a provascular cell-specific spermine synthase involved in vein definition and in polar auxin transport. *Plant Physiol.* **138**: 767-777.

Cloos P.A., Christensen J., Agger K., Maiolica A., Rappsilber J., Antal T., Hansen K.H., Helin K. (2006) The putative oncogene *GASC1* demethylates tri- and dimethylated lysine 9 on histone H3. *Nature* **442**: 307-311.

Cohen S.S. (1998) A guide to polyamines. Oxford University Press, New York.

Cona A., Cenci F., Cervelli M., Federico F., Mariottini P., Moreno S., Angelini R. (2003) Polyamine oxidase, a hydrogen peroxide-producing enzyme, is up-regulated by light and down-regulated by auxin in the outer tissue of maize mesocotyl. *Plant Physiol.* **131**: 803-813.*

Cona A., Moreno S., Cenci F., Federico R., Angelini R. (2005) Cellular re-distribution of flavin-containing polyamine oxidase in differentiating root and mesocotyl of *Zea mays* L. seedlings. *Planta* **221**: 265-276.*

Cona A., Rea G., Angelini R., Federico R., Tavladoraki P. (2006) Functions of amine oxidases in plant development and defence. *Trends Plant Sci.* **11**: 80-88.*

Culhane J.C., Szewczuk L.M., Liu X., Da G., Marmorstein R., Cole P.A. (2006) A mechanism-based inactivator for histone demethylase LSD1. *J. Am. Chem. Soc.* **128**: 4536-4537.*

Cuthbert G.L., Daujat S., Snowden A.W., Erdjument-Bromage H., Hagiwara T., Yamada M., Schneider R., Gregory P.D., Tempst P., Bannister A.J., Kouzarides T. (2004) Histone deimination antagonizes arginine methylation. *Cell* **118**: 545-553.*

Edmondson D.E. and Newton-Vinson P. (2001) The covalent FAD of monoamine oxidase: structural and functional role and mechanism of the flavinylation reaction. *Antioxid. Redox Signal* **3**: 789-806.*

Edmondson D.E., Mattevi A., Binda C., Li M., Hubálek F. (2004) Structure and mechanism of monoamine oxidase. *Curr. Med. Chem.* **11**: 1983-1993.*

Federico R., Cona A., Angelini R., Schininà M.E., Giartosio A. (1990) Characterization of maize polyamine oxidase. *Phytochemistry* **29**: 2411-2414.*

Federico R. and Angelini R. (1991) Polyamine catabolism. In: Slocum R. D., Flores H.E.(Eds.), Biochemistry and physiology of polyamines in plants. *CRC Press*, Boca Raton, FL. 41-56.

Feng Q., Wang H., Ng H.H., Erdjument-Bromage H., Tempst P., Struhl K., Zhang Y. (2002) Methylation of H3-lysine 79 is mediated by a new family of HMTases without a SET domain. *Curr. Biol.* **12**: 1052-1058.

Feng C. P. and Mundy J. (2006) Gene discovery and functional analyses in the model plant *Arabidopsis*. *J. Integr. Plant Biol.* **48**: 5-14.*

Forneris F., Binda C., Vanoni M.A., Battaglioli E., Mattevi A. (2005a) Human histone demethylase LSD1 reads the histone code. *J. Biol. Chem.* **280**: 41360-41365.*

Forneris F., Binda C., Vanoni M.A., Mattevi A., Battaglioli E. (2005b) Histone demethylation catalysed by LSD1 is a flavin-dependent oxidative process. *FEBS Lett.* **579**: 2203-2207.*

Forneris F., Binda C., Dall'Aglio A., Fraaije M.W., Battaglioli E., Mattevi A. (2006) A highly specific mechanism of histone H3-K4 recognition by histone demethylase LSD1. *J. Bio.l Chem.* **281**: 35289-35295.*

Forneris F., Binda C., Adamo A., Battaglioli E., Mattevi A. (2007) Structural basis of LSD1-CoREST selectivity in histone H3 recognition. *J. Biol. Chem.* **282**: 20070-20074.*

Forneris F., Binda C., Battaglioli E., Mattevi A. (2008) LSD1: oxidative chemistry for multifaceted functions in chromatin regulation. *Trends Biochem. Sci.* **33**: 181-189.*

Fraaije M.W., van Den Heuvel R.H., van Berkel W.J., Mattevi A. (2000) Structural analysis of flavinylation in vanillyl-alcohol oxidase. *J. Biol. Chem.* **275**: 38654-38658.*

Frescas D., Guardavaccaro D., Bassermann F., Koyama-Nasu R., Pagano M. (2007) JHDM1B/FBXL10 is a nucleolar protein that represses transcription of ribosomal RNA genes. *Nature* **450**: 309-313.

Frye R.A. (2000) Phylogenetic classification of prokaryotic and eukaryotic Sir2-like proteins. *Biochem. Biophys. Res. Commun.* **273**: 793-798.

Galston A.W. and Sawhney R.K. (1990) Polyamines in plant physiology. *Plant Physiol.* **94**: 406-410.

Galston A.W. and Sawhney R.K. (1995) Polyamines as endogenous growth regulators. In *Plant hormones: Physiology, biochemistry and molecular biology (2nd edn)*. Davies PJ (Ed). Kluwer Academic Publishers, Dordrecht, The Netherlands. 158-178.

Ge C., Cui X., Wang Y., Hu Y., Fu Z., Zhang D., Cheng Z., Li J. (2006) *BUD2*, encoding an S-adenosylmethionine decarboxylase, is required for *Arabidopsis* growth and development. *Cell Res.* **16**: 446-456.

Gendrel A.V., Lippman Z., Yordan C., Colot V., Martienssen R.A. (2002) Dependence of heterochromatic histone H3 methylation patterns on the Arabidopsis gene *DDM1*. *Science* **297**: 1871-1873.

Gilad G.M., Gilad V.H., Rabey J.M. (1996) Arginine and ornithine decarboxylation in rodent brain: coincidental changes during development and after ischemia. *Neurosci. Lett.* **216**: 33-36.

Gregoretti I.V., Lee Y.M., Goodson H.V. (2004) Molecular evolution of the histone deacetylase family: functional implications of phylogenetic analysis. *J. Mol. Biol.* **338**: 17-31.

Groppa M.D. and Benavides M.P. (2008) Polyamines and abiotic stress: recent advances. *Amino Acids* **34**: 35-45.*

Ha H.C., Sirisoma N.S., Kuppusamy P., Zweier J.L., Woster P.M., Casero R.A. Jr. (1998) The natural polyamine spermine functions directly as a free radical scavenger. *Proc. Natl. Acad. Sci. USA* **95**: 11140-11145.

Hanfrey C., Sommer S., Mayer M.J., Burtin D., Michael A.J. (2001) Arabidopsis polyamine biosynthesis: absence of ornithine decarboxylase and the mechanism of arginine decarboxylase activity. *Plant J.* **27**: 551-560.*

Hanson A.D., Rathinasabapathi B., Rivoal J., Burnet M., Dillon M.O., Gage D.A. (1994) Osmoprotective compounds in the *Plumbaginaceae*: a natural experiment in metabolic engineering of stress tolerance. *Proc. Natl. Acad. Sci. USA* **91**: 306-310.

Hanzawa Y., Takahashi T., Komeda Y. (1997) *ACL5*: an *Arabidopsis* gene required for internodal elongation after flowering. *Plant J.* **12**: 863-874.*

Hanzawa Y., Imai A.,. Michael A.J., Komeda Y., Takahashi T. (2002) Characterization of the spermidine synthase-related gene family in *Arabidopsis thaliana*. *FEBS Lett.* **527**: 176-180.*

Hartley J.L., Temple G.F., Brasch M.A. (2000) DNA cloning using *in vitro* site-specific recombination. *Genome Res.* **10**: 1788-1795.

Hartzog G.A. and Tamkun J.W. (2007) A new role for histone tail modifications in transcription elongation. *Genes Dev*. **21**: 3209-3213.*

Hashimoto Y., Hibasami H., Tamaki S., Kamei A., Ikoma J., Kaito M., Imoto I., Watanabe S., Nakashima K., Adachi Y. (1999) Induction of apoptotic cell death in human hepatocellular carcinoma SK-HEP-1 cells by a polyamine synthesis inhibitor, methylglyoxal bis(cyclopentylamidinohydrazone). *Anticancer Drugs* **10**: 323-327.

Hassa P.O., Haenni S.S., Elser M., Hottiger M.O. (2006) Nuclear ADP-ribosylation reactions in mammalian cells: where are we today and where are we going? *Microbiol. Mol. Biol. Rev.* **70**: 789-829.*

He L., Nada K., Kasukabe Y., Tachibana S. (2002) Enhanced susceptibility of photosynthesis to low-temperature photoinhibition due to interruption of chill-induced increase of S-adenosylmethionine decarboxylase activity in leaves of spinach (*Spinacia oleracea* L.). *Plant Cell Physiol.* **43**: 196-206.

He H. and Lehming N. (2003) Global effects of histone modifications. *Brief. Funct. Genomic Proteomic.* **2**: 234-243.*

He Y., Michaels S.D., Amasino R.M. (2003) Regulation of flowering time by histone acetylation in *Arabidopsis*. *Science* **302**: 1751-1754.*

He Y. and Amasino R. M. (2005) Role of chromatin modification in flowering-time control. *Trends Plant Sci.* **10**: 30-35.*

Hebbes T.R., Thorne A.W., Crane-Robinson C. (1988) A direct link between core histone acetylation and transcriptionally active chromatin. *EMBO J.* **7**: 1395-1402.

Hochstrasser M. (1996) Ubiquitin-dependent protein degradation. *Annu. Rev. Genet.* **30**: 405-439.

Holt A. and Baker G.B. (1995) Metabolism of agmatine (clonidine-displacing substance) by diamine oxidase and the possible implications for studies of imidazoline receptors. *Prog. Brain Res.* **106**: 187-197.

Huang J., Sengupta R., Espejo A.B., Lee M.G., Dorsey J.A., Richter M., Opravil S., Shiekhattar R., Bedford M.T., Jenuwein T., Berger S.L. (2007) p53 is regulated by the lysine demethylase LSD1. *Nature* **449**: 105-108.*

Hummel I., Bourdais G., Gouesbet G., Couée I., Malmberg R.L., El Amrani A. (2004) Differential expression of arginine decarboxylase *ADC1* and *ADC2* in *Arabidopsis thaliana*: characterization of transcriptional regulation during seed germination and seedling development. *New Phyt.* **163**: 519-531.

Igarashi K. and Kashiwagi K. (2000) Polyamines: mysterious modulators of cellular functions. *Biochem. Biophys. Res. Commun.* **271**: 559-564.*

Imai S., Armstrong C.M., Kaeberlein M., Guarente L. (2000) Transcriptional silencing and longevity protein Sir2 is an NAD-dependent histone deacetylase. *Nature* **403**: 795-800.

Imai A., Matsuyama T., Hanzawa Y., Akiyama T., Tamaoki M., Saji H., Shirano Y., Kato T., Hayashi H., Shibata D., Tabata S., Komeda Y., Takahashi T. (2004) Spermidine Synthase Genes Are Essential for Survival of *Arabidopsis*. *Plant Physiol.* **135**: 1565-1573.*

Ivaldi M.S., Karam C.S., Corces V.G. (2007) Phosphorylation of histone H3 at Ser10 facilitates RNA polymerase II release from promoter-proximal pausing in *Drosophila*. *Genes Dev.* **21**: 2818-2831.

Jackson J.P., Lindroth A.M., Cao X., Jacobsen S.E. (2002) Control of CpNpG DNA methylation by the KRYPTONITE histone H3 methyltransferase. *Nature* **416**: 556-560.

Jackson J.P., Johnson L., Jasencakova Z., Zhang X., PerezBurgos L., Singh P.B., Cheng X., Schubert I., Jenuwein T., Jacobsen S.E. (2004) Dimethylation of histone H3 lysine 9 is a critical mark for DNA methylation and gene silencing in *Arabidopsis thaliana*. *Chromosoma* **112**: 308-315.*

Jason L.J.M., Moore S.C., Lewis J.D., Lindsey G., Ausió J. (2002) Histone ubiquitination: a tagging tail unfolds? *Bioessays* **24**: 166-174.*

Jensen L.R., Amende M., Gurok U., Moser B., Gimmel V., Tzschach A., Janecke A.R., Tariverdian G., Chelly J., Fryns J.P., Van Esch H., Kleefstra T., Hamel B., Moraine C., Gecz J., Turner G., Reinhardt R., Kalscheuer V.M., Ropers H.H., Lenzner S. (2005) Mutations in the *JARID1C* gene, which is involved in transcriptional regulation and chromatin remodeling, cause X-linked mental retardation. *Am. J. Hum. Genet*. **76**: 227-236.

Jenuwein T., Laible G., Dorn R., Reuter G. (1998) SET domain proteins modulate chromatin domains in eu- and heterochromatin. *Cell Mol. Life Sci.* **54**: 80-93.

Jenuwein T. and Allis C.D. (2001) Translating the Histone Code. *Science* **293**: 1074-1080.*

Jiang D., Yang W., He Y., Amasino R.M. (2007) *Arabidopsis* relatives of the human lysine-specific demethylase 1 repress the expression of *FWA* and *FLOWERING LOCUS C* and thus promote the floral transition. *Plant Cell* **19**: 2975-2987.*

Jin J.B., Jin Y.H., Lee J., Miura K., Yoo C.Y., Kim W.Y., Van Oosten M., Hyun Y., Somers D.E., Lee I., Yun D.J., Bressan R.A., Hasegawa P.M. (2008) The SUMO E3 ligase, *AtSIZ1*, regulates flowering by controlling a salicylic acid-mediated floral promotion pathway and through affects on *FLC* chromatin structure. *Plant J.* **53**: 530-540.*

Kakehi J., Kuwashiro Y., Niitsu M., Takahashi T. (2008) Thermospermine is Required for Stem Elongation in *Arabidopsis thaliana*. *Plant Cell Physiol.* **49**: 1342-1349.*

Kamada-Nobusada T., Hayashi M., Fukazawa M., Sakakibara H., Nishimura M. (2008) A putative peroxisomal polyamine oxidase, AtPAO4, is involved in polyamine catabolism in *Arabidopsis thaliana*. *Plant Cell Physiol.* **49**: 1272-1282.*

Kaneko H., Hibasami H., Mori K., Kawarada Y., Nakashima K. (1998) Apoptosis induction in human breast cancer MRK-nu-1 cells by a polyamine synthesis inhibitor, methylglyoxal bis(cyclopentylamidinohydrazone) (MGBCP). *Anticancer Res.* **18**: 891-896.

Karimi M., Inzé D., Depicker A. (2002) GATEWAY vectors for *Agrobacterium*-mediated plant transformation. *Trends Plant Sci.* **7**: 193-195.*

Kasukabe Y., He L., Nada K., Misawa S., Ihara I., Tachibana S. (2004) Overexpression of spermidine synthase enhances tolerance to multiple environmental stresses and up-regulates the expression of various stress-regulated genes in transgenic *Arabidopsis thaliana*. *Plant Cell Physiol.* **45**: 712-722.

Kasukabe Y., He L., Watakabe Y., Otani M., Shimada T., Tachibana S. (2006) Improvement of environmental stress tolerance of sweet potato by introduction of genes for spermidine synthase. *Plant Biotechnol*. **23**: 75-83.

Klose R.J., Kallin E.M., Zhang Y. (2006) JmjC-domain-containing proteins and histone demethylation. *Nat. Rev. Genet.* **7**: 715-727.*

Knott J.M., Römer P., Sumper M. (2007) Putative spermine synthases from *Thalassiosira pseudonana* and *Arabidopsis thaliana* synthesize thermospermine rather than spermine. *FEBS Lett.* **581**: 3081-3086.*

Koc E.C., Bagga S., Songstad D.D., Betz S.R., Kuehn G.D., Phillips G.C. (1998) Occurrence of uncommon polyamines in cultured tissues of maize. *In vitro Cell. Dev. Biol. Plant* **34**: 252-255.

Koyama-Nasu R., David G., Tanese N. (2007) The F-box protein Fbl10 is a novel transcriptional repressor of *c-Jun*. *Nat. Cell Biol.* **9**: 1074-1080.

Krichevsky A., Gutgarts H., Kozlovsky S.V., Tzfira T., Sutton A., Sternglanz R., Mandel G., Citovsky V. (2007) C2H2 zinc finger-SET histone methyltransferase is a plant-specific chromatin modifier. *Dev. Biol.* **303**: 259-269.*

Kubicek S. and Jenuwein T. (2004) A crack in histone lysine methylation. *Cell* **119**: 903-906.*

Kuehn G.D., Rodriguez-Garay B., Bagga S., Phillips G.C. (1990) Novel Occurrence of Uncommon Polyamines in Higher Plants. *Plant Physiol.* **94**: 855-857.*

Kumar V., Dooley D.M., Freeman H.C., Guss J.M., Harvey I., McGuirl M.A., Wilce M.C., Zubak V.M. (1996) Crystal structure of a eukaryotic (pea seedling) copper-containing amine oxidase at 2.2 Å resolution. *Structure* **4**: 943-955.*

Kumar A., Altabella T., Taylor M., Tiburcio A.F. (1997) Recent advances in polyamine research. *Trends Plant Sci.* **2**: 124-130.*

Kuo M.H. and Allis C.D. (1998) Roles of histone acetyltransferases and deacetylases in gene regulation. *Bioessays* **20**: 615-626.

Kusano T., Yamaguchi K., Berberich T., Takahashi Y. (2007a) Advances in polyamine research in 2007. *J. Plant Res.* **120**: 345-350.*

Kusano T., Yamaguchi K., Berberich T., Takahashi Y. (2007b) The polyamine spermine rescues *Arabidopsis* from salinity and drought stresses. *Plant Signal Behav*. **2**: 250-251.

Kusano T., Berberich T., Tateda C., Takahashi Y. (2008) Polyamines: essential factors for growth and survival. *Planta* **228**: 367-381.*

Landry J. and Sternglanz R. (2003) Yeast Fms1 is a FAD-utilizing polyamine oxidase. *Biochem. Biophys. Res. Commun.* **303**: 771-776.*

Laurenzi M., Rea G., Federico R., Tavladoraki P., Angelini R. (1999) De-etiolation causes a phytochrome-mediated increase of polyamine oxidase expression in outer tissues of the maize mesocotyl: a role in the photomodulation of growth and cell wall differentiation. *Planta* **208**: 146-154.

Laurenzi M., Tipping A.J., Marcus S.E., Knox J.P., Federico R., Angelini R., McPherson M.J. (2001) Analysis of the distribution of copper amine oxidase in cell walls of legume seedlings. *Planta* **214**: 37-45.

Lee M.G., Wynder C., Cooch N., Shiekhattar R. (2005) An essential role for CoREST in nucleosomal histone 3 lysine 4 demethylation. *Nature* **437**: 432-435.*

Lee M.G., Wynder C., Bochar D.A., Hakimi, M.A., Cooch N., Shiekhattar R. (2006) Functional interplay between histone demethylase and deacetylase enzymes. *Mol. Cell. Biol.* **26**: 6395-6402.*

Liu K., Fu H., Bei Q., Luan S. (2000) Inward potassium channel in guard cells as a target for polyamine regulation of stomatal movements. *Plant Physiol.* **124**: 1315-1326.

Liu J-H., Kitashiba H., Wang J., Ban Y., Moriguchi T. (2007) Polyamines and their ability to provide environmental stress tolerance to plants. *Plant Biotechnol.* **24**: 117-126.

Lo W.S., Duggan L., Emre N.C., Belotserkovskya R., Lane W.S., Shiekhattar R., Berger S.L. (2001) Snf1--A histone kinase that works in concert with the histone acetyltransferase Gcn5 to regulate transcription. *Science* **293**: 1142-1146.

Lu F., Li G., Cui X., Liu C., Wang X.J., Cao X.J. (2008) Comparative analysis of JmjC domain-containing proteins reveals the potential histone demethylases in Arabidopsis and rice. *Integr. Plant Biol.* **50**: 886-896.*

Luger K., Rechsteiner T.J., Flaus A.J., Waye M.M.Y., Richmond T.J. (1997) Characterization of nucleosome core particles containing histone proteins made in bacteria. *J. Mol. Biol.* **272**: 301-311.

Mackintosh C.A and Pegg A.E. (2000) Effect of spermine synthase deficiency on polyamine biosynthesis and content in mice and embryonic fibroblasts, and the sensitivity of fibroblasts to 1,3-bis-(2-chloroethyl)-N-nitrosourea. *Biochem. J.* **2**: 439-447.

Malmberg R.L., Watson M.B., Galloway G.L., Yu W. (1998) Molecular genetic analyses of plant polyamines. *Crit. Rev. Plant Sci.* **17**: 199-224.

Mansour M.M.F. and Al-Mutawa M.M. (1999) Stabilization of plasma membrane by polyamines against salt stress. *Cytobios.* **100**: 7-17.

Marini F., Betti L., Scramagli S., Biondi S., Torrigiani P. (2001) Polyamine metabolism is upregulated in response to tabacco mosaic virus in hypersensitive, but not in susceptible, tobacco. *New Phytol.* **149**: 301-309.

Martin-Tanguy J. (1997) Conjugated polyamines and reproductive development: biochemical, molecular and physiological approaches. *Physiol. Plant.* **100**: 675-688.*

Medda R., Padiglia A., Pedersen J.Z., Rotilio G., Finazzi Agrò A., Floris G. (1995) The reaction mechanism of copper amine oxidase: detection of intermediates by the use of substrates and inhibitors. *Biochemistry* **34**: 16375-16381.

Metzger E., Wissmann M., Yin N., Muller J.M., Schneider R., Peters A.H., Gunther T., Buettner R., Schule R. (2005) LSD1 demethylates repressive histone marks to promote androgen-receptor-dependent transcription. *Nature* **437**: 436-439.*

Metzger E., Yin N., Wissmann M., Kunowska N., Fischer K., Friedrichs N., Patnaik D., Higgins J.M.G., Potier N., Scheidtmann K.H., Buettner R., Schüle R. (2008) Phosphorylation of histone H3 at threonine 11 establishes a novel chromatin mark for transcriptional regulation. *Nat. Cell Biol.* **10**: 53-60.*

Mittler R., Vanderauwera S., Gollery M., Van Breusegem F. (2004) Reactive oxygen gene networks of plants. *Trends Plant Sci.* **9**: 490-498.

Møller S.G. and McPherson M.J. (1998) Developmental expression and biochemical analysis of the Arabidopsis *atao1* gene encoding an H_2O_2-generating diamine oxidase. *Plant J.* **13**: 781-791.*

Møller S.G., Urwin P.E., Alkinson H.J., McPherson M.J. (1998) Nematode-induced expression of *atao1*, a gene encoding an extracellular diamine oxidase associated with developing vascular tissue. *Physiol. Mol. Plant Pathol.* **53**: 73-79.*

Moschou P.N., Sanmartin M., Andriopoulou A.H., Rojo E., Sanchez-Serrano J.J., Roubelakis-Angelakis K.A. (2008) Bridging the gap between plant and mammalian polyamine catabolism: a novel peroxisomal polyamine oxidase responsible for a full back-conversion pathway in Arabidopsis. *Plant Physiol.* **47**: 1845-1857.*

Muskett P.R., Clissold L., Marocco A., Springer P.S., Martienssen R., Dean C. (2003) A resource of mapped dissociation launch pads for targeted insertional mutagenesis in the *Arabidopsis* genome. *Plant Physiol.* **132**: 506-516.

Nayyar H., Kaur S., Singh S., Kumar S., Singh K.J., Dhir K.K. (2005) Involvement of polyamines in the contrasting sensitivity of chickpea (*Cicer arietinum* L.) and soybean (*Glycine max* (L.) Merrill.) to water deficit stress. *Bot. Bull. Acad. Sin.* **46**: 333-338.

Ng H.H., Feng Q., Wang H., Erdjument-Bromage H., Tempst P., Zhang Y., Struhl K. (2002) Lysine methylation within the globular domain of histone H3 by Dot1 is important for telomeric silencing and Sir protein association. *Genes Dev.* **16**: 1518-1527.

Nicolas E., Lee M.G., Hakimi M.A., Cam H.P., Grewal S.I., Shiekhattar R. (2006) Fission yeast homologs of human histone H3 lysine 4 demethylase regulate a common set of genes with diverse functions. *J. Biol. Chem.* **281**: 35983-35988.*

Nowak S.J. and Corces V.G. (2004) Phosphorylation of histone H3: a balancing act between chromosome condensation and transcriptional activation. *Trends Genet.* **20**: 214-220.

Ooi L. and Wood I.C. (2007) Chromatin crosstalk in development and disease: lessons from REST. *Nat. Rev. Genet.* **8**: 544-554.*

Ozawa K. (2008) Reduction of phosphorylated histone H3 serine 10 and serine 28 cell cycle marker intensities after DNA damage. *Cytometry A.* **73**: 517-527.

Panicot M., Minguet E.G., Ferrando A., Alcázar R., Blázquez M.A., Carbonell J., Altabella T., Koncz C., Tiburcio A.F. (2002) A polyamine metabolon involving aminopropyl transferase complexes in *Arabidopsis*. *Plant Cell* **14**: 2539-2551.

Park M.H. (2006) The post-translational synthesis of a polyamine-derived amino acid, hypusine, in the eukaryotic translation initiation factor 5A (eIF5A). *J. Biochem.* **139**: 161-169.

Paschalidis K.A. and Roubelakis-Angelakis K.A. (2005) Sites and regulation of polyamine catabolism in the tobacco plant. Correlations with cell division/expansion, cell cycle progression, and vascular development. *Plant Physiol.* **138**: 2174-2184.

Perez-Amador M.A., Leon J., Green P.J., Carbonell J. (2002) Induction of the arginine decarboxylase *ADC2* gene provides evidence for the involvement of polyamines in the wound response in *Arabidopsis*. *Plant Physiol.* **130**: 1454-1463.

Peters A.H., O' Carroll D., Scherthan H., Mechtler K., Sauer S., Schöfer C., Weipoltshammer K., Pagani M., Lachner M., Kohlmaier A., Opravil S., Doyle M., Sibilia M., Jenuwein T. (2001) Loss of the Suv39h histone methyltransferases impairs mammalian heterochromatin and genome stability. *Cell* **107**: 323-337.

Polticelli F., Basran J., Faso C., Cona A., Minervini G., Angelini R., Federico R., Scrutton N.S., Tavladoraki P. (2005) Lys300 plays a major role in the catalytic mechanism of maize polyamine oxidase. *Biochemistry* **44**: 16108-16120.*

Probst A.V., Fagard M., Proux F., Mourrain P., Boutet S., Earley K., Lawrence R.J., Pikaard C.S., Murfett J., Furner I., Vaucheret H., Scheid O.M. (2004) *Arabidopsis* histone deacetylase HDA6 is required for maintenance of transcriptional gene silencing and determines nuclear organization of rDNA repeats. *Plant Cell* **16**: 1021-1034.

Provencher S.W. (1982) A constrained regularization method for inverting data represented by linear algebraic or integral-equations. *Comput. Phys. Commun.* **27**: 213-227.

Raman S.B. and Rathinasabapathi B. (2003) B-alanine N-methyltransferase of *Limonium latifolium* cDNA cloning and functional expression of a novel N-methyltransferase implicated in the synthesis of the osmoprotectant β-alanine betaine. *Plant Physiol.* **132**: 1642-1651.

Rea G., Laurenzi M., Tranquilli E., D'Ovidio R., Federico R., Angelini R. (1998) Developmentally and wound regulated expression of the gene encoding a cell wall copper amine oxidase in chickpea seedlings. *FEBS Lett.* **437**: 177-182.*

Rea G., Metoui O., Infantino A., Federico R., Angelini R. (2002) Copper amine oxidase in defense response to wounding and *Ascochyta rabiei* invasion. *Plant Physiol.* **128**: 865-875.*

Rodriguez-Garay B., Phillips G.C., Kuehn G.D. (1989) Detection of Norspermidine and Norspermine in *Medicago sativa* L. (Alfalfa). *Plant Physiol.* **89**: 525-529.*

Roth S.Y., Denu J.M., Allis C.D. (2001) Histone acetyltransferases. *Ann. Rev. Biochem*. **70**: 81-120.

Roy M. and Ghosh B. (1996) Polyamines, both common and uncommon, under heat stress in rice (*Oryza sativa*) callus. *Physiol. Plant.* **98**: 196-200.

Schipper R.G., Penning L.C., Verhofstad A.A. (2000) Involvement of polyamines in apoptosis. Facts and controversies: effectors or protectors? *Semin. Cancer Biol.* **10**: 55-68.*

Schmitz R.J., Sung S., Amasino R.M. (2008) Histone arginine methylation is required for vernalization-induced epigenetic silencing of *FLC* in winter-annual *Arabidopsis thaliana*. *PNAS* **105**: 411-416.*

Šebela M., Radova A., Angelini R., Tavladoraki P., Frebort I., Pec P. (2001) FAD-containing polyamine oxidase: a timely challenge for researchers in biochemistry and physiology of plants. *Plant Sci.* **160**: 197-207.*

Seiler N. (1995) Polyamine oxidase, properties and functions. *Prog. Brain Res.* **106**: 333-344.*

Seiler N. (2004) Catabolism of polyamines. *Amino Acids* **26**: 217-233.*

Seiler N. and Raul F. (2005) Polyamines and apoptosis. *J. Cell. Mol. Med.* **9**: 623-642.*

Shabala S., Cuin T.A., Pottosin I. (2007) Polyamines prevent NaCl-induced K^+ efflux from pea mesophyll by blocking non-selective cation channels. *FEBS Lett*. **581**: 1993-1999.

Shi Y., Sawada J., Sui G., Affar el B., Whetstine J.R., Lan F., Ogawa H., Luke M.P., Nakatani Y., Shi Y. (2003) Coordinated histone modifications mediated by a CtBP co-repressor complex. *Nature* **422**: 735-738.

Shi Y., Lan F., Matson C., Mulligan P., Whetstine J.R., Cole P.A., Casero R.A., Shi Y. (2004) Histone demethylation mediated by the nuclear amine oxidase homolog LSD1. *Cell* **119**: 941-953.*

Shi Y.J., Matson C., Lan F., Iwase S., Baba T., Shi Y. (2005) Regulation of LSD1 histone demethylase activity by its associated factors. *Mol. Cell* **19**: 857-864.*

Shiio Y. and Eisenman R.N. (2003) Histone sumoylation is associated with transcriptional repression. *Proc. Natl. Acad. Sci. USA* **100**: 13225-13230.*

Sreerama N., Venyaminov S.Y., Woody R.W. (1999) Estimation of the number of alpha-helical and beta-strand segments in proteins using circular dichroism spectroscopy. *Protein Sci.* **8**: 370-380.

Stavropoulos P., Blobel G., Hoelz A. (2006) Crystal structure and mechanism of human lysine-specific demethylase-1. *Nat. Struct. Mol. Biol.* **13**: 626-632.*

Takahashi Y., Berberich T., Miyazaki A., Seo S., Ohashi Y., Kusano T. (2003) Spermine signalling in tobacco: activation of mitogen-activated protein kinases by spermine is mediated through mitochondrial dysfunction. *Plant J.* **36**: 820-829.

Tavladoraki P., Schininà M.E., Cecconi F., Di Agostino S., Manera F., Rea G., Mariottini P., Federico R., Angelini R. (1998) Maize polyamine oxidase: primary structure from protein and cDNA sequencing. *FEBS Lett.* **426**: 62-66.*

Tavladoraki P., Rossi M.N., Saccuti G., Perez-Amador M.A., Polticelli F., Angelini R., Federico R. (2006) Heterologous expression and biochemical characterization of a polyamine oxidase from Arabidopsis involved in polyamine back-conversion. *Plant Physiol.* **141**: 1519-1532.*

Terano S. and Suzuki Y. (1978) Formation of β-alanine from spermine and spermidine in maize shoots. *Phytochemistry* **7**: 148-149.

Thomas T. and Thomas T.J. (2001) Polyamines in cell growth and cell death: molecular mechanisms and therapeutic applications. *Cell. Mol. Life Sci.* **58**: 244-258.*

Tian L. and Chen Z.J. (2001) Blocking histone deacetylation in *Arabidopsis* induces pleiotropic effects on plant gene regulation and development. *Proc. Natl. Acad. Sci. USA* **98**: 200-205.*

Tian L., Fong M.P., Wang J.J., Wei N.E., Jiang H., Doerge R.W., Chen Z.J. (2005) Reversible histone acetylation and deacetylation mediate genome-wide, promoter-dependent and locus-specific changes in gene expression during plant development. *Genetics* **169**: 337-345.

Torrigiani P., Rabiti A.L., Bortolotti G., Betti L., Marani F., Canova A., Bagni N. (1997) Polyamine synthesis and accumulation in the hypersensitive response to TMV in *Nicotiana tabacum*. *New Phytol*. **135**: 467-473.

Tsukada Y., Fang J., Erdjument-Bromage H., Warren M.E., Borchers C.H., Tempst P., Zhang Y. (2005) Histone demethylation by a family of JmjC domain-containing proteins. *Nature* **439**: 811-816.*

Urano K., Yoshiba Y., Nanjo T., Igarashi Y., Seki M., Sekiguchi F., Yamaguchi-Shinozaki Y., Shinozaki K. (2003) Characterization of Arabidopsis genes involved in biosynthesis of polyamines in abiotic stress responses and developmental stages. *Plant Cell Environ.* **26**: 1917-1926.*

Urano K., Hobo T., Shinozaki K. (2005) *Arabidopsis* ADC genes involved in polyamine biosynthesis are essential for seed development. *FEBS Lett.* **579**: 1557-1564.*

Vergnolle C., Vaultier M.N., Taconnat L., Renou J.P., Kader J.C., Zachowski A., Ruelland E. (2005) The cold-induced early activation of phospholipase C and D pathways determines the response of two distinct clusters of genes in Arabidopsis cell suspensions. *Plant Physiol*. **139**: 1217-1233.

Vlachonasios K.E., Thomashow M.F., Triezenberg S.J. (2003) Disruption mutations of *ADA2b* and *GCN5* transcriptional adaptor genes dramatically affect Arabidopsis growth, development, and gene expression. *Plant Cell* **15**: 626-638.

Vujcic S., Diegelman P., Bacchi C.J., Kramer D.L., Porter C.W. (2002) Identification and characterization of a novel flavin-containing spermine oxidase of mammalian cell origin. *Biochem. J.* **367**: 665-675.*

Vujcic S., Liang P., Diegelman P., Kramer D.L., Porter C.W. (2003) Genomic identification and biochemical characterization of the mammalian polyamine oxidase involved in polyamine back-conversion. *Biochem. J.* **370**: 19-28.*

Walden R., Cordeiro A., Tiburcio A.F. (1997) Polyamines: Small Molecules Triggering Pathways in Plant Growth and Development. *Plant Physiol.* **3**: 1009-1013.*

Wallace H.M., Fraser A.V., Hughes A. (2003) A perspective of polyamine metabolism. *Biochem. J.* **376**: 1-14.*

Walters D.R. (1989) Polyamines and plant disease. *Plants Today* January-February. 22-26.

Walters D.R. (2000) Polyamines in plant-microbe interactions. *Physiol. Mol. Plant Pathol.* **57**: 137-146.

Walters D.R. (2003) Polyamines and plant disease. *Phytochemistry* **64**: 97-107.*

Wang Y., Devereux W., Woster P.M., Stewart T.M., Hacker A., Casero Jr. R.A. (2001) Cloning and characterization of a human polyamine oxidase that is inducible by polyamine analogue exposure. *Cancer Res.* **61**: 5370-5373.

Wang Y., Stewart T.M., Devereux W., Hacker A., Frydman B., Woster P.M., Casero R.A. (2003) Properties of purified recombinant human polyamine oxidase, PAOh1/SMO. *Biochem. Biophys. Res. Commun.* **304**: 605-611.*

Wang X., Ikeguchi Y., McCloskey D.E., Nelson P., Pegg A.E. (2004a) Spermine synthesis is required for normal viability, growth, and fertility in the mouse. *J. Biol. Chem.* **279**: 51370-51375.

Wang Y., Wysocka J., Sayegh J., Lee Y.H., Perlin J.R., Leonelli L., Sonbuchner L.S., McDonald C.H., Cook R.G., Dou Y., Roeder R.G., Clarke S., Stallcup M.R., Allis C.D., Coonrod S.A. (2004b) Human PAD4 regulates histone arginine methylation levels via demethylimination. *Science* **306**: 279-283.*

Wang J., Scully K., Zhu X., Cai L., Zhang J., Prefontaine G.G., Krones A., Ohgi K.A., Zhu P., Garcia-Bassets I., Liu F., Taylor H., Lozach J., Jayes F.L., Korach K.S., Glass C.K., Fu X.D., Rosenfeld M.G. (2007) Opposing LSD1 complexes function in developmental gene activation and repression programmes. *Nature* **446**: 882-887.*

Watson M.B. and Malmberg R.L. (1996) Regulation of *Arabidopsis thaliana* (L.) Heynh Arginine decarboxylase by potassium deficiency stress. *Plant Physiol.* **111**: 1077-1083.

Watson M.W., Yu W., Galloway G.L., Malmberg R.L. (1997) Isolation and characterization of a second arginine decarboxylase cDNA from *Arabidopsis* (PGR97–114). *Plant Physiol*. **114**: 1569.

Wissmann M., Yin N., Müller J.M., Greschik H., Fodor B.D., Jenuwein T., Vogler C., Schneider R., Günther T., Buettner R., Metzger E., Schüle R. (2007) Cooperative demethylation by JMJD2C and LSD1 promotes androgen receptor-dependent gene expression. *Nat. Cell Biol.* **9**: 347-353.*

Wortham B.W., Patel C.N., Oliveira M.A. (2007) Polyamines in bacteria: pleiotropic effects yet specific mechanisms. *Adv. Exp. Med. Biol.* **603**: 106-115.

Wu K., Malik K., Tian L., Brown D., Miki B. (2000) Functional analysis of a RPD3 histone deacetylase homologue in *Arabidopsis thaliana*. *Plant Mol. Biol.* **44**: 167-176.

Wu T., Yankovskaya V., McIntire W.S. (2003) Cloning, sequencing, and heterologous expression of the murine peroxisomal flavoprotein, N^1-acetilated polyamine oxidase. *J. Biol. Chem.* **278**: 20514-20525.*

Yamaguchi K., Takahashi Y., Berberich T., Imai A., Miyazaki A., Takahashi T., Michael A., Kusano T. (2006) The polyamine spermine protects against high salt stress in *Arabidopsis thaliana*. *FEBS Lett*. **580**: 6783-6788.

Yamaguchi K., Takahashi Y., Berberich T., Imai A., Takahashi T., Michael A., Kusano T. (2007) A protective role for the polyamine spermine against drought stress in Arabidopsis. *Biochem. Biophys. Res. Commun.* **352**: 486-490.

Yamane K., Toumazou C., Tsukada Y., Erdjument-Bromage H., Tempst P., Wong J., Zhang Y. (2006) JHDM2A, a JmjC-containing H3K9 demethylase, facilitates transcription activation by androgen receptor. *Cell* **125**: 483-495.

Yamane K., Tateishi K., Klose R.J., Fang J., Fabrizio L.A., Erdjument-Bromage H., Taylor-Papadimitriou J., Tempst P., Zhang Y. (2007) PLU-1 is an H3K4 demethylase involved in transcriptional repression and breast cancer cell proliferation. *Mol. Cell* **25**: 801-812.

Yan L., Loukoianov A., Blechl A., Tranquilli G., Ramakrishna W., SanMiguel P., Bennetzen J.L., Echenique V., Dubcovsky J. (2004) The wheat *VRN2* gene is a flowering repressor down-regulated by vernalization. *Science* **303**: 1640-1644.

Yang M., Gocke C.B., Luo X., Borek D., Tomchick D.R., Machius M., Otwinowski Z., Yu H. (2006) Structural basis for CoREST-dependent demethylation of nucleosomes by the human LSD1 histone demethylase. *Mol. Cell* **23**: 377-387.*

Yang M., Culhane J.C., Szewczuk L.M., Gocke C.B., Brautigam C.A., Tomchick D.R., Machius M., Cole P.A., Yu H. (2007) Structural basis of histone demethylation by LSD1 revealed by suicide inactivation. *Nat. Struct. Mol. Biol.* **14**: 535-539.*

Yesbergenova Z., Yang G., Oron E., Soffer D., Fluhr R., Sagi M. (2005) The plant Mo-hydroxylases aldehyde oxidase and xanthine dehydrogenase have distinct reactive oxygen species signatures and are induced by drought and abscisic acid. *Plant J.* **42**: 862-876.

Yoda H., Yamaguchi Y., Sano H. (2003) Induction of hypersensitive cell death by hydrogen produced through polyamine degradation in tabacco plant. *J. Plant Physiol.* **132**: 1973-1981.

Yoda H., Hiroi Y. Sano H. (2006) Polyamine oxidase is one of the key elements for oxidative burst to induce programmed cell death in tobacco cultured cells. *Plant Physiol*. **142**: 193-206.*

Zhang Y. and Reinberg D. (2001) Transcription regulation by histone methylation: interplay between different covalent modifications of the core histone tails. *Genes Dev.* **15**: 2343-2360.*

Zhao F., Song C.P., He J., Zhu H. (2007) Polyamines improve K^+/Na^+ homeostasis in barley seedlings by regulating root ion channel activities. *Plant Physiol.* **145**: 1061-1072.

Zhou C., Zhang L., Duan J., Miki B., Wu K. (2005) Histone deacetylase 19 is involved in jasmonic acid and ethylene signaling of pathogen response in Arabidopsis. *Plant Cell* **17**: 1196-1204.

* consulted references

Acknowledgements:

I wish to thank Dr. Paraskevi Tavladoraki. She has been like a guide for me during these three years of PhD research and she has given to me the possibility to acquire a good and deep knowledge about Vegetable Biotechnologies.

A grateful thanks goes to Prof. Rodolfo Federico for taking me in to work in his laboratory, for revealing the “tricks of the trade” and for always giving me great ideas.

A special thanks goes to Prof. Riccardo Angelini for always being there for me, for having always listened attentively to my presentations and for his suggestions and fundamental encouragements in the most difficult moments.

Many thanks to Dr. Alessandra Cona for always being there for me, not only as a “neighbor” in the laboratory, but also an invaluable colleague.

Thanks to Dr. Fabio Polticelli and Dr. Viviana Capodaglio for all their collaboration and helpfulness.

I wish to thank Dr. Pasquale Stano for his helpful collaboration, professionalism and for all his kindness too.

I would also like to show my deep gratitude to Prof. Paolo Mariottini and Dr. Manuela Cervelli for their endless support and for always having left their laboratory doors open to me.

A special thanks also goes to Prof. Giancarlo Gibertini, Dr. Livia Leoni and Dr. Giordano Rampioni for having made my stay more pleasant and more interesting.

Of course thanks to all my friends in the laboratory, and particular thanks to Dr. Valerio Giarrizzo whit whom I shared two years of work, Marco Leone for his constant support and kindness, Dr. Alessandra Tisi always there for me, Dr. Annarita Fiorillo for her joy and advice, Dr.Maria Elena Ricci and Dr. Paola Fincato who I knew for a short time but admire for her ongoing hard work.

A very special thanks to Dr. Lucia Pomettini, a person who has always dedicated herself to her research projects with great interest and enthusiasm and who has always helped out in maintaining the smooth running of the laboratory. A valued colleague and a very good friend too.

Thanks to all my friends who have accompanied me and beared with me during these three years of PhD research.

A special thanks to my family for being by my side and supporting me every step along the way.

Finally a very deep and grateful thanks to my boy friend, Tiziano, for all his patience and understanding during these three long years and for helping to make them special.

TABLE OF CONTENTS

MATERIALS AND METHODS

Materials

Put, Spd, Spm, N^1-acetyl-Spm, 4-aminoantipyrine, 3,5-dichloro-2-hydroxybenzenesulfonic acid and horseradish peroxidase were purchased from Sigma-Aldrich-Fluka. Guazatine was obtained from Rhone-Poulenc Agro-Italia. Restriction and DNA-modifying enzymes were purchased from New England Biolabs, Invitrogen, Stratagene and Promega. Other chemicals were obtained from Sigma-Aldrich-Fluka, Bio-Rad and J.T. Baker. *Escherichia coli* strains were purchased from Invitrogen and Novagen. *Pichia Pastoris* strain was purchased from Invitrogen. *Agrobacterium tumefaciens* GV301 (pMP90) strain was kindly provided by Prof. Felice Cervone (University of Rome, "La Sapienza"). All oligonucleotides were synthesized by Invitrogen and PRIMM. [^{14}C]Spd (N-(3-aminopropyl)-[1,4-^{14}C]tetramethylene-1,4-diamine) trihydrochloride (112 mCi/mmol) and [^{14}C]Spermine (N',N'-Bis-(3-aminopropyl)-[1,4-^{14}C]tetramethylene-1,4-diamine) trihydrochloride (113 mCi/mmol) were purchased from GE Healthcare. Synthetic Thermo-Spm was a kind gift from Prof. Armin Geyer, Marburg. The synthetic human histone H3 peptides with specific modifications H3K4me1 (1–21 aa), H3K4me1-S10pho (1–21 aa), H3K4me2 (1–21 aa), H3K9me2 (1–21 aa), and H3K27me2 (21–44 aa) were purchased from Upstate Group Inc. or synthesized by Thermo Scientific. Recombinant HsLSD1 in complex with CoREST was kindly provided by Prof. Andrea Mattevi and Dr. Claudia Binda (University of Pavia, Italy).

<u>Microbiological techniques</u>

Bacterial strains

<u>*Escherichia coli DH5α*</u> (strain for DNA cloning): F- φ80(*lac*Z)ΔM15 Δ(*lac*ZYA-*arg*F) U169 *rec*A1 *end*A1 *hsd*R17 (r_k-, m_k+) *pho*A *sup*E44 λ- *thi*-1 *gyr*A96 *rel*A1. The φ80d*lac*ZΔM15 marker provides α-complementation of the *β-galactosidase* gene from pUC or similar vectors and, therefore, can be used for blue/white screening of colonies on bacterial plates containing Bluo-gal or X-gal.

<u>*E. coli BL21 (DE3)*</u> (strain for recombinant protein expression): F- *ompT* $hsdS_B$ (r_B-m_B-) *gal dcm* (DE3). The DE3 designation means that the strain contains the λDE3 lysogen that carries the gene encoding for T7 RNA polymerase under the control of the *lacUV5* promoter. Thus, isopropyl β-D-thiogalactoside (IPTG), a molecular mimic of allolactose, is required to induce expression of the T7 RNA polymerase. This strain is deficient in both lon and

ompT proteases. The lack of these two key proteases reduces degradation of heterologous proteins.

E. coli BL21 (DE3)pLysS (strain for recombinant protein expression): F- *ompT hsdS*$_B$ (r_B-m_B-) *gal dcm* (DE3) pLysS (Cam^R). Deficient in both lon and ompT proteases. pLysS strains produce T7 lysozyme to reduce basal expression levels of heterologous genes.

E. coli BL21-CodonPlus(DE3)-RIPL (strain for recombinant protein expression): F- *ompT hsdS*$_B$ (r_B-m_B-) *gal dcm* (DE3) *endA* Hte [*argU proL* Cam^R] [*argU ileY leuW* Strep/Spec^R]. Deficient in both lon and ompT proteases. In this strain, the gene that encodes endonuclease I (*endA*), an enzyme that rapidly degrades plasmid DNA, has been inactivated. This strain also contains extra copies of the *argU*, *ileY*, *leuW* and *proL* tRNA genes and thus rescues expression of heterologous proteins from organisms that have either AT- or GC-rich genomes.

E. coli One Shot® OmniMAX™ 2-T1^R (strain for DNA cloning through Gateway technology): F′ {*pro*AB$^+$ *lac*I^q *lac*ZΔM15 *Tn*10(Tet^R) Δ(*ccd*AB)} *mcr*A Δ(*mrr-hsd*RMS-*mcr*BC) φ80(*lac*Z)ΔM15 Δ(*lac*ZYA-*arg*F) U169 *end*A1 *rec*A1 *sup*E44 *thi*-1 *gyr*A96 *rel*A1 *ton*A *pan*D. The OmniMAX™ 2-T1^R strain presents Δ(*ccd*AB) for sensitivity to the toxic effects of the *ccdB* gene product, allowing negative selection of vectors containing the *ccdB* gene.

Agrobacterium tumefaciens GV301 (pMP90) strain: This strain carries a gene for rifampicin resistance on the chromosome and a gene for gentamycin resistance on the helper plasmid.

Bacterial culture media

LB (Luria Bertani) broth: Tryptone (pancreatic digest of casein) 10 g/L, yeast extract 5 g/L and NaCl 10 g/L, pH 7.0. For agar plates, 15 g/L agar was used.

Low salt LB broth: Tryptone (pancreatic digest of casein) 10 g/L, yeast extract 5 g/L and NaCl 5 g/L, pH 7.0. It was used for selection with Zeocin.

Preparation of competent *Escherichia coli* cells

A single colony grown for 16-20 h at 37°C, was inoculated into 4 mL LB broth. After overnight incubation at 37°C with constant shaking at 250 rpm, 1.0 mL of the culture was inoculated into 100 mL LB broth in a sterile 1-L flask and grown at 37°C with shaking at 250 rpm to an A_{600} value of ~ 0.6. The culture was then transferred aseptically into sterile, ice-cold 50 mL falcon tubes

and was cooled to 0°C on ice for 30 min. After centrifugation at 1500 x g for 15 min at 4°C, the supernatant was completely removed and the bacterial pellet was resuspended gently in 25 mL of ice-cold 70 mM $CaCl_2$ and the suspension was stored on ice for 60 min. Cell suspension was centrifuged at 1500 x g for 10 min at 4°C and, after discarding the supernatant, the pellet was resuspended in 5 mL of ice-cold 50mM $CaCl_2$ / 15% glycerol. Aliquots of competent cell suspension (100 μL) were used for transformation or stored at – 80 °C until use.

Transformation of competent *E. coli* cells

Before transformation, frozen aliquots of competent cells were thawed on ice. Plasmid DNA (10 to 50 ng) was added into the tube and the content of the tube was mixed by swirling gently and incubated on ice for 30 min. Following incubation, the tube was heated at 42°C for 2 min (30 s in the case of *E. coli* One Shot® OmniMAX™ 2-T1^R) and then transferred immediately on ice. Cells were chilled for 2 min and, after addition of 800 μL LB broth (250 μL LB broth in the case of *E. coli* One Shot® OmniMAX™ 2-T1^R), the culture was incubated at 37°C for 1 h with constant agitation to obtain antibiotic resistance. Following incubation, cells were plated on LB agar plates containing appropriate antibiotics for selection of transformants and the plates were incubated at 37°C for 16 h.

Conditions for heterologous protein expression in *E. coli*

A single colony of *E. coli* cells (*E. coli* BL21 (DE3), *E. coli* BL21 (DE3)pLysS or *E. coli* BL21-CodonPlus(DE3)-RIPL cells) transformed with the expression construct was inoculated into LB broth containing appropriate antibiotics. After overnight growth at 30°C to an A_{600} value of 0.7 - 1.0, IPTG was added to the culture to a final concentration 0.4 mM to induce recombinant protein expression. The culture was incubated at 25°C or 30°C or 37°C for various time intervals (for time-course studies) or directly at 25°C for 5 h (for recombinant protein purification). The culture was centrifuged at 1500 rpm and the cell paste was used to determine expression levels and/or to purify recombinant protein. To determine total expression level by western-blot analysis, the cell paste was resuspended in loading buffer for SDS-PAGE analysis and lysed by boiling. To determine recombinant protein accumulation in the soluble protein fraction, cells were resuspended in extraction buffer composed of 50 mM Tris-HCl, pH 8.0, 0.5 M NaCl for AtPAO1 (Tavladoraki *et al*., 2006), 100 mM Tris-HCl, pH 8.0, 0.5 M NaCl, 40% (v/v) glycerol for AtPAO2, 100 mM Tris-HCl, pH 8.0, 40% (v/v) glycerol for AtPAO4 and 50 mM Tris-HCl, pH 8.0, 0.1 M NaCl, 10% (v/v) glycerol for AtLSD1. Cells transformed with AtPAO5-pET17 b plasmid were resuspended in 100 mM sodium phosphate (pH 6.0 or pH 7.0) or Tris-HCl (pH 7.0 or pH 8.0). In all

extraction buffers, 1 mM phenylmethanesulfonyl fluoride (PMSF) was added and the cells were disrupted by sonication. After centrifugation at 6500 x g for 30 min at 4 °C, the clear supernatant (bacterial extract) containing the soluble proteins was either analyzed for recombinant protein accumulation by immunoblotting or further processed for recombinant protein purification. The remaining pellet was extensively washed with the extraction buffer, by three to four cycles of sonication/centrifugation to eliminate the whole amount of the soluble recombinant protein and resuspended in SDS-PAGE loading buffer to determine recombinant protein accumulation in inclusion bodies.

Preparation of competent *Agrobacterium tumefaciens* cells

A single colony of *A. tumefaciens* GV301 cells was inoculated into LB broth containing 50 µg mL^{-1} rifampicin and 50 µg mL^{-1} gentamycin. After growth at 28°C with constant shaking at 250 rpm to an A_{600} value of ~ 1.0, the culture was transferred aseptically into sterile, ice-cold 50 mL falcon tubes and was cooled to 0°C on ice for 20 min. Culture was then centrifuged at 2000 x g for 15 min at 4°C, the supernatant was completely removed and the bacterial pellet was resuspended gently in 30 mL of ice-cold sterile water. After centrifugation, the wash procedure was repeated twice. Bacterial pellet was resuspended in 5 mL of ice cold 10% glycerol and after centrifugation the new bacterial pellet was resuspended in 400 µL of ice-cold 10% glycerol. Aliquots of competent cell suspension (40µL) were either used immediately or stored at – 80 °C until use.

Electroporation of competent *A. tumefaciens* cells

One µL of a 150 ng/µL plasmid DNA was added to a microcentrifuge tube containing 40 µL of thawn on ice competent cells. The mixture was incubated on ice for 1 min and then transferred immediately into a prechilled electroporation cuvette (Biorad). The cuvette was then placed into the sample chamber. The electroporation apparatus (microPulser electroporator, Biorad) was set to 2.4 kV, 25 µF and the pulse controller was set to 200 ohms. After application of the pulse to perform the electroporation, the cuvette was immediately removed from the chamber and 1 mL of LB broth was added. The mixture was transferred to a sterile microcentrifuge tube and incubated at 28°C for 3h with constant agitation. After incubation, cells were plated on LB agar plates containing appropriate antibiotics for selection of trasformants.

Pichia pastoris strains

P. pastoris strain X-33 (for recombinant protein expression): It is the wild-type strain. This strain allows the expression of recombinant proteins from vectors with Zeocin resistance as the only selectable marker.

P. pastoris culture media

YPD (Yeast extract Peptone Dextrose) broth: 1% yeast extract, 2% peptone and 2% dextrose (D-glucose).

YPD agar: 1% yeast extract, 2% peptone, 2% dextrose (D-glucose) and 2% agar.

Preparation of competent *P. pastoris* cells

Competent *P. pastoris* cells were prepared following the protocol of the *Pichia* EasyComp™ Kit (Invitrogen). A single colony of *P. pastoris* X-33 cells was inoculated into YPD broth. After growth at 30°C with constant shaking at 250 rpm to an A_{600} value of 0.6 - 1.0, cells were centrifuged at 500 x g for 5 min at room temperature. The supernatant was completely removed and the pellet was resuspended gently in 10 mL of Solution I (Sorbitol solution containing ethylene glycol and DMSO). Aliquots of competent cell suspension were either used immediately or stored at – 80 °C until use.

Transformation of competent *P. pastoris* cells

Transformation of Competent *P. pastoris* cells were obtained following the protocol of the *Pichia* EasyComp™ Kit (Invitrogen). Thawn competent cells were mixed with 3 µg of linearized plasmid. After addition of 1 mL of Solution II (PEG solution), the suspension was mixed by vortexing and incubated at 30°C for a period of 1 hour during which the vortexing was repeated every 15 min. The tube was heated at 42°C for 10 min and the cells were splitted into 2 microcentrifuge tubes. 1 mL of YPD medium was added to each tube and the cells were incubated at 30°C for 1 hour. At the end of incubation, cells were centrifuged at 3000 x g for 5 min at room temperature and the supernatant was completely removed. Cells were resuspended in 500 µL of Solution III (Salt solution) per tube and combined into one tube. After centrifugation, the pellet was resuspended in 100 - 150 µL of Solution III. Transformed competent cells were plated on LB agar plates containing appropriate antibiotics and incubated at 30°C for 2 to 4 days.

Conditions for heterologous protein expression in *P. pastoris*

Expression in shake flasks was performed following the instructions of the pGAPZα A, B, and C *Pichia* expression vectors for constitutive expression and purification of recombinant proteins manual (Invitrogen). A single colony of *P. pastoris* X-33 cells transformed with the AtPAO5-pGAPZαA plasmid was inoculated into YPD broth containing 100 µg mL^{-1} Zeocin. After growth at 30°C with constant shaking at 250 rpm to an A_{600} value of 2 - 4, cells were centrifuged and transferred to a new YPD medium without Zeocin. The culture medium was tested for AtPAO5 expression levels by enzymatic activity assay and western blot analysis at various days post-inoculation.

<u>Techniques for manipulation of nucleic acids</u>

Plasmid vectors

<u>*pDrive Cloning Vector*</u> (Qiagen) (Fig. 1): The pDrive Cloning Vector has a number of useful features designed to facilitate cloning and analysis of PCR products. These include a large number of unique restriction enzyme recognition sites and a T7 and SP6 promoter on either side of the cloning site, allowing *in vitro* transcription of cloned PCR products as well as sequence analysis using standard sequencing primers. In addition, the pDrive Cloning Vector has a phage f1 origin to allow preparation of single-stranded DNA.

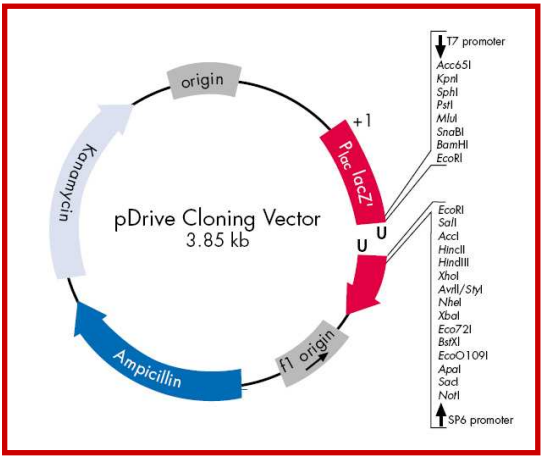

Fig. 1. **Map of pDrive Cloning Vector.** Representation of the linearized pDrive Cloning Vector with U overhangs. The unique restriction endonuclease recognition sites on either side of the cloning site are listed.

The vector allows both ampicillin and kanamycin selection as well as blue/white screening of recombinant colonies. Furthermore, the pDrive Cloning Vector provides highly efficient cloning of PCR products through UA hybridization. The vector is supplied in a linear form with a U overhang at each 3' end, which hybridizes with high specificity to the A overhang of PCR products generated by *Taq* and other non-proofreading DNA polymerases.

pET-17b expression Vector (Novagen) (Fig. 2): The pET-17b vector carries an N-terminal T7 Tag sequence followed by a region of useful cloning sites. Target genes are cloned in pET plasmids under control of strong bacteriophage T7 transcription and expression is induced by providing a source of T7 RNA polymerase in the host cell. Another important characteristic of this vector is its ability to maintain target genes transcriptionally silent in the uninduced state. Target genes are initially cloned using hosts that do not contain the T7 RNA polymerase gene, thus eliminating plasmid instability due to the production of proteins potentially toxic to the host cell. Once established in a non-expression host, target protein expression may be initiated by transferring the plasmid into an expression host containing a chromosomal copy of the *T7 RNA polymerase* gene under l*acUV5* control. Expression is induced by the addition of IPTG or lactose to the bacterial culture or using an autoinduction medium. In addition, this vector contains an ampicillin resistance gene for selection in *E. coli*.

pDONR^{TM} 221 (Invitrogen) (cloning vector) (Fig. 3): It is a Gateway donor vector used for cloning of PCR products. It contains two *att* sites (*att*P1 and *att*P2 sites). *att* sites are bacteriophage λ-derived DNA recombination sequences that permit recombinational cloning of the gene of interest. Between the two *att* sites there is a cassette (Gateway cassette) containing the *ccdB* gene for negative selection of donor/destination vectors in *E. coli* (following recombination and transformation) and a chloramphenicol resistance gene (Cm^R) for counterselection. After the recombination reaction, this cassette is replaced by the gene of interest. This vector presents also *rrnB* T1 and T2 transcription terminators which protect the cloned gene from expression by vector-encoded promoters and M13 Forward and M13 Reverse priming sites for sequencing of the insert. In addition, this vector contains a kanamycin resistance gene for selection in *E. coli* and a pUC origin for replication and maintenance of the plasmid in *E. coli*.

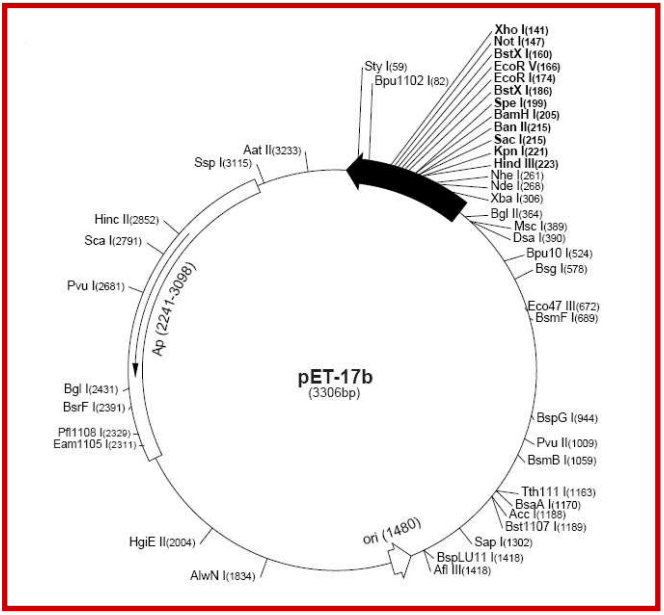

Fig. 2. **Map of pET-17b expression Vector.** Unique sites (except for the two BstX I sites) are shown on the circle map.

<u>*pKGWFS7*</u> (a plant Gateway destination vector for promoter analysis) (Fig. 4): It is a Gateway destination vector for *A. tumefaciens*-mediated plant transformation (Karimi *et al*., 2002). This vector contains an origin for replication in *E. coli* (ColE1) and in *A. tumefaciens* (pVS1), a pBR322 *bom* site for mobilization from *E. coli* to *A. tumefaciens* and the two T-DNA borders: left border (LB) and right border (RB). This vector also possesses a streptomycin and/or spectinomycin resistance gene for plasmid selection in bacteria and a kanamycin resistance marker, under the transcriptional regulation of *nos* promoter and *nos* terminator for selection of transformant plant cells, is present near the left border of the T-DNA. The vector contains also two *att* sites (*att*R1 and *att*R2 sites) which are bacteriophage λ-derived DNA recombination sequences that permit recombinational cloning of the DNA of interest. Between these two *att* sites there is a Gateway cassette which is replaced, after the recombination reaction, by the DNA of interest. Downstream of the Gateway cassette an in frame fusion of the genes for enhanced green-fluorescent protein (*Egfp*) and β-glucuronidase (*gus*) is present under the control of the 35S CaMV terminator (T35S). In this way, after ricombination the *Egfp-gus* fusion is under the control of the promoter of interest.

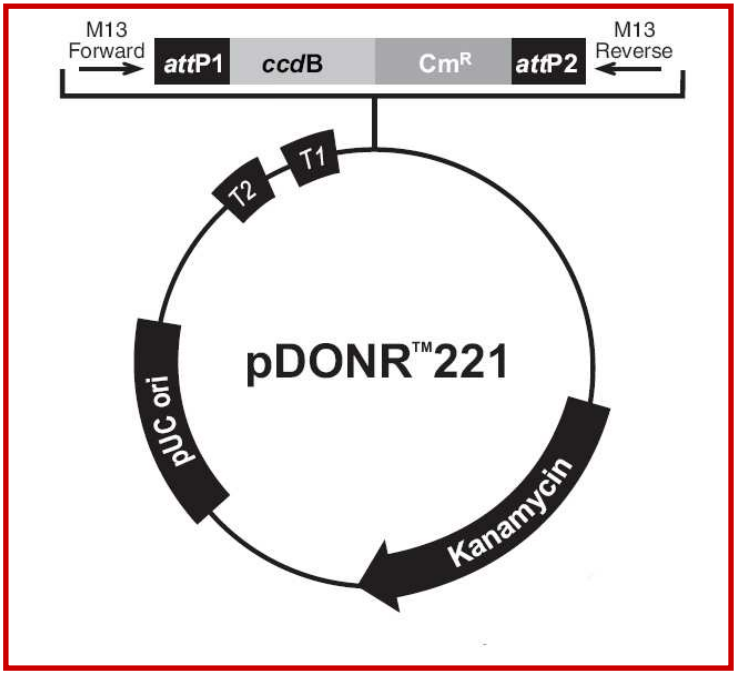

***Fig. 3*. Map of pDONR™ 221 Vector.**

<u>*pK2GW7*</u> (a plant Gateway destination vector for protein overexpression) (Fig. 5): It is a Gateway destination vector for *A. tumefaciens*-mediated plant transformation (Karimi *et al*., 2002). This vector contains an origin for replication in *E. coli* (ColE1) and in *A. tumefaciens* (pVS1), a pBR322 *bom* site for mobilization from *E. coli* to *A. tumefaciens* and the two T-DNA borders: left border (LB) and right border (RB). This vector also possesses a streptomycin and/or spectinomycin resistance gene for plasmid selection in bacteria and a kanamycin resistance marker, under the transcriptional regulation of *nos* promoter and *nos* terminator for selection of transformant plant cells, is present near the left border of the T-DNA. The vector contains also two bacteriophage λ-derived *att* sites (*att*R1 and *att*R2 sites) to permit recombinational cloning of the DNA of interest and removal of the Gateway cassette. The gateway cassette is present between the highly active and constitutive 35S CaMV promoter (p35S) and the T35S to guide the expression of the gene of interest after recombination. Downstream of the p35S, the tobacco mosaic virus (TMV) Ω leader ensures efficient translation of the inserted coding sequences.

pGAPZαA expression vector (Invitrogen) (Fig. 6): The pGAPZαA vector uses the promoter of the gene encoding the glyceraldehyde-3-phosphate dehydrogenase (*GAP*) to constitutively express recombinant proteins in *P. pastoris*. Proteins can be expressed as fusions to a C-terminal peptide containing the *myc* epitope for detection and a poly-His tag for purification on metal-chelating resin. In addition, pGAPZαA produces proteins fused to an N-terminal peptide encoding the *Saccharomyces cerevisiae* α-factor secretion signal. Selection of this vector is based on the dominant selectable marker, Zeocin, which is bifunctional in both *P. Pastoris* and *E. coli*.

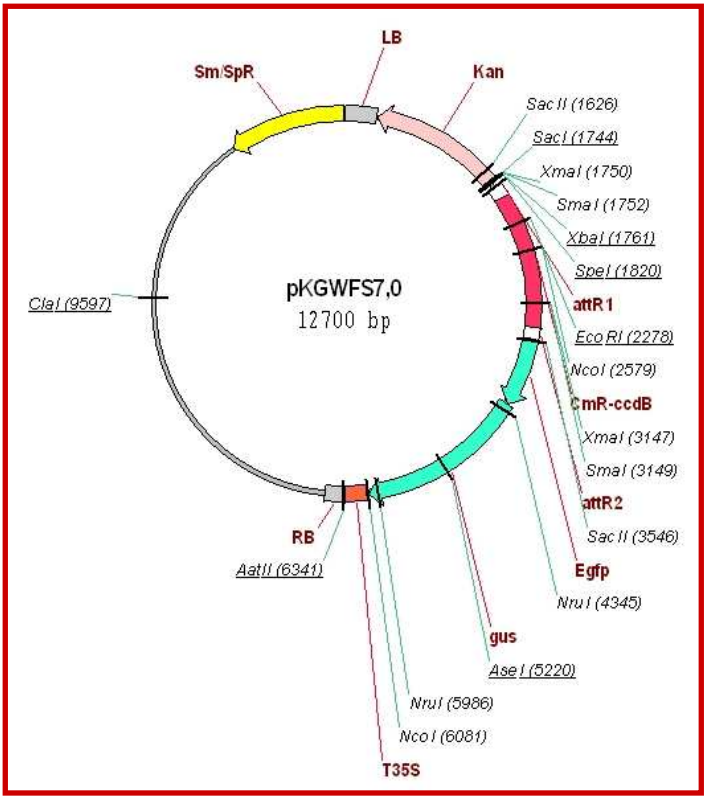

***Fig. 4*. Map of pKGWFS7 plant Gateway destination vector for promoter analysis.**

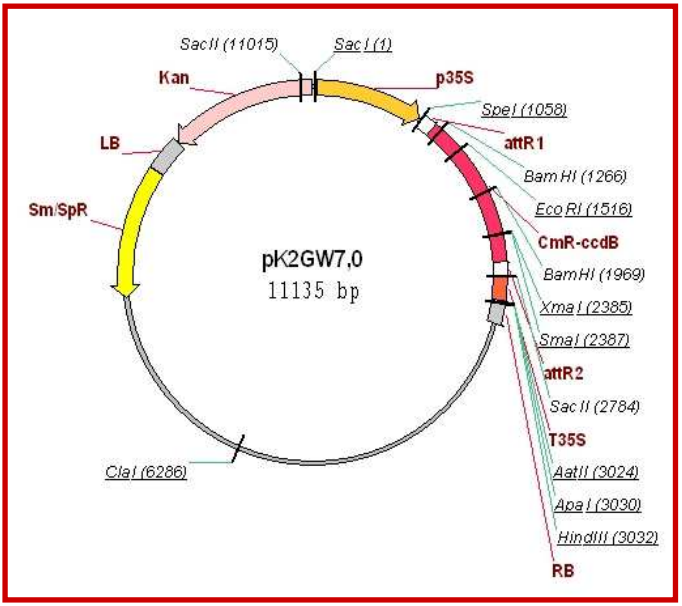

***Fig. 5*. Map of pK2GW7 plant Gateway destination vector for protein overexpression.**

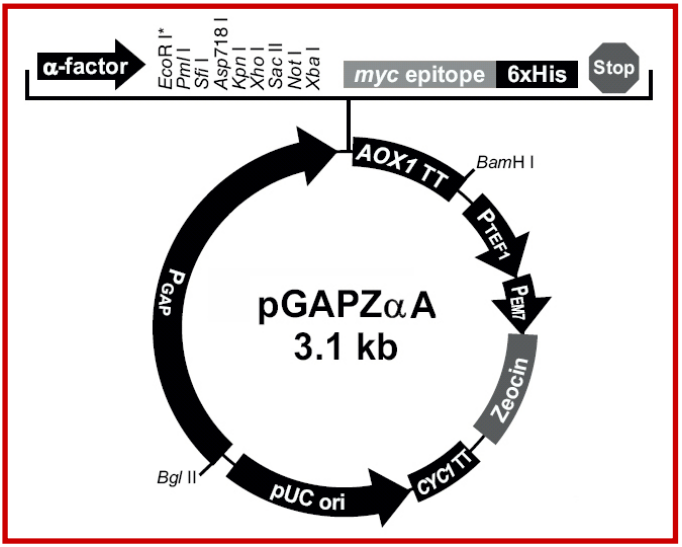

***Fig. 6*. Map of pGAPZαA vector.**

Plasmid DNA preparation

For small- and large-scale preparation of plasmid DNA from *E.coli*, a single colony was inoculated into 4 mL and 100 mL LB broth, respectively, containing appropriate antibiotics. After overnight incubation at 37°C with constant shaking at 250 rpm, the culture was centrifuged at 6000 x g for 15 min at 4°C. Small-scale preparation of plasmid DNA from the bacterial pellet was performed following the instructions of the QIAprep Spin Miniprep Kit (Qiagen), whereas large-scale preparation of plasmid DNA was performed following the instructions of the HiSpeed Plasmid Midi Kit (Qiagen). In the last case, the final plasmid DNA preparation was concentrated by ethanol precipitation. Ethanol precipitation of DNA was performed adding 200 mN NaCl and 2.5 volumes of 100% cold ethanol. After incubation for 1h at -80°C or overnight at -20°C, the precipitated DNA was recovered by centrifugation at 18000 x g for 15 min at 4°C. The DNA pellet was rinsed with cold 80% ethanol, dried at room temperature and resuspended in an appropriate volume of sterile water.

To determine the yield of the plasmid DNA preparation, DNA concentration was determined by both quantitative analysis on an agarose gel and UV spectrophotometry at 260 nm and 280 nm taking into consideration that A_{260} value of 1.0 corresponds to a DNA of 50 μg mL^{-1} and A_{260}/A_{280} should be > 1.6 for adequate purity.

Isolation of total DNA from plant tissue

Isolation of total DNA from leaf tissue was obtained following the protocol of the DNeasy Plant Mini Kit (Qiagen). In detail, fresh leaf tissue from *A. thaliana* (≤ 100 mg wet weight) was ground to a fine powder under liquid nitrogen using a mortar and pestle. The tissue powder and liquid nitrogen were transferred to an appropriately sized tube and the liquid nitrogen was allowed to evaporate. 400 μL AP1 buffer and 4 μL RNase A stock solution (100 mg/mL) were added to the tube containing the tissue powder and the suspension was vigorously mixed by vortexing. After incubation at 65°C for a period of 10 min during which the mixing was repeated 2 or 3 times, 130 μL AP2 buffer were added to the cell lysate. Following incubation for 5 min on ice, the lysate was centrifuged for 5 min at 20000 x g and the supernatant containing the DNA was applied to a QIAshredder Mini spin column placed in a 2 mL collection tube. The column was centrifuged for 2 min at 20000 x g and the flow-through fraction was transferred into a new tube without disturbing the cell-debris pellet. 1.5 volumes of Buffer AP3/E were added to the cleared lysate and the mixture, including any precipitate that may have formed, was transferred into a DNeasy Mini spin column placed in a 2 mL collection tube, which was centrifuged for 1 min at 6000 x g. The flow-through was discarded and the

DNeasy Mini spin column was washed twice with 500 µL AW Buffer. Following centrifugation of the DNeasy Mini spin column to dry it, DNA was eluted with 100 µL AE Buffer pipetted directly onto the DNeasy membrane. After incubation for 5 min at room temperature, the DNA was collected to a new tube following centrifugation.

Alkali treatment for rapid isolation of total DNA from leaf tissue

Rapid isolation of DNA from small amounts of leaf tissue was obtained following a protocol developed for preparing DNA templates for PCR analysis from tomato tissues (Klimyuk *et al*., 1993) and adapting the protocol to Arabidopsis tissues. A young leaf piece of *A. thaliana* was collected into a sterile microcentrifuge tube containing 40 µL of 0.25 M NaOH. The sample was incubated in a boiling water bath for 30 s and subsequently neutralized by addition of 40 µL 0.25 M HCl and 20 µL 0.5 M Tris-HCl pH 8.0, before boiling for a further 2 min. Tissue sample or cell extract was used immediately for PCR analysis or stored at -20°C for several weeks.

Restriction enzyme digestion of DNA

The digestion reactions were prepared according to the manufacturer's instructions and using buffers supplied with the enzymes. For an analytical digestion of plasmid DNA, the reaction was performed using 1 µg of substrate DNA and using a 5-fold excess of restriction enzyme over DNA (5 units per 1 µg DNA) and the reaction mixture was incubated at 25°C or 37°C (depending on the restriction enzyme used) for 1 to 2 h. For large amounts of plasmid DNA, the reaction was performed in a volume of 50 µL on 3-6 µg of substrate DNA using 15 - 30 units of restriction enzyme and the mixture was incubated at the appropriate temperature for 3 h. After incubation, a small aliquot of the reaction was run on a agarose gel to check for digestion.

Agarose gel electrophoresis of DNA

Samples containing DNA were mixed with gel-loading buffer (6X buffer; 0.25% bromophenol blue, 0.25% xylene cyanol FF, 30% glycerol) and loaded on 1% or 1.5% agarose gel made in Tris-acetate-EDTA buffer (40 mM Tris-acetate, 1 mM EDTA, pH 8.0) and containing ethidium bromide (0.5 µg/mL). The electrophoresis run was performed at 100V in Tris-acetate-EDTA buffer and the Gene Ruler™ 1 kb DNA Ladder (Fermentas) was used as molecular weight marker to estimate the size of the separated and ethidium bromide-stained DNA fragments which are visualized as fluorescent bands under UV light.

DNA extraction from agarose gel

DNA fragment of interest visualized as fluorescent band under UV light was extracted and eluted from an agarose gel following the protocol of QIAquick Gel Extraction Kit (Qiagen). The gel slice containing the DNA of interest was transferred into a microcentrifuge tube and its weight was determined. Three volumes of Buffer QG were added to 1 volume of gel (100 mg ~ 100 μL) and the sample was incubated at 50°C for about 10 min or until the gel slice has completely dissolved mixing every 2-3 min. After the gel slice has dissolved completely, 1 gel volume of isopropanol was added. To bind DNA, the mixture was applied to a QIAquick spin column placed in a 2 mL collection tube and the column was centrifuged for 1 min at 18000 x g. The flow-through was discarded and the QIAquick column was washed first with 0.5 mL of Buffer QG and then with 0.75 mL of Buffer PE. Following centrifugation of the empty QIAquick column to dry it, DNA was eluted with EB buffer (10 mM Tris-HCl, pH 8.5) which was added to center of the QIAquick membrane. DNA was collected by centrifugation.

DNA ligation

Ligation reactions were performed using the T4 DNA Ligase (Promega) according to the manufacturer's instructions. In detail, 50 - 100 ng plasmid vector, DNA fragment in a 1:3 molar ratio (vector:insert DNA), 1 μL ligation buffer 10X, 1 μL T4 DNA Ligase (0.5 units) and distilled water to a final volume of 10 μL were added into a sterile microcentrifuge tube and the mixture was incubated overnight at 16°C.

In the case of ligation of a PCR product in the pDrive cloning vector (Qiagen), ligation was performed following the protocol of the PCR Cloning Kit (Qiagen). In detail, 1 μL (50 ng/μL) pDrive cloning vector, DNA fragment in a 1:5 molar ratio (vector:insert DNA), 5 μL ligation master mix 2X and distilled water to a final volume of 10 μL were added into a sterile microcentrifuge tube and the mixture was incubated at 16°C for 2 h.

Polymerase Chain Reaction (PCR)

For DNA cloning, the PCR reaction was carried out with the *Pfu Turbo*® DNA polymerase (Stratagene) in an iCycler thermal cycler (Bio-Rad) with the following parameters: 2 min of denaturation at 95 °C, 30 cycles of 95°C for 1 min, 58 °C for 1 min and 72 °C for 1 min per Kb and 10 min at 72°C for final extension.

For PCR analysis of bacterial colonies and of total DNA from *Atlsd1*, *Atlsd2*, *Atlsd3* and *Atlsd4* mutant seedlings, the PCR reaction was carried out with the Dream*Taq*™ DNA Polymerase (Fermentas) in a iCycler™ Thermal

Cycler (Bio-Rad) with the following parameters: 2-4 min of denaturation at 95 °C, 35 cycles of 95°C for 1 min, 58 °C for 1 min and 72 °C for 1 min per Kb and 10 min at 72°C for final extension.

Primers used for the various PCR performed are indicated in Tables I, II and III.

AtPAO2-His for	5'-GCATATGGAGTCCAGGAAAAACTCTGATCG-3'
AtPAO2-His rev	5'-GCGGCCGCCTAGTGGTGGTGGTGGTGGTGTCCTCCGAGACGA GATATAAGAAGAGGTACAGAGGC-3'
AtPAO4-His for	5'-GCCTCGCATATGGATAAGAAGAAGAATTCGTTTCCAG-3'
AtPAO4-His rev	5'-GGTACGCTCGAGCTAGTGGTGGTGGTGGTGGTGTCCTCCCAT CCTGGAGATTTGGAGAGGCACAG-3'
AtPAO5-His for1	5'-GGCTCCCATATGGCGAAGAAAGCAAGAATTGTTATAATCG-3'
AtPAO5-His rev	5'- GTGTACTGCGGCCGCCTAGTGGTGGTGGTGGTGGTGTCCTCC AAAATTACATTTGTAATGCTTGAGAAG-3
AtPAO5-His for2	5'-GCCTCGGAATTCGCGAAGAAAGCAAGAATTGTTATAATC-3'
AtLSD1-His for	5'-GTCTAGAAATAATTTTGTTTAACTTTAAGAAGGAGATATACAT ATGTCAACAGAGACTAAAGAAACCCGACCC-3'
AtLSD1-His rev	5'-GCTCGAGCTAGTGGTGGTGGTGGTGGTGTCCTCCATCAAAGAT CTGTCGATTCAGTCTTGCAGC-3'

Table I. Sequences of primers used for *AtPAO2, AtPAO4, AtPAO5* and *AtLSD1* cDNAs amplification for cloning in vectors for heterologous expression in *E. coli* and/or *P. Pastoris*. The underlined regions in *AtPAO2-His for*, *AtPAO4-His for* and *AtPAO5-His for1* primers indicate *Nde*I restriction sites, in *AtPAO2-His rev* and *AtPAO5-His rev* primers indicate *Not*I restriction sites, in *AtPAO4-His rev* primer indicate *Xho*I restriction site and in *AtPAO5-His for2* primer indicate *Eco*RI restriction site. The *AtPAO2-His rev*, *AtPAO4-His rev*, *AtPAO5-His rev* and *AtLSD1-His rev* primers were designed to insert the coding sequence for two Gly residues (in orange) followed by a 6-His tag (in blue) prior to the stop codon of the corresponding cDNA.

AtLSD1prom for	5'-GGGGACAAGTTTGTACAAAAAAGCAGGCTGGGTCTTG ATGTCTCCACTACCTGCAG-3'
AtLSD1prom rev	5'-GGGGACCACTTTGTACAAGAAAGCTGGGTAGCTCTAG CTCTGTGTGTGATGATGTGAGTG-3'
overAtLSD1-His for	5'-GGGGACAAGTTTGTACAAAAAAGCAGGCTATGTCAAC AGAGACTAAAGAAACCCGACCC-3'
overAtLSD1-His rev	5'-GGGGACCACTTTGTACAAGAAAGCTGGGTCTAGTGGT GGTGGTGGTGGTGTCCTC-3'
overAtLSD1-HA FLAG for1	5'-CCATACGATGTTCCAGATTACGCTGCTGCTTCAACAGA GACTAAAGAAACCCGACCCG-3'
overAtLSD1-HA FLAG for2	5'-ATGGATTACAAGGATGACGACGATAAGACCAGCTACC CATACGATGTTCCAGATTACGCTGCT-3'
overAtLSD1-HA FLAG for3	5'-GGGGACAAGTTTGTACAAAAAAGCAGGCTATGGATTA CAAGGATGACGACGATAAGACC-3'
overAtLSD1-HA FLAG rev	5'-GGGGACCACTTTGTACAAGAAAGCTGGGTCTAATCAAA GATCTGTCGATTCAGTCTTGCAGC-3'

Table II. Sequences of primers used for *AtLSD1* cDNA and *AtLSD1* promoter amplification for cloning in Gateway destination vectors. The underlined regions in *AtLSD1prom for*, *overAtLSD1-His for*, and *overAtLSD1-HA FLAG for3* primers indicate *att*B1 recombination site and in *AtLSD1prom rev*, *overAtLSD1-His rev* and *overAtLSD1-HA FLAG rev* primers indicate *att*B2 recombination site. In the *overAtLSD1-His rev* primer the coding sequence for 6-His tag is evidenced in blue. O*verAtLSD1-HA FLAG for1*, *overAtLSD1-HA FLAG for2* and *overAtLSD1-HA FLAG for3* primers were designed to insert the coding sequences for the FLAG tag (in red) and the HA tag (in green) downstream of the start codon of the *AtLSD1* cDNA.

AtLSD1-LP	5'-CCCAGCTTTCTCAAGAAACCGCCG-3'
AtLSD1-RP	5'-GATGATGACGCTCTTCTTCTAGCAACTCTAAG-3'
AtLSD2-LP	5'-GTGGGACCTGCTTCTGCCTCTGCGTGCG-3'
AtLSD2-RP	5'-GATAACGTCATGAACCTTTTGCTGCTTC-3'
AtLSD3-LP	5'-CTTATGCCTCGGGCCTTTGCAGATTGAGC-3'
AtLSD4-LP	5'-GTTAATTGTGCGTTCGAATTTGAGAGTTTTG-3'
AtLSD4-RP	5'-CCCTCGGAAATTTTCATCTTCGCAGG-3'
LBb1	5'-GCGTGGACCGCTTGCTGCAACT-3'
Lba1	5'-GATGGTTCACGTAGTGGGCCATCGC-3'
Lb3sail	5'-GAATTTCATAACCAATCTCGATAC-3'

Table III. Sequences of the primers used for the PCR analysis of *Atlsd1, Atlsd2, Atlsd3* and *Atlsd4* mutant seedlings. *Lba1*, *LBb1* and *Lb3 sail* are T-DNA left border-specific primers.

Gateway cloning technology

DNA cloning using the Gateway technology (Hartley *et al.*, 2000) was performed following the procedure of the Gateway® Technology with Clonase™ II manual (Invitrogen). The Gateway system takes advantage of the recombination reactions which involve specific sites (*att* sites) and which enable the bacteriophage λ to integrate and excise itself in and out of a bacterial chromosome. Gateway protocols rely essentially on the BP and LR clonase reactions (Hartley *et al.*, 2000). The BP reaction is catalyzed by the BP Clonase II enzyme mix that consists of the phage integrase and the integration host factor. The BP clonase mix transfers a DNA fragment of interest, for example a PCR product, flanked by two *att*B sites into a donor vector (pDONR) carrying two *att*P sites. After recombination of the matching *att*B and *att*P sites, the DNA fragment is inserted into the donor backbone, resulting in an entry clone, and is flanked by two *att*L sites (Fig. 7). Entry clones are key substrates in the LR reaction that is catalyzed by the LR Clonase II enzyme mix that consists of integrase, integration host factor, and the phage excisionase. The LR clonase mix transfers the DNA fragment of interest flanked by two *att*L sites (in the entry clone) into a destination vector carrying two *att*R sites. After recombination of the matching *att*L and *att*R sites, the DNA fragment of interest is inserted into a novel expression clone and again flanked by *att*B sites (Fig. 7). To enable directional cloning, the Gateway vectors contain engineered variants of the original *att*B, *att*P, *att*L, and *att*R sites so that for example *att*B1 will react specifically with *att*P1, but not with *att*P2, *att*P3. The Gateway Technology permits rapid and highly efficient transfer of DNA sequences into multiple vector systems for protein expression and functional analysis.
The BP reaction was performed using an equimolar amount of a PCR product flanked by two *att*B sites (*att*B-PCR product) and the donor vector (containig the *att*P sites). In particular, 1 μL of pDONR™ vector (150 ng/ μL), 1-7 μL of *att*B-PCR product, 2 μL of BP Clonase™ II enzyme mix and TE Buffer (10 mM Tris-HCl, pH 8.0, 1 mM EDTA) to a final volume of 10 μL were added into a sterile microcentrifuge tube and the mixture was incubated

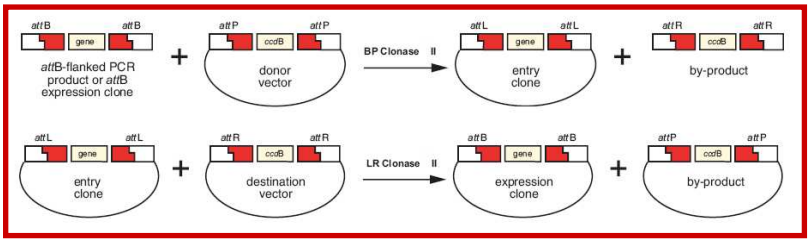

Fig. 7. **Schematic representation of Gateway recombination reactions.**

overnight at 25°C. After incubation, 1 µL of the Proteinase K solution was added to the reaction and the tube was incubated for 10 min at 37°C.

The LR reaction was performed using also in this case an equimolar amount of an *att*L-containing entry clone (in TE, pH 8.0) and an *att*R-containing destination vector and the LR Clonase™ II enzyme mix. The reaction was carried out under the same experimental conditions used for the BP reaction.

The BP and LR reaction products were used to transform One Shot® OmniMAX™ 2-T1^{R} chemically competent *E. coli* cells. At the end, LR reaction products were used to tranform *A. tumefaciens* competent cells.

DNA sequencing

DNA sequencing was performed on double-stranded plasmid DNA using the automated fluorescent dye terminator technique (Perkin-Elmer ABI model 373A).

Isolation of total RNA from plant tissue

Total RNA was isolated from various plant organs (rosette leaves, cauline leaves, stems, inflorescences, silique, and roots) of *A. thaliana* plants using TRIZOL® reagent (Invitrogen) and/or the RNeasy Plant Mini kit (Qiagen) according to the manufacturer's instructions.

For RNA extraction using TRIZOL® reagent (Invitrogen), plant tissue sample was ground to a fine powder under liquid nitrogen using a mortar and pestle and was homogenized using 1 mL of TRIZOL reagent per 100 mg of tissue. The homogenized sample was transferred to an appropriately sized tube and incubated for 5 min at room temperature to permit the complete dissociation of nucleoprotein complexes. 0.2 mL of chloroform per 1 mL of TRIZOL reagent were added to the sample and the tube was vigorously shaked by hand for 15 seconds and was incubated at room temperature for 2 to 3 min. After incubation, the sample was centrifuged at 12000 x g for 15 min at 4°C. The aqueous phase containing RNA was transferred to a fresh microcentrifuge tube and the RNA was precipitated adding to the aqueous phase 0.5 mL of

isopropyl alcohol per 1 mL of TRIZOL reagent used for the initial homogenization. The mixture was then mixed and incubated at room temperature for 10 min. Following incubation, the sample was centrifuged at 12000 x g for 10 min at 4°C and the RNA pellet was washed once with 75% ethanol. After centrifugation, the RNA pellet was briefly dried and resuspended in RNase-free water.

For RNA extraction using the RNeasy Plant Mini kit (Qiagen), plant tissue (100 mg) was ground to a fine powder under liquid nitrogen and transferred to an appropriately sized tube. 450 µL Buffer RLC containing 1% β-Mercaptoethanol were added to the tissue powder and the mixture was vigorously vortexed and was incubated at 56°C for 2 min. The lysate was transferred to a QIAshredder spin column placed in a 2 mL collection tube, and the column was centrifuged for 2 min at full speed. After centrifugation, the supernatant of the flow-through was carefully transferred to a new microcentrifuge tube without disturbing the cell-debris pellet in the collection tube and 0.5 volume of ethanol (96–100%) were added to the cleared lysate. The mixture was immediately mixed by pipetting and was transferred, including any precipitate that may have formed, to an RNeasy spin column placed in a 2 mL collection tube. The column was centrifuged for 15 s at 8000 x g and the flow-through was discarded. The column was washed once with 700 µL of RW1 Buffer and twice with 500 µL Buffer RPE. After centrifugation of the empty column at full speed to dry it, the RNA was eluted with 30-50 µL of RNase-free water and collected to a new tube by centrifugation at 8000 x g for 1 min.

To extract total RNA from the siliques, a method modified from the RNeasy Plant Mini kit was used (Gehrig *et al.*, 2000). In particular, PEG 20,000 mol wt (2% w/v) was added to the RLC buffer containing 1% β-Mercaptoethanol to improve the integrity and yield of isolated RNA.

To determine the yield of the total RNA preparation, RNA concentration was determined by UV spectrophotometry at 260 nm and 280 nm taking into consideration that A_{260} value of 1.0 corresponds to a RNA of 40 µg mL^{-1} and A_{260}/A_{280} should be > 1.8 for adequate purity.

Agarose gel electrophoresis of RNA

For RNA Electrophoresis, agarose gel was prepared using 1% agarose, 1X MOPS running buffer (20 mM MOPS pH 8.0, 1 mM EDTA, 5 mM sodium acetate pH 5.2) and 37% formaldehyde. Samples containing RNA were mixed with 3 volumes of gel-loading buffer (1X MOPS running buffer pH 8.0, 50% formamide, 6% formaldehyde and Bromophenol Blue) and 1 µg ethidium bromide and were incubated at 65°C for 5 min. After incubation, the samples were loaded on agarose gel and the electrophoresis run was performed at 80V

in 1X MOPS running buffer pH 7.0. At the end, the gel was visualized on a UV transilluminator.

Reverse Transcription Polymerase Chain Reaction (RT-PCR) and Semiquantitative RT-PCR

RNA samples were treated with RNase-free DNase I (Invitrogen) to avoid amplification from genomic DNA following the manufacturer's instructions. The first cDNA strand was synthesized from total RNA following the protocol of the the SuperScript III first-strand synthesis system for RT-PCR (Invitrogen) and using random primers (random hexamers). Each RNA/primer mixture was prepared adding 1-8 μL of total RNA (up to 5 μg of total RNA), 1 μL of random hexamers (50 ng/μL), 1 μL of 10 mM dNTP mix and RNase-free water to a final volume of 10 μL. The mixture was incubated at 65°C for 5 min and was then placed on ice for at least 1 min. For each RNA/primer mixture, a cDNA synthesis mix containing 2 μL of 10X RT buffer, 4 μL of 25 mM $MgCl_2$, 2 μL of 0.1 M DTT, 1 μL of RNaseOUT (40 U/μL) and 1 μL SuperScript III RT (200 U/μL) was prepared. The cDNA synthesis mix (10 μL) was added to each RNA/primer mixture and the cDNA synthesis was carried out in a iCycler™ Thermal Cycler (Bio-Rad) with the following parameters: 10 min at 25°C, 50 min at 50°C and 5 min at 85°C. After chilling on ice, 1 μL of RNase H was added to the reaction. Following incubation for 20 min at 37°C, the mixture was stored at -20°C or immediately used for PCR.

For RT-PCR analysis of total RNA from *Atlsd1*, *Atlsd2* and *Atlsd3* mutant seedlings, the PCR reaction was carried out with the Dream*Taq*™ DNA Polymerase (Fermentas) in a iCycler™ Thermal Cycler (Bio-Rad) with the following parameters: 2 min of denaturation at 95 °C, 35 cycles of 95°C for 1 min, 58 °C for 1 min and 72 °C for 1 min per Kb and 10 min at 72°C for final extension.

For semiquantitative RT-PCR analysis of *AtLSD* genes in various Arabidopsis organs, aliquots of reverse-transcribed RNA were amplified by 25, 28, 30, 35, or 40 PCR cycles. PCR amplification was carried out with the BIOTAQ DNA polymerase (Bioline) in a iCycler™ Thermal Cycler (Bio-Rad) with the following parameters: 1 min of denaturation at 94 °C, annealing at 58 °C and extension at 72 °C for 1 min. To confirm equal amounts of RNA among the various samples, *UBQ5* expression was used. Results at the exponential phase (usually at 28 cycles for *AtLSD1*, *AtLSD2* and *AtLSD3*, at 30 cycles for *AtLSD4*, and at 25 cycles for *UBQ5*) were analyzed.

Primers used for semiquantitative RT-PCR analysis are shown in Table IV.

AtLSD1for	5'-CAACAGAGACTAAAGAAACCCGACC-3′
AtLSD1rev	5′-CGGCGGTTTCTTGAGAAAGCTGGG-3′
AtLSD2for	5'-CCGAGGAGGAACAGGAG AAAAGTAAG-3'
AtLSD2rev	5'-AGTACCCTCTTCAGGAATATAAGGAGCAA-3'
AtLSD3for	5'-GCACCAAAGAAACGAAGGAGAGGACG-3'
AtLSD3rev	5′-GCCGAATCTAAGAGACTACTACAATGTTTAGGAATC-3′
AtLSD4for	5′-CAGCGCCAGGGTTTTTCTGTAACC-3′
AtLSD4rev	5′-TCTCAGCCGTTGAAGGCCATATTCT-3′
UBQ5for	5′-GGAAGAAGAAGACTTACACC-3′
UBQ5rev	5′-AGTCCACACTTACCACAGTA-3′

Table IV. Sequences of primers used for semiquantitative RT-PCR analysis of *AtLSD* genes in various Arabidopsis organs.

Plant manipulation

Plant material and growth conditions

The Columbia (Col-0) ecotype of *A. thaliana* was used as the wild-type. *Atlsd1*, *Atlsd2* and *Atlsd3* mutants were obtained from the SALK Institute (SALK_142477.31.30x, SALK_135831.43.30.x and SALK_015053.35.80.x, respectively; Alonso *et al.*, 2003). *Atlsd4* mutant was obtained from the SAIL collection (SAIL_640_B10; Sessions *et al*., 2002). Insertion mutant information was obtained from the SIGnAL website at http://signal.salk.edu. Plants were grown in soil and/or *in vitro* in a growth chamber at a temperature of 23°C under long-day conditions (16 h of light and 8 h of dark) and 75% RH.
For *in vitro* growth, seeds were surface sterilized by washing first with 70% (v/v) ethanol for 2 min and then with 50% bleach containing 0.2% (v/v) Triton X-100 for 10 min. After rinsing several times with sterile water, seeds were sown in Petri dishes containing ½ x Murashige and Skoog (MS) medium, including Gamborg B5 vitamins (Sigma-Aldrich-Fluka), supplemented with 2% (w/v) sucrose and 0.8% (w/v) plant agar (Duchefa). Plates were placed in horizontal or vertical position in the growth chamber.

For plant transformation, plants were planted in moistened potting soil. To prevent the soil in larger pots from falling into inoculation medium, soil was mounded slightly above the rim of plant containers, seeds were planted and soil was then covered with tulle (veil) fabric and secured by a rubber band. To obtain more floral buds per plant, inflorescences were clipped after most plants had formed primary bolts, relieving apical dominance and encouraging synchronized emergence of multiple secondary bolts. Plants were transformed when most secondary inflorescences were about 1-10 cm tall (4-8 days after clipping).

Protoplast preparation

Arabidopsis leaf tissues were incubated at 25 °C for 2.5-3 h with gentle shaking at 50-75 rpm in enzymatic solution containing 2% Cellulase, 0.25% Macerozyme R-10 and Driselase 0,5% in K_3 medium (B5 medium including Vitamins, 136.92 g/L sucrose, 250 mg/L xylose, 250 mg/L NH_4NO_3, 750 mg/L $CaCl_2 \cdot 2H_2O$, 63.3 mg/L $CaHPO_4 \cdot 2H_2O$, 25.35 mg/L $NaH_2PO_4 \cdot 2H_2O$, 1 mg/L NAA, 0.2 mg/L 6-BAP, 0.1 mg/L 2,4-D, pH 5.6). The isolated protoplasts were filtered through a 88µm nylon mesh and centrifuged for 5 min at 100 x *g*. The pelleted protoplasts were gently resuspended and washed two times with washing buffer (9 g/L NaCl, 18.4 g/L $CaCl_2$, 0.4 g/L KCl, 1.0 g/L glucose). The protoplasts were resuspended to 1 x 10^5 cells/mL in K_3 medium.

Transformation of *A. thaliana* plants

A. thaliana plant transformation was performed using the floral dip method. *A. tumefaciens* GV301(pMP90) cells transformed with the expression construct of interest were grown at 28°C with constant shaking to stationary phase in LB broth containing appropriate antibiotics. Cells were harvested by centrifugation at 5500 x g for 20 min at room temperature and then resuspended in infiltration medium (5.0% sucrose and 0.05% Silwet L-77) to a final A_{600} of approximately 0.8 prior to use.

For floral dip, the inoculation medium was added to a beaker, plants were inverted into this suspension such that all above-ground tissues were submerged, and plants were then removed after 1 min of gentle agitation. Dipped plants were then placed in a plastic tray and covered with a tall clear-plastic dome to maintain humidity. Plants were left in a low light or dark location overnight and returned to the growth chamber the next day; care was taken to keep domed plants out of direct sunlight. After removing the dome, plants were grown for a further 3-5 weeks until siliques were brown and dry, keeping the bolts from each pot together and separated from neighboring pots using tape and/or wax paper. Seeds were harvested and stored in microfuge tubes and kept at 4°C. For selection of transformants, sterilized seeds were plated on selection plates containing ½ x MS medium, 1% (w/v) sucrose, 0.8% (w/v) plant agar and 50 µg mL^{-1} kanamycin monosulfate. Petri plates were placed in the growth chamber and transformants were identified as kanamycin-resistant seedlings producing green leaves and well-established roots within the selective medium. Transformants were grown to maturity by transplanting, preferably after the development of 3-5 adult leaves, into heavily moistened potting soil.

Biochemical techniques

Protein purification

Recombinant AtPAO2, AtPAO4 and AtLSD1 were purified from bacterial extracts by affinity chromatography using a Ni^{2+}-charged resin (Amersham Biosciences). In detail, bacterial extracts containing the recombinant proteins were applied to the Ni^{2+}-charged resin equilibrated in extraction buffer (see Conditions for heterologous protein expression in *E. coli*). The resin was then washed first with 10 volumes of extraction buffer and then with 100 mM Tris-HCl, pH 8.0, 40% (v/v) glycerol for AtPAO2 and AtPAO4 or with 50 mM Tris-HCl, pH 8.0, 50 mM NaCl, and 10% (v/v) glycerol for AtLSD1.

Recombinant AtPAO2 and AtPAO4 were eluted with 100 mM Tris-HCl, pH 8.0, 40% (v/v) glycerol, 300 mM imidazole and immediately dialysed against 100 mM Tris-HCl, pH 8.0, 40% (v/v) glycerol using centrifugal filter devices (Millipore).

Recombinant AtLSD1 was eluted with 50 mM Tris-HCl, pH 8.0, 50 mM NaCl, 10% (v/v) glycerol, and 100 mM imidazole. The fractions enriched in recombinant AtLSD1 were pooled, diluted 5-fold with 50 mM Tris-HCl, pH 8.0, and 10% (v/v) glycerol, and chromatographed on a HiTrap heparin HP column (Amersham Biosciences) equilibrated in 50 mM Tris-HCl, pH 8.0, 10 mM NaCl, and 10% (v/v) glycerol. Elution was performed with a nonlinear gradient of NaCl (50 mM-2M) in Tris-HCl, pH 8.0, and 10% (v/v) glycerol. AtLSD1-containing fractions (fractions of 200 or 400 mM NaCl) were dialyzed against 50 mM Tris-HCl, pH 8.0, and 10% (v/v) glycerol and concentrated using centrifugal filter devices (Millipore).

Recombinant AtPAO1 was purified from bacterial extract by affinity chromatography using guazatine (a good competitive PAO inhibitor; Federico *et al*.,2001; Cona *et al*., 2004; Bianchi *et al*., 2006) bound on CNBr-activated Sepharose 4B (Amersham Biosciences). In detail, bacterial extract was applied to the guazatine-Sepharose 4B resin prepared as described by Tavladoraki *et al*. (2006). After binding, the column was washed with 50 mM Tris-HCl, 0.5 M NaCl, pH 8.0, and with 50 mM Tris-HCl, pH 7.0. The recombinant AtPAO1 was eluted with 50 mM 1,12-diaminododecane in 50 mM Tris-HCl, pH 7.0, and immediately dialyzed against 50 mM Tris-HCl, pH 8.0, using centrifugal filter devices (Millipore).

Recombinant proteins were quantified by absorption spectroscopy using an extinction coefficient of 10790 M^{-1} cm^{-1} at 458 nm and stored at 4 °C. The purity of the recombinant enzyme was determined by SDS-PAGE analysis and by the ratio A_{280}/A_{458}.

SDS PAGE and Western blot analysis

SDS-PAGE was carried out according to the method of Laemmli (1970). Recombinant proteins from bacterial extracts were subjected to SDS-PAGE (10% polyacrylamide) and analyzed either by staining with Coomassie Brilliant Blue or by Western blot using a mouse anti-6-His monoclonal antibody (Sigma-Aldrich-Fluka) and a rabbit anti-mouse antibody coupled to horseradish peroxidase (Amersham Biosciences). In the latter case, proteins were transferred to a nitrocellulose membrane (Schleicher & Schuell) using a Mini Trans-Blot apparatus (Bio-Rad), following the manufacturer's instructions. The detection of the labeled proteins was done with a chemiluminescence kit (Boehringer-Mannheim).

Circular dichroism spectroscopy

CD spectra were recorded at 25 °C using a Jasco J-600 spectropolarimeter and quartz cells having 0.05 cm path length. Recombinant AtLSD1 was at a concentration of 0.3 mg/mL in 15 mM Tris-HCl and 3% (v/v) glycerol, pH 8.0. Instrumental ellipticity was converted into mean residue molar ellipticity [θ] (deg cm^2 $dmol^{-1}$) after spectrophotometric determination of the protein concentration. For each sample, nine CD spectra in the far-UV region (198–250 nm) were recorded and averaged. Secondary structures were estimated by using CONTIN, K2D, and SELCON3 algorithms provided by the free software Dicroprot2000 (Deleage and Geourjon, 1993).

Determination of enzyme catalytic parameters

The catalytic parameters (K_m and k_{cat}) of recombinant AtPAO1, AtPAO2 and AtPAO4 and recombinant AtLSD1 and HsLSD1-CoREST were determined using purified proteins through an enzymatic activity assay based on a horseradish peroxidase-coupled reaction (Holt and Baker, 1995; Tavladoraki *et al*., 2006). In detail, the catalytic parameters of recombinant proteins were determined by following spectrophotometrically the formation of a pink adduct (ε_{515} = 2.6 x 10^4 $M^{-1}cm^{-1}$), as a result of oxidation of 4-aminoantipyrine and 3,5-dichloro-2-hydroxybenzesulfonic acid catalyzed by horseradish peroxidase in the reaction buffer at 25°C. The reaction buffer was 100 mM Tris-HCl buffer, pH 7.5 for AtPAO2 and AtPAO4, 100 mM Tris-HCl buffer, pH 8.0 for recombinant AtPAO1 and 50 mM Tris-HCl and 30% glycerol, pH 8.0 (except as otherwise indicated) for recombinant AtLSD1 and HsLSD1-CoREST. For recombinant AtLSD1 and HsLSD1-CoREST, k_{cat} values were calculated using saturating concentrations of methylated H3K4 peptides (147 μM) and keeping the O_2 concentration constant at the air-saturated level (apparent k_{cat}). K_m values were determined from Michaelis-

Menten plots and nonlinear least-squares fitting of data was performed using Graphpad Prism software.

Studies of the pH dependence of recombinant AtPAO2, AtPAO4 and AtLSD1 activity were conducted in 100 mM Tris-HCl buffer (for pH range 7.0–9.5) or in 100 mM sodium phosphate buffer (for pH range 5.0-7.5) at 25°C.

Histone demethylation assay by western blot analysis

H3K4me2 peptide (0.29 mM) was incubated with purified recombinant AtLSD1 (0.02 mM) in 50 mM Tris-HCl, pH 8.0, and 30% (v/v) glycerol for 2 h at room temperature. The demethylase activity of AtLSD1 was evaluated by Western blot analysis using a rabbit anti-H3K4me2 (Upstate Group Inc.) methylation-specific antibody. For Western blot analysis, proteins were separated by SDS-PAGE (15% polyacrylamide), electrophoretically transferred to a polyvinylidene difluoride (PVDF) membrane (Immobilon PSQ; Millipore) at 150 mA for 45 min, and incubated first with the rabbit anti-H3K4me2 methylation-specific antibody and then with a goat anti-rabbit antibody coupled to horseradish peroxidase (Vector Laboratories, Inc.). The detection of the labeled proteins was done with a chemiluminescence kit (Boehringer-Mannheim).

High-Performance Liquid Chromatography analysis of polyamines

Analysis of the polyamine products of Spm and Spd oxidation by recombinant AtPAO2 and AtPAO4 was performed as described by Tavladoraki *et al*. (2006). In detail, a reaction mixture containing purified recombinant AtPAO2 or AtPAO4 at 1 nM final concentration and 0.2 mM Spm or Spd in 100 mM Tris-HCl, pH 7.5 was prepared and aliquots were analyzed for polyamine content at various time intervals after addition of an equal volume of 5% (w/v) perchloric acid (PCA) containing 0.15 mM 1,6-diaminohexane (Dah) as an internal standard. Polyamines were derivatizated with dansyl chloride according to Smith and Davies (1985) and separated by High-Performance Liquid Chromatography (HPLC) (Spectra SystemP 2000; ThermoFinnigan) on a reverse-phase C18 column (Spherisorb S5 ODS2, 5-µm particle diameter, 4.6 x 250 mm) using a discontinued **solution A** [acetonitrile, methanol and water in a ratio 3:2:5 (v:v)] to **solution B** [acetonitrile and methanol in a ratio 3:2 (v/v)] gradient (78% solution A for 5 min, 78%-36% solution A in 42 min, 36%-20% in 3 min, 20%-10% in 10 min, 10%–78% in 10 min at a flow rate of 1.0 mL min^{-1}). Eluted peaks were detected by a spectrofluorometer (Spectra System FL 3000; excitation 365 nm, emission 510 nm), recorded, and integrated by an attached computer using Thermo Finnigan Chrom-Card 32-bit software. To establish retention times, a reference solution containing Dap, Put, Dah, Spd and Spm treated as above was first analyzed.

Analysis of polyamine content of Arabidopsis protoplasts using Thin-Layer Chromatography

Protoplasts prepared from *A. thaliana* leaves and resuspended in K_3 medium (at a final concentration of 1.5 x 10^5 protoplasts/mL) were incubated with 7 µM of [^{14}C]Spd or [^{14}C]Spm. For inhibition experiments, protoplasts were in parallel incubated with 50 µM guazatine. Aliquots of protoplasts were removed at various time intervals and homogenized with 5% (v/v) PCA containing 0.15 mM Dah. Polyamines were derivatized by dansyl chloride, separated by thin layer chromatography (TLC) in a solvent system of chloroform/triethylammine (25:2, v/v) and visualized under UV light. To detect radioactivity, the silica gel TLC-plates (AL SIL G, Whatman) were exposed to radiographic film for 2 to 4 days.

SUPPLEMENTARY FIGURES

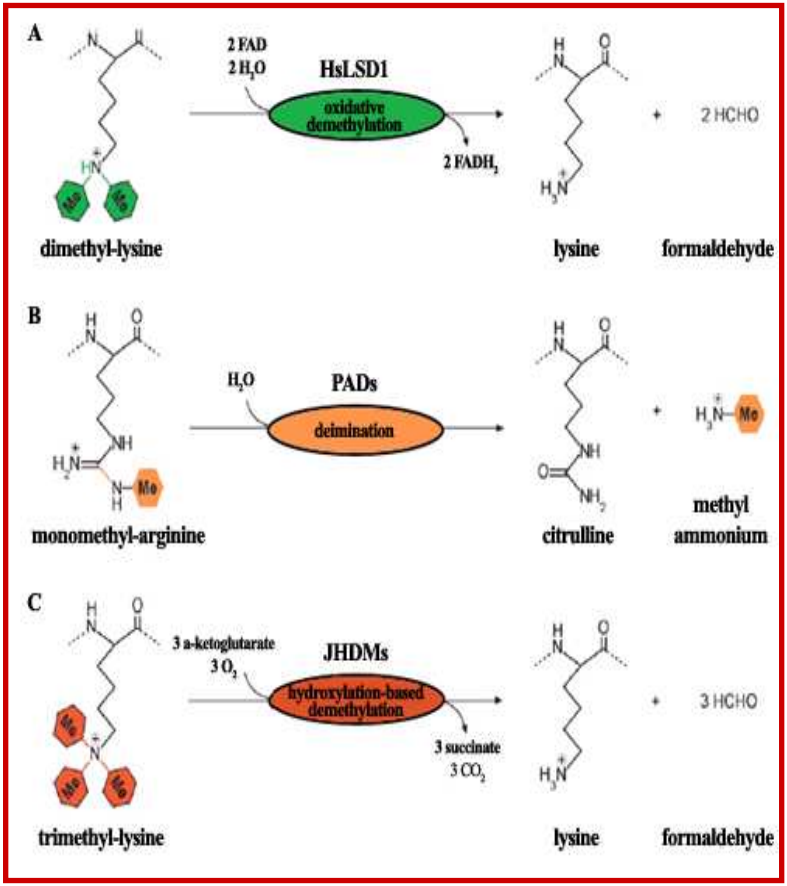

***Supplementary Fig. 1*. Enzymatic Mechanisms to Remove Histone Methylation.** (A) Human lysine-specific demethylase 1 (HsLSD1) specifically acts on mono- and dimethylated Lys4 of histone H3 in a FAD dependent oxidative reaction to form an imine intermediate that is hydrolyzed to produce formaldehyde and the unmodified lysine. The formation of the imine intermediate requires a protonated nitrogen (shown in green), therefore restricting this reaction to mono- and di-methylated lysine substrates. (B) Arg methylation can be by cleaved at the guanidino C-N bond (shown in orange) by peptidyl-Arg demethylases (PADs) to generate citrulline and methyl-ammonium. (C) Jumonji C histone demethylases (JHDMs) remove methyl groups on lysine residues through a hydroxylation-based reaction (Tsukada *et al*., 2005). JHDMs catalytic mechanism, not requiring a protonated nitrogen for activity, permits demethylation of trimethylated Lys residues. Figure modified by Kubicek and Jenuwein, 2004.

```
AtPAO1          -------------------------MSTASVIIIGAGISGISAAKVLVENGVED--VLIL 33
AtPAO2          MESRKNSDRQMRRANCFSAGERMKT-RSPSVIVIGGGFGGISAARTLQDASFQ---VMVL 56
AtPAO3          MESGGKTNRQLRKAICVSTDEKMKKKRSPSVIVIGGGMAGISAARTLQDASFQ---VVVL 57
AtPAO4          MDKKKNSFPDNLPEGTISELMQKQNNVQPSVIVIGSGISGLAAARNLSEASFK---VTVL 57
ATPAO5          -----------------------MAKKARIVIIGAGMAGLTAANKLYTSSNNTFELSVV 36
ZmPAO           -----------------------ATVGPRVIVVGAGMSGISAAKRLSEAGITD--LLIL 34

AtPAO1          EATDRIGGRIHKQNFGDVPVELGAGWIAGVGGKESNPVWELA--------SRFNLRTCFS 85
AtPAO2          ESRDRIGGRVHTDYSFGFPVDLGASWLHGVC--KENPLAPVIGRLGLPLYRTSGDNSVLY 114
AtPAO3          ESRDRIGGRVHTDYSFGFPVDLGASWLHGVC--KENPLAAVIGRLGLPLYRTSGDNSVLY 115
AtPAO4          ESRDRIGGRIHTDYSFGCPVDMGASWLHGVS--DENPLAPIIRRLGLTLYRTSGDDSILY 115
ATPAO5          EGGSRIGGRINTSEFSSEKIEMGATWIHGIGGSPVYRIAKETGSLVSDEPWECMDSTIDK 96
ZmPAO           EATDHIGGRMHKTNFAGINVELGANWVEGVNGGKMNPIWPIVN-------STLKLRNFRS 87

AtPAO1          DYTNAR-------------FNIYDRSGKIFPTGIAS------DSYKKAVDSAILKLKS-- 124
AtPAO2          DHDLES-------------YALFDMDGNQVPQELVTQIG---VTFERILEEINKVRDEQD 158
AtPAO3          DHDLES-------------YALFDKAGNQVSQELVTKVG---ENFEHILEEICKVRDEQD 159
AtPAO4          DHDLES-------------YGLFDMHGNKIPPQLVTKVG---DAFKRILEETEKIRDETA 159
ATPAO5          AKTFAEGGFEIEPSIVESISGLFTALMELAQGKEISQSDADLSRLAHIYETATRVCSKGS 156
ZmPAO           DFDYLA-------------QNVYKEDGGVYDEDYVQKRIELADSVEEMGEKLSATLHASG 134

AtPAO1          ---LEAQCSG-------QVAEEAPSSPKTPIELAIDFILHDFEMAE---------VEPIS 165
AtPAO2          ADISISQAFS-------IVFSRKP-------ELRLEGLAHNVLQWYVCRMEGWFAADAET 204
AtPAO3          EDMSIAQAFS-------IVFKRNP-------ELRLEGLAHNVLQWYLCRMEGWFAADAET 205
AtPAO4          NDMSVLQGIS-------IVLDRNP-------ELRQEGMAYEVLQWYLCRMEAWFAVDANL 205
ATPAO5          STSVGSFLKSGFDAYWDSISNGGEEGVKGYGKWSRKSLEEAIFTMFSNTQRTYTSADELS 216
ZmPAO           RDDMSILAMQ-------RLNEHQPNGPATPVDMVVDYYKFDYEFAEPPRVTSLQNTVPLA 187

AtPAO1          TYVDFGEREF-LVADERGYECLLYKMAEEFLVTS--HGNILDYRLKLNQVVREVQQSRNG 222
AtPAO2          ISAKCWDQEE-LLPGGHGLMVRGYRPVINTLAKG------LDIRVG-HRVTKIVRRYNG- 255
AtPAO3          ISAKCWDQEE-LLPGGHGLMVRGYRPVINTLSKG------LDIRLS-HRITKISRRYSG- 256
AtPAO4          ISLKCWDQDE-CLSGGHGLMVQGYEPVIRTIAKD------LDIRLN-HRVTKVVRTSNNK 257
ATPAO5          TLDFAAESEYQMFPGEEITIAKGYLSVIHHLASV-----LPQGVIQLNRKVTKIEWQSNE 271
ZmPAO           TFSDFGDDVY-FVADQRGYEAVYYYLAGQYLKTDDKSGKIVDPRLQLNKVVREIKYSPGG 246

AtPAO1          VVVKTEDGSVYEANYVIVSASIGVLQS----DLLSFQPLLPRWKTEAIQKCDVMVYTKIF 278
AtPAO2          VKVTTENGQTFVADAAVIAVPLGVLKS----GTIKFGPKLPEWKQEAINDLGVGIENKII 311
AtPAO3          VKVTTEKGDTFVADAAVIALPLGVLKS----GMITFEPKLPQWKQEAINDLGVGIENKII 312
AtPAO4          VIVAVEGGTNFVADAVIITVPIGVLKA----NLIQFEPELPQWKTSAISGLGVGNENKIA 313
ATPAO5          VKLHFSDGSVVFADHVIVTVSLGVLKAGIETDAELFSPPLPDFKSDAIRRLGYGVVNKLF 331
ZmPAO           VTVKTEDNSVYSADYVMVSASLGVLQS----DLIQFKPKLPTWKVRAIYQFDMAVYTKIF 302

AtPAO1          LKFPQCFWPCGPGQEFFIYAHEQRG-------YFTFWQHMENAYPGSNI----------K 321
AtPAO2          LHFEKVFWP---KVEFLGVVAETSY-------GCSYFLNLHKAT-GHPVLVYMPAGQLAK 360
AtPAO3          LNFDNVFWP---NVEFLGVVAETSY-------GCSYFLNLHKAT-SHPVLVYMPAGQLAR 361
AtPAO4          LRFDRAFWP---NVEFLGMVAPTSY-------ACGYFLNLHKAT-GHPVLVYMAAGNLAQ 362
ATPAO5          VEMSQRKFP---SLQLVFDREDSEFRFVKIPWWMRRTATITPIHSNSKVLLSWFAGKEAL 388
ZmPAO           LKFPRKFWPEGKGREFFLYASSRRG-------YYGVWQEFEKQYPDANVLLVTVTDEESR 355

AtPAO1          RVEAQSDQETMKEAMSVL-----RDMF-GATIPYA-------------TDILVPRWWNNR 362
AtPAO2          DIEKMSDEAAANFAVLQL-----QRILPDALPP---------------VQYLVSRWGSDV 400
AtPAO3          DIEKKSDEAAANFAFSQL-----QKILPDASSP---------------INYLVSRWGSDI 401
AtPAO4          DLEKLSDEATANFVMLQL-----KKMFPDAPDP---------------AQYLVTRWGTDP 402
ATPAO5          ELEKLTDEEIKDAVMTTISCLTGKEVKNDTAKPLTNGSLNDDDEAMKITKVLKSKWGSDP 448
ZmPAO           RIEQQSDEQTKAEIMQVL-----RKMFPGKDVPDA-------------TDILVPRWWSDR 397

AtPAO1          FQRGSYSNYPMISDNQLLQNIKAPVGRIFFTGEHTSEKFSGYVHGGYLAGIDTSKSLLEE 422
AtPAO2          NSMGSYSYDIVGKPHDLYERLRVPVDNLFFAGEATSSSFPGSVHGAYSTGLMAAEDCRMR 460
AtPAO3          NSLGSYSYDIVNKPHDLYERLRVPLDNLFFAGEATSSSYPGSVHGAYSTGVLAAEDCRMR 461
AtPAO4          NTLGCYAYDVVGMPEDLYPRLGEPVDNIFFGGEAVNVEHQGSAHGAFLAGVSASQNCQRY 462
ATPAO5          LFRGSYSYVAVGSSGDDLDAMAEPLPKINKKVGQVNGHDQAKVHELQVMFAGEATHRTHY 508
ZmPAO           FYKGTFSNWPVGVNRYEYDQLRAPVGRVYFTGEHTSEHYNGYVHGAYLSGIDSAEILINC 457

AtPAO1          MKQSLLLQPLLAFTESLTLTHQKPNNSQIYTNVKFISGTS 462      (45%)
AtPAO2          VLERYGELDLF--QPVMGEE---GPASVPLLISRL----- 490      (23%)
AtPAO3          VLERYGEL-----EHEMEEE---APASVPLLISRM----- 488      (24%)
AtPAO4          IFERLGAWEKLKLVSLMGNSDILETATVPLQISRM----- 497      (24%)
ATPAO5          STTHGAYYSGLREANRLLKHYKCNF--------------- 533      (22%)
ZmPAO           AQKKMCKYHVQGKYD------------------------- 472      (100%)
```

***Supplementary Fig. 2*. Alignment of the amino acid sequence of AtPAOs and ZmPAO.** Multialignment was done using the program ClustalW sequence alignment (Altschul *et al.*, 1990). Numbering of amino acid residues is shown at the right side. In ZmPAO, numbering starts from the first amino acid of the mature protein. Percentage of identity refers to ZmPAO. The identical residues and the conserved residues are indicated in red and blue, respectively.

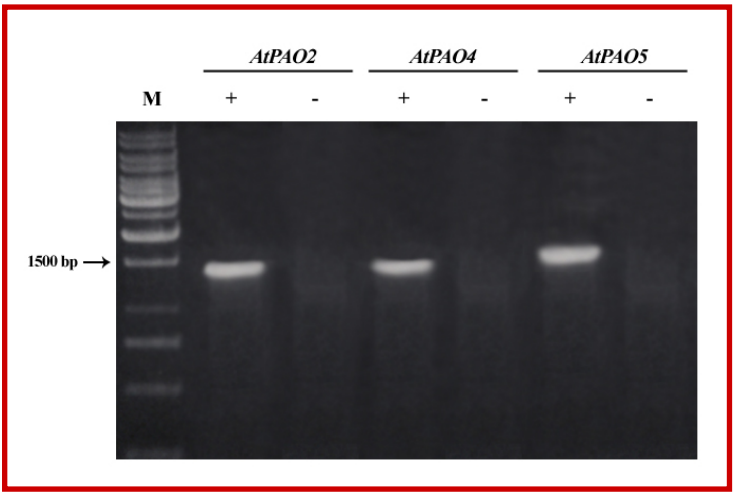

Supplementary Fig. 3. **Amplification of *AtPAO2, AtPAO4* and *AtPAO5* cDNAs.**
cDNAs of *AtPAOs* were obtained by RT-PCR from Arabidopsis leaves. The RT reaction was performed in the presence of reverse transcriptase (+) and in absence of the enzyme (−). **M**: DNA Marker.

REFERENCES (Materials and methods – Supplementary Figures)

Alonso J.M., Stepanova A.N., Leisse T.J., Kim C.J., Chen H., Shinn P., Stevenson D.K., Zimmerman J., Barajas P., Cheuk R., Gadrinab C., Heller C., Jeske A., Koesema E., Meyers C.C., Parker H., Prednis L., Ansari Y., Choy N., Deen H., Geralt M., Hazari N., Hom E., Karnes M., Mulholland C., Ndubaku R., Schmidt I., Guzman P., Aguilar-Henonin L., Schmid M., Weigel D., Carter D.E., Marchand T., Risseeuw E., Brogden D., Zeko A., Crosby W.L., Berry C.C., Ecker J.R. (2003) Genome-wide insertional mutagenesis of *Arabidopsis thaliana*. *Science* **301**: 653-657.*

Altschul S.F., Gish W., Miller W., Myers E.W., Lipman D.J. (1990) Basic local alignment search tool. *J. Mol. Biol.* **215**: 403-410.

Bianchi M., Polticelli F., Ascenzi P., Botta M., Federico R., Mariottini P., Cona A. (2006) Inhibition of polyamine and spermine oxidases by polyamine analogues. *FEBS J.* **273**: 1115-1123.*

Cona A., Manetti F., Leone R., Corelli F., Tavladoraki P., Polticelli F., Botta M. (2004) Molecular basis for the binding of competitive inhibitors of maize polyamine oxidase. *Biochemistry* **43**: 3426-3435.*

Deleage G. and Geourjon C. (1993) An interactive graphic program for calculating the secondary structure content of proteins from circular dichroism spectrum. *Comput. Appl. Biosci.* **2**: 197-199.

Federico R., Leone L., Botta M., Binda C., Angelini R., Venturini G., Ascenzi P. (2001) Inhibitor of pig liver and *Zea mays* L. polyamine oxidase: a comparative study. *J. Enzyme Inhib.* **13**: 465-471.*

Gehrig H.H., Winter K., Cushman J., Borland A., Taybi T. (2000) An improved RNA isolation method for succulent plant species rich in polyphenols and polysaccharides. *Plant Mol. Biol. Rep.* **18**: 369-376.*

Hartley J.L., Temple G.F., Brasch M.A. (2000) DNA cloning using *in vitro* site-specific recombination. *Genome Res.* **10**: 1788-1795.

Holt A. and Baker G.B. (1995) Metabolism of agmatine (clonidine-displacing substance) by diamine oxidase and the possible implications for studies of imidazoline receptors. *Prog. Brain Res.* **106**: 187-197.

Karimi M., Inzé D., Depicker A. (2002) GATEWAY vectors for *Agrobacterium*-mediated plant transformation. *Trends Plant Sci.* **7**: 193-195.*

Klimyuk V.I., Carroll B.J., Thomas C.M., Jones J.D. (1993) Alkali treatment for rapid preparation of plant material for reliable PCR analysis. *Plant J.* **3**: 493-494.*

Kubicek S. and Jenuwein T. (2004) A crack in histone lysine methylation. *Cell* **119**: 903-906.*

Laemmli U.K. (1970) Cleavage of structural proteins during the assembly of the head of bacteriophage T4. *Nature* **277**: 680-685.

Sessions A., Burke E., Presting G., Aux G., McElver J., Patton D., Dietrich B., Ho P., Bacwaden J., Ko C., Clarke J.D., Cotton D., Bullis D., Snell J., Miguel T., Hutchison D., Kimmerly B., Mitzel T., Katagiri F., Glazebrook J., Law M., Goff S.A. (2002) A high-throughput Arabidopsis reverse genetics system. *Plant Cell* **14**: 2985-2994.*

Smith T.A. and Davies P.J. (1985) Separation and quantitation of polyamines in plant tissue by high performance liquid chromatography of their dansyl derivatives. *Plant Physiol*. **78**: 89-91.

Tavladoraki P., Rossi M.N., Saccuti G., Perez-Amador M.A., Polticelli F., Angelini R., Federico R. (2006) Heterologous expression and biochemical characterization of a polyamine oxidase from Arabidopsis involved in polyamine back-conversion. *Plant Physiol.* **141*:*** 1519-1532.*

Tsukada Y., Fang J., Erdjument-Bromage H., Warren M.E., Borchers C.H., Tempst P., Zhang Y. (2005) Histone demethylation by a family of JmjC domain-containing proteins. *Nature* **439**: 811-816.*

* consulted references

Characterization of a Lysine-Specific Histone Demethylase from *Arabidopsis thaliana*†

Valentina Spedaletti,‡ Fabio Polticelli,‡ Viviana Capodaglio,‡ M. Eugenia Schininà,§ Pasquale Stano,‡ Rodolfo Federico,‡ and Paraskevi Tavladoraki*,‡

Department of Biology, University Roma Tre, 00146 Rome, Italy, and Department of Biochemical Science and Laboratory of Functional Genomics and Proteomics, University of Rome La Sapienza, 00185 Rome, Italy

Received October 1, 2007; Revised Manuscript Received February 22, 2008

ABSTRACT: *Arabidopsis thaliana* has four genes with close homology to human histone H3 lysine 4 demethylase (HsLSD1), a component of various transcriptional corepressor complexes that often also contain histone deacetylases and the corepressor protein CoREST. All four *Arabidopsis* proteins contain a flavin amine oxidase domain and a SWIRM domain, the latter being present in a number of proteins involved in chromatin regulation. Here, we describe the heterologous expression and biochemical characterization of one of these *Arabidopsis* proteins (AtLSD1) and show that, similarly to HsLSD1, it has demethylase activity toward mono- and dimethylated Lys4 but not dimethylated Lys9 and Lys27 of histone 3. Modeling of the AtLSD1 three-dimensional structure using the HsLSD1 crystal structure as a template revealed a high degree of conservation of the residues building up the active site and some important differences. Among these differences, the most prominent is the lack of the HsLSD1 Tower domain, which has been shown to interact with CoREST and to be indispensable for HsLSD1 demethylase activity. This observation, together with AtLSD1 peculiar surface electrostatic potential distribution, suggests that the molecular partners of AtLSD1 are probably different from those of the human orthologue.

In eukaryotes, the histone N-terminal tails are subjected to multiple covalent modifications, such as acetylation, methylation, phosphorylation, ubiquitination, sumoylation, and ADP-ribosylation (*1*−*3*). These histone modifications act in a combinatorial manner, thus defining a "histone code", to control chromatin state and gene expression (*4*–*6*). Among these modifications, histone lysine acetylation is the best characterized. This modification is generally associated with transcriptional activation and is dynamically regulated by histone acetyltransferases and deacetylases (*4*). Histone methylation mediated by multiple classes of methyl transferases has emerged as another important mechanism which regulates chromatin structure and function (*4, 7, 8*). Five lysine residues on the tails of histones H3 and H4 (H3K4,[1] H3K9, H3K27, H3K36, and H4K20) as well as K79 located within the core of histone H3 have been shown to be target sites for methylation (*6, 9*). Methylation at these sites has been linked to both transcriptional activation and repression, as well as DNA-damage response (*6, 10*), demonstrating a widespread role for histone methylation in various aspects of chromatin biology. Histone lysine residues can be methylated in three different modes, i.e., mono-, di-, or trimethylation. These differentially methylated lysine residues could serve as docking sites for different effector proteins and/or platforms for chromatin modifiers including histone methylases, deacetylases, or remodeling activities, which then could result in potentially diverse functional outcomes (*11*). Arginine residues within the tails of histones H3 (R2, R17, R26) and H4 (R3) can also be methylated, and this generally leads to transcriptional activation (*12*).

Although some histone modifications, such as acetylation, phosphorylation, and ubiquitination, are highly dynamic, histone methylation had been regarded as irreversible. However, the recent discovery of several histone demethylases which can reverse methylation of arginine and lysine residues has altered this view of histone methylation (*11, 13*−*17*). PAD4/PADI4 was the first reported histone arginine demethylase that demethyliminates monomethylarginine to produce citrulline (*13, 14*). Human lysine-specific demethylase 1 (HsLSD1), also known as KIAA0601, has been recently identified as the first histone demethylase that specifically acts on mono- and dimethylated Lys4 of histone H3 (H3K4me1 and H3K4me2, respectively) in a flavin adenine dinucleotide (FAD) dependent oxidative reaction (*15*). More recently, a new family of histone demethylases has been discovered which contains a jumonji C domain capable of removing methyl groups on lysine residues by hydroxylation-based demethylation (*11, 16, 17*).

† This work was supported by the University Roma Tre, the Italian Ministry of University and Research (COFIN-PRIN 2005, p.c. 2005052297_002), and the Federated Ateneum of Science and Technology, University of Rome La Sapienza.

* To whom correspondence should be addressed. Tel: +39 06 57336352. Fax: +39 06 57336321. E-mail: tavlador@uniroma3.it.

‡ University Roma Tre.

§ University of Rome La Sapienza.

[1] Abbreviations: H3K4, Lys4 of histone 3; HsLSD1, human lysine-specific demethylase 1; H3K4me1, monomethylated H3K4; H3K4me2, dimethylated H3K4; FLC, flowering locus C; FLD, flowering locus D; H3K4me1-S10pho, monomethylated Lys4 and phosphorylated Ser10 of H3; AtLSD1, *Arabidopsis thaliana* lysine-specific demethylase 1; FAD, flavin adenine dinucleotide; ZmPAO, *Zea mays* polyamine oxidase; IPTG, isopropyl β-D-thiogalactoside.

10.1021/bi701969k CCC: $40.75
Published on Web 04/05/2008

HsLSD1 comprises an N-terminal SWIRM domain and a C-terminal flavin domain which displays homology with members of the amine oxidase family (*15*). The HsLSD1-catalyzed reaction regenerates the methyl-free lysine with concomitant release of formaldehyde and H_2O_2. HsLSD1 has been found in association with the corepressor protein CoREST, the histone deacetylases 1 and 2, the PHD-domain-containing protein BHC80, and the HMG-domain-containing protein BRAF35, among others (*18–20*), and recent studies suggest that its specificity and activity can be modulated by its interacting factors (*19–21*). However, the molecular mechanism by which this regulation is achieved still remains unclear. The crystal structure of HsLSD1, determined in free form or in complex with an HsLSD1-stimulatory domain of human CoREST and substrate-like peptide inhibitors, provided the structural framework to explain its catalytic properties and the active role of CoREST in substrate recognition (*22–27*). Furthermore, mutagenesis studies showed that DNA binding by the CoREST domain is crucial for the demethylation of H3K4 within nucleosomes by the HsLSD1−CoREST complex (*24*). Biochemical assays have also shown that HsLSD1 is able to "read and interpret" the histone code discriminating between peptides bearing different covalent modifications (*5, 28*).

In plants, little is known about histone tail modifications in general and about histone methylation/demethylation processes in particular. Available data provide evidence that *Arabidopsis* euchromatin, in general, is enriched in H3K4me2, while heterochromatin is depleted in H3K4me2 but enriched in H3K9me2 (*29, 30*). Furthermore, it has been demonstrated that the acceleration of flowering by prolonged cold, a process called vernalization, causes changes in histone methylation in discrete domains within a negative regulator of flowering, the flowering locus C (FLC), increasing H3K9 and H3K27 dimethylation and decreasing H3K4 dimethylation (*31*). On the other hand, it has been shown that an *Arabidopsis* homologue of HsLSD1, termed flowering locus D (FLD) and shown to interact with a plant-specific C2H2 zinc finger-SET domain protein (*32*), represses the FLC by histone deacetylation (*33*).

In plants, despite the growing information available on histone methylation, the existence of an enzyme which is able to revert histone methylation has not been demonstrated yet. Here, we report the first biochemical characterization of a plant lysine-specific histone demethylase. More specifically, a lysine-specific histone demethylase from *Arabidopsis thaliana* homologous to HsLSD1 was expressed in a bacterial heterologous system, and the catalytic properties of the recombinant enzyme were determined. The three-dimensional structure of this *Arabidopsis* histone demethylase was also modeled using the HsLSD1 crystal structure as a template and analyzed in comparison with the human orthologue.

MATERIALS AND METHODS

Materials. 4-Aminoantipyrine, 3,5-dichloro-2-hydroxybenzenesulfonic acid, and horseradish peroxidase were purchased from Sigma-Aldrich-Fluka. Restriction and DNA-modifying enzymes were purchased from New England Biolabs, Invitrogen, Stratagene, and Promega. The synthetic human histone H3 peptides with specific modifications H3K4me1 (1–21 aa), monomethylated Lys4 and phosphorylated Ser10 (H3K4me1-S10pho) (1–21 aa), H3K4me2 (1–21 aa), H3K9me2 (1–21 aa), and H3K27me2 (21–44 aa) were purchased from Upstate Group Inc. or synthesized by Thermo Scientific. Recombinant HsLSD1 was kindly provided by Prof. Andrea Mattevi and Dr. Claudia Binda (University of Pavia, Italy).

Sequence Analysis and cDNA Acquisition. EST database searches were performed using the basic local alignment search tool (BLAST) (*34*). Multiple sequence alignment of the amino acid sequences was done using the program CLUSTAL W (*35*). The cDNA encoding for the putative *A. thaliana* histone demethylase (*AtLSD1*; At1g62830; GenBank accession number NM_104961) was obtained from the DNA Stock Center of the *Arabidopsis* Biological Resource Centre (U21563 clone) and completely sequenced to exclude sequence changes compared to the corresponding *A. thaliana* genomic sequence.

Expression of Recombinant AtLSD1 in Escherichia coli. The pET17b vector (Novagen) was used to construct an *AtLSD1* prokaryotic expression system. To clone *AtLSD1* cDNA between restriction sites *Xba*I and *Xho*I of this vector, the whole coding region of the *AtLSD1* cDNA was amplified using the U21563 clone (*Arabidopsis* Biological Resource Center) as a template and the sequence-specific oligonucleotides *AtLSD1for1* (5′-GTCTAGAAATAATTTTGTTTAACTTTAAGAAGGAGATATACATATGTCAACAGAGACTAAAGAAACCCGACCC-3′)/*AtLSD1rev1* (5′-GCTCGAGCTAGTGGTGGTGGTGGTGGTGTCCTCCATCAAAGATCTGTCGATTCAGTC TTGCAGC-3′). The underlined regions in *AtLSD1for1* and *AtLSD1rev1* oligonucleotides indicate *Xba*I and *Xho*I restriction sites, respectively. The *AtLSD1rev1* primer was designed to insert the coding sequence for two Gly residues and a 6-His tag prior to the stop codon of the *AtLSD1* cDNA. The amplified *AtLSD1* cDNA was subcloned into the pDrive vector (Qiagen), completely sequenced, and then cloned in the pET17b plasmid yielding the construct *AtLSD1*-pET17b. This plasmid was then used to transform *E. coli* BL21 (DE3) cells. Expression of recombinant AtLSD1 was induced by 0.4 mM isopropyl β-D-thiogalactoside (IPTG) at 25 °C for 5 h. Cells were resuspended in extraction buffer [50 mM Tris-HCl, pH 8.0, 0.1 M NaCl, 10% (v/v) glycerol, 1 mM phenylmethanesulfonyl fluoride] and disrupted by sonication. After centrifugation at 13000*g* for 30 min at 4 °C, the clear supernatant (bacterial extract) containing the soluble proteins was either analyzed for recombinant protein accumulation by immunoblotting or further processed for recombinant protein purification.

Purification of Recombinant AtLSD1 from Bacterial Extracts. Recombinant AtLSD1 was purified from bacterial extracts by affinity chromatography. In detail, bacterial extracts were applied to a Ni^{2+}-charged resin (Amersham Biosciences) equilibrated in extraction buffer. The resin was washed first with extraction buffer and then with 50 mM Tris-HCl, pH 8.0, 50 mM NaCl, and 10% (v/v) glycerol. The protein was eluted with 50 mM Tris-HCl, pH 8.0, 50 mM NaCl, 10% (v/v) glycerol, and 100 mM imidazole. The fractions enriched in recombinant AtLSD1 were pooled, diluted 5-fold with 50 mM Tris-HCl, pH 8.0, and 10% (v/v) glycerol, and chromatographed on a HiTrap heparin HP column (Amersham Biosciences) equilibrated in 50 mM Tris-HCl, pH 8.0, 10 mM NaCl, and 10% (v/v) glycerol. Elution was performed with a nonlinear gradient of NaCl (50 mM−2

M) in Tris-HCl, pH 8.0, and 10% (v/v) glycerol. AtLSD1-containing fractions (fractions of 200 or 400 mM NaCl) were dialyzed against 50 mM Tris-HCl, pH 8.0, and 10% (v/v) glycerol and concentrated using centrifugal filter devices (Millipore). Recombinant protein was quantified by absorption spectroscopy using an extinction coefficient of 10790 M^{-1} cm^{-1} at 458 nm (*36*) and stored at 4 °C. The purity of the recombinant enzyme was determined by SDS−PAGE analysis and by the ratio A_{280}/A_{458}, which was about 10. Using this two-step purification protocol, a yield of 1 mg/L of culture has been obtained.

CD Spectroscopy. CD spectra were recorded at 25 °C using a Jasco J-600 spectropolarimeter and quartz cells having 0.05 cm path length. Recombinant AtLSD1 was at a concentration of 0.3 mg/mL in 15 mM Tris-HCl and 3% (v/v) glycerol, pH 8.0. Instrumental ellipticity was converted into mean residue molar ellipticity [θ] (deg cm^2 $dmol^{-1}$) after spectrophotometric determination of the protein concentration. For each sample, nine CD spectra in the far-UV region (198–250 nm) were recorded and averaged. Secondary structures were estimated by using CONTIN, K2D, and SELCON3 algorithms provided by the free software Dicroprot2000 (*37*).

Determination of AtLSD1 and HsLSD1 Catalytic Parameters. The catalytic parameters (K_m and k_{cat}) of recombinant AtLSD1 and HsLSD1 were determined using about 2.0 μM purified protein in a 300 μL reaction volume by following spectrophotometrically the formation of a pink adduct (ϵ_{515} = 2.6 × 10^4 M^{-1} cm^{-1}), as a result of oxidation of 4-aminoantipyrine and 3,5-dichloro-2-hydroxybenzenesulfonic acid catalyzed by horseradish peroxidase in 50 mM Tris-HCl and 30% glycerol, pH 8.0 (except as otherwise indicated) at 25 °C (*5, 36, 38*). k_{cat} values were calculated using saturating concentrations of methylated H3K4 peptides (147 μM) and keeping the O_2 concentration constant at the air-saturated level (apparent k_{cat}). K_m values were determined from Michaelis–Menten plots using variable concentrations of peptides (2–147 μM) and a constant O_2 concentration at the air-saturated level (apparent K_m).

Demethylation Assay by Western Blot Analysis. H3K4met2 peptide (0.29 mM) was incubated with purified recombinant AtLSD1 (0.02 mM) in 50 mM Tris-HCl, pH 8.0, and 30% (v/v) glycerol for 2 h at room temperature. The demethylase activity of AtLSD1 was evaluated by Western blot analysis using an anti-H3K4met2 (Upstate Group Inc.) methylation-specific antibody.

Demethylation Assay by Matrix-Assisted Laser Desorption/Ionization (MALDI) Mass Spectrometry. H3K4me1, H3K4me2, H3K9me2, and H3K27me2 peptides at a concentration of 0.2 mM were incubated with purified recombinant AtLSD1 (0.02 mM) in 50 mM Tris-HC, pH 8.0, and 10% (v/v) glycerol for 4 h at room temperature. An aliquot of each sample (1 μL) was mixed with the α-cyano-4-hydroxy-*trans*-cinnamic acid matrix solution (10 mg/mL in 70% acetonitrile containing 0.2% trifluoroacetic acid) in different ratios (1:3, 1:5, 1:10); 1 μL of each mixture was deposited onto a MALDI target plate and allowed to dry on air. MALDI-TOF MS analyses were performed in a Voyager-DE STR instrument (Applied Biosystems, Framingham, MA) equipped with a 337 nm nitrogen laser and operating in reflector mode. Mass data were obtained by accumulating spectra from 200 laser shots with an accelerating voltage of 20 kV. All mass spectra were externally calibrated using a standard peptide mixture (Sequizyme; Applied Biosystems).

SDS−PAGE and Western Blot Analysis. SDS−PAGE was carried out according to the method of Laemmli (*39*). Recombinant AtLSD1 from bacterial extracts was subjected to SDS−PAGE (10% polyacrylamide) and analyzed either by staining with Coomassie Brilliant Blue or by Western blot using a mouse anti-6-His monoclonal antibody (Sigma-Aldrich-Fluka) and a rabbit anti-mouse antibody coupled to horseradish peroxidase (Amersham Biosciences). In the latter case, proteins were transferred to a nitrocellulose membrane (Schleicher & Schuell) using a Mini Trans-Blot apparatus (Bio-Rad), following the manufacturers' instructions. For Western blot analysis of the H3K4me2 peptide, proteins were separated by SDS−PAGE (15% polyacrylamide), electrophoretically transferred to a polyvinylidene difluoride (PVDF) membrane (Immobilon PSQ; Millipore) at 150 mA for 45 min, and incubated first with a rabbit anti-H3K4me2 methylation-specific antibody (Upstate Group Inc.) and then with a goat anti-rabbit antibody coupled to horseradish peroxidase (Vector Laboratories, Inc.). The detection of the labeled proteins was done with a chemiluminescence kit (Boehringer-Mannheim).

DNA Sequencing. DNA sequencing was performed on double-stranded plasmid DNA using the automated fluorescent dye terminator technique (Perkin-Elmer ABI model 373A).

Semiquantitative RT-PCR Analysis of Lysine-Specific Histone Demethylase Genes in Various Arabidopsis Organs. Total RNA was isolated from various plant organs (rosette leaves, cauline leaves, stems, inflorescences, silique, and roots) of *A. thaliana* (ecotype Columbia) plants using TRIZOL reagent (Invitrogen) and/or the RNeasy Mini kit (Qiagen) according to the manufacturers' instructions. To extract total RNA from the silique, a method modified from the RNeasy Mini kit was used (*40*). RNA samples were treated with RNase-free DNase I (Invitrogen) to avoid amplification from genomic DNA. The first cDNA strand was synthesized from total RNA using the SuperScript III first-strand synthesis system for RT-PCR (Invitrogen) and random primers. Aliquots of reverse-transcribed RNA were amplified by 25, 28, 30, 35, or 40 PCR cycles (denaturation at 94 °C for 1 min, annealing at 58 °C for 30 s, and extension at 72 °C for 1 min) using gene-specific primers. The *AtLSD1*-specific primers were *AtLSD1for2* (5-CAACAGAGACT-AAAGAAACCCGACC-3′) and *AtLSD1rev2* (5′-CGGCG-GTTTCTTGAGAAAGCTGGG-3′); the *AtLSD2*-specific primers were *AtLSD2for* (5′-CCGAGGAGGAACAGGAG-AAAAGTAAG-3′) and *AtLSD2rev* (5′-AGTACCCTCTT-CAGGAATATAAGGAGCAA); the *AtLSD3*-specific primers were *AtLSD3for* (5′-GCACCAAAGAAACGAAGGAGA-GGACG-3′) and *AtLSD3rev* (5′-GCCGAATCTAAGAGAC-TACTACAATGTTTAGGAATC-3′); the *AtLSD4*-specific primers were *AtLSD4for* (5′-CAGCGCCAGGGTTTTTCT-GTAACC-3′) and *AtLSD4rev* (5′-TCTCAGCCGTTGAAG-GCCATATTCT-3′). PCR amplification was carried out with the BIOTAQ DNA polymerase (Bioline) in an iCycler thermal cycler (Bio-Rad). To confirm equal amounts of RNA among the various samples, UBQ5 expression was used using the gene-specific primers *UBQ5for* (5′-GGAAGAAGAA-GACTTACACC-3′) and *UBQ5rev* (5′-AGTCCACACTTA-CCACAGTA-3′). Results at the exponential phase (usually

at 28 cycles for *AtLSD1*, *AtLSD2*, and *AtLSD3*, at 30 cycles for *AtLSD4*, and at 25 cycles for *UBQ5*) were analyzed.

Molecular Modeling and Structure Analysis. The three-dimensional structure of AtLSD1 was homology modeled using the structure of HsLSD1 as a template [PDB code 2IW5 (*24*)]. In detail, a PSI-BLAST (*34*) search on the nonredundant sequence database was carried out to retrieve amino acid sequences displaying significant similarity to AtLSD1. The best 18 sequences, which included the template HsLSD1 sequence, were then subjected to a multiple alignment procedure using CLUSTAL W (*35*). From the multiple alignment obtained with this procedure a pairwise alignment between AtLSD1 and HsLSD1 was extracted and used for the homology modeling procedure. The AtLSD1 model was then built using the program NEST, a software to build protein models based on a given alignment between query sequence and template which uses an artificial evolution method (*41*). The NEST option −*tune 2* was used to refine the alignment, avoiding the unlikely occurrence of insertions and deletions within template secondary structure elements. The quality of the final AtLSD1 model was then probed using the program PROCHECK (*42*). The overall *G*-value of the model resulted in being –0.22, well above the PROCHECK threshold of –0.5 for good quality models. The complex between AtLSD1 and a substrate-like peptide inhibitor was modeled by superimposition of the three-dimensional model of AtLSD1 with the three-dimensional structure of the complex formed by HsLSD1 with the peptide inhibitor [PDB code 2V1D (*26*)]. Surface electrostatic potential of AtLSD1 and HsLSD1 was calculated using the DelPhi program (*43*) and visualized using Chimera (*44*). In detail, hydrogen atoms were added to the structures using the routine HBUILD of the CHARMM package (*45*) and the CHARMM27 parameters and force field (*46*). Structures were then stereochemically regularized by energy minimization, applying a harmonic force of 10 kcal/mol to non-hydrogen atoms. In the DelPhi calculations, values of 2 and 80 were used for the dielectric constant of the protein interior and solvent, respectively. The ionic strength value was set to 0.05 M.

RESULTS

Description of a Lysine-Specific Histone Demethylase Gene Family in A. thaliana. A search of the *A. thaliana* genome database using the amino acid sequence of *Zea mays* polyamine oxidase (ZmPAO) revealed the presence of five cDNAs encoding for putative PAOs (*47*), plus four additional ones (*At1g62830*, *At3g13682*, *At3g10390*, *At4g16310*) coding for proteins bearing a flavin amine oxidase domain signature together with a SWIRM domain (Figure 1) (*15, 32*). The latter proteins display 26−30% sequence homology with HsLSD1, which is also known to possess both a flavin amine oxidase domain and a SWIRM domain and which specifically demethylates histone H3K4me1 and H3K4me2 (*5, 15*). Thus, it was hypothesized that these four *A. thaliana* cDNAs also encode for lysine-specific histone demethylases, and they were termed *AtLSD1* (*A. thaliana* lysine-specific demethylase 1), *AtLSD2*, *AtLSD3*, and *AtLSD4*, respectively. Interestingly, despite the high sequence homology with HsLSD1, the amino acid sequence homology of the four AtLSDs with the two yeast demethylases [SWIRM1 and SWIRM2 (*48*)], for which, however, histone demethylase activity has not yet been demonstrated, is very low (11–18%). AtLSD1, AtLSD2, and AtLSD3 display a fairly high overall sequence homology with each other (48–52%) and with AtLSD4 (25%–30%), which extends to both the amine oxidase and the SWIRM domains (Figure 1B).

To determine the possible subcellular localization of the four putative *Arabidopsis* histone demethylases, the amino acid sequences were analyzed using PSORT (www.psort.ims.u-tokio.ac.jp). This analysis predicted the presence of a nuclear localization signal at positions 517–534 of the AtLSD1 amino acid sequence, suggesting sorting to the nucleus similarly to HsLSD1 (*49*). This has been recently confirmed by transient expression studies of AtLSD1 tagged with green fluorescent protein (*32*). Nuclear localization was predicted also for AtLSD2 and AtLSD4, while mitochondrial/chloroplastic localization was predicted for AtLSD3. Furthermore, analysis of the amino acid sequence of the four AtLSDs for the presence of specific sequence motifs did not evidence the presence of HMG DNA-binding domains, as has been shown for the two yeast demethylases (*48*).

The expression pattern of the *AtLSD* gene family in different *Arabidopsis* organs (rosette and cauline leaves, stem, flowers, roots, and siliques) was also analyzed by semiquantitative RT-PCR using gene-specific primers (Figure 2). This analysis showed that the AtLSD1 transcript is present at similar levels in all tested organs, even though expression levels were expected to be higher in the flowers than in the other tissues considering the proposed role of chromatin remodeling enzymes in flowering control (*50*). Similar results were obtained also for AtLSD2, AtLSD3, and AtLSD4 transcripts (Figure 2). These data are in agreement with microarray data obtained from the *A. thaliana* database (Genevestigator expression analysis), which, however, demonstrate the differential expression pattern in specific parts or at specific developmental stages of the various organs, as, for example, in the shoot apex during transition from the vegetative to the inflorescence state.

Heterologous Expression and Biochemical Characterization of AtLSD1 in E. coli. To verify whether the *AtLSD* gene family encodes for proteins with a lysine-specific histone demethylase activity, heterologous expression of AtLSD1, chosen as representative member of the family, in *E. coli* was attempted using the pET17b vector which guides cytoplasmic expression of recombinant proteins. To facilitate purification of the recombinant protein, a sequence encoding for a 6-His tag was added at the 3′ terminus of the *AtLSD1* cDNA in the *AtLSD1*-pET17b plasmid. Western blot analysis using an anti-6-His tag antibody of bacteria transformed with *AtLSD1*-pET17b plasmid and treated with IPTG confirmed recombinant AtLSD1 accumulation in the soluble bacterial extracts (data not shown).

To purify the recombinant AtLSD1, affinity chromatography on a resin charged with Ni^{2+} was performed, which, however, was not sufficient to purify the recombinant protein to electrophoretic homogeneity (Figure 3). Thus, the pooled elution fractions from the Ni^{2+} resin were further chromatographed on a HiTrap heparin HP column from which the protein was recovered at a homogeneity greater than 95% (Figure 3). The purified protein displayed the characteristic

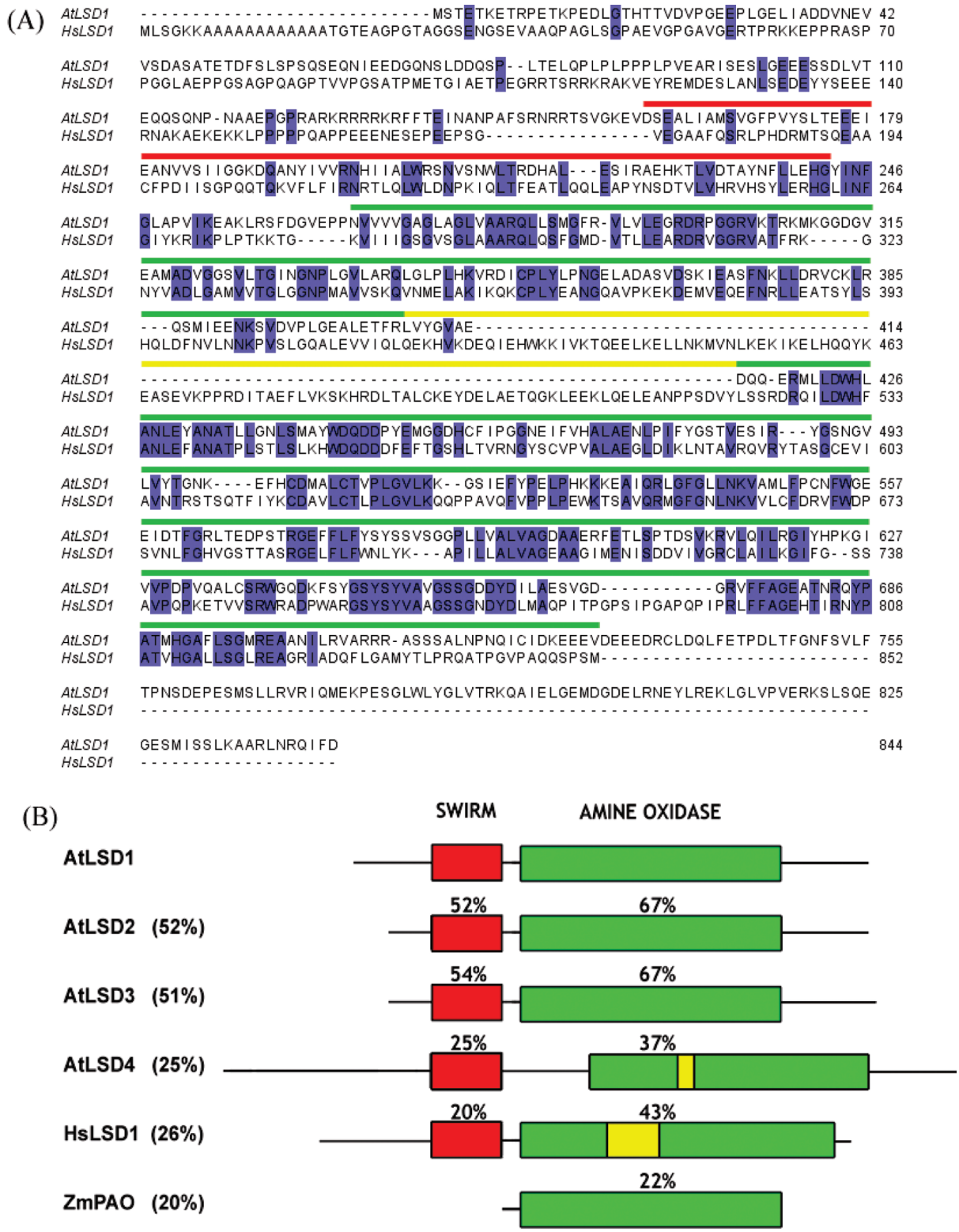

FIGURE 1: AtLSDs, HsLSD1, and ZmPAO sequence comparison. (A) Amino acid sequence alignment of AtLSD1 and HsLSD1. Strictly conserved residues are indicated by blue boxes. Red lines above the alignment indicate the SWIRM domain, green lines indicate the amine oxidase domain, and yellow lines indicate the Tower domain. (B) Schematic representation of the various domains of AtLSD1 (At1g62830; GenBank accession number NM_104961), AtLSD2 (At3g13682; GenBank accession number NM_112218), AtLSD3 (At3g10390; FLD; GenBank accession number NM_111874), AtLSD4 (*At4g16310*; GenBank accession number NM_117726), HsLSD1 (GenBank accession number NM_015013), and ZmPAO (GenBank accession number AJ002204). Red boxes indicate the SWIRM domains, green boxes indicate the amine oxidase domains, and yellow boxes the Tower domain. Numbers indicate the percentage of amino acid sequence homology, as a whole or by domain, of the various proteins with respect to AtLSD1.

UV–visible spectrum of the oxidized flavoproteins with three absorbance peaks at 280, 380, and 460 nm (data not shown) and an apparent molecular mass of 94 kDa (Figure 3), the molecular mass expected for the recombinant protein from amino acid sequence analysis. Precipitation of purified AtLSD1 with trichloroacetic acid resulted in the release of

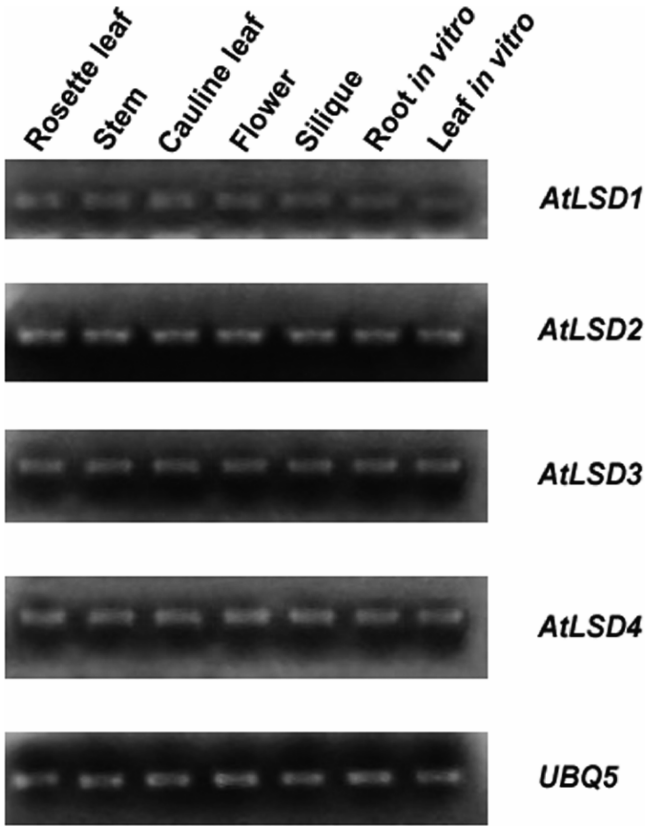

FIGURE 2: Expression pattern of *AtLSD1*, *AtLSD2*, *AtLSD3*, and *AtLSD4* in various *Arabidopsis* organs. The expression of the four *AtLSD* genes in various *Arabidopsis* organs (rosette and cauline leaves, stems, flowers, roots, and siliques) was analyzed by semi-quantitative RT-PCR using gene-specific primers. *UBQ5* expression was used to confirm an equal amount of RNA among the various samples. Results at the exponential phase (at 28 cycles for *AtLSD1*, *AtLSD2*, and *AtLSD3*, at 30 cycles for *AtLSD4*, and at 25 cycles for *UBQ5*) are shown.

the cofactor into the supernatant, indicating noncovalent binding to the protein.

Purified recombinant AtLSD1 was tested for its ability to oxidize various methylated H3 peptides and various polyamines using a peroxidase-coupled assay to quantify H_2O_2 levels (*5, 36, 38*). The results evidenced that, similarly to HsLSD1, the recombinant enzyme is able to demethylate H3K4me2 and H3K4me1 peptides, the specific activity with the H3K4me2 peptide being higher than that with the H3K4me1 peptide (Table 1). Furthermore, the results also showed that AtLSD1 is not able to oxidize either the H3K9me2 and H3K27me2 peptides or the common polyamines spermine, spermidine, and putrescine. The ability of recombinant AtLSD1 to demethylate the H3K4me2 peptide was also analyzed by a Western blot based assay using an anti-H3K4me2 methylation-specific antibody to detect the dimethylation status of the peptide (*15*). This analysis confirmed that the recombinant protein efficiently reduces the dimethylation level of the H3K4me2 peptide (Figure 4). Demethylase activity of AtLSD1 was further confirmed by mass spectrometry analysis. Demethylation of the H3K4me1 and H3K4me2 peptides by AtLSD1 is expected to regenerate the unmodified peptide with the net loss of 14 and 28 Da, respectively, corresponding to the molecular mass of one or two CH_2 group(s). The H3K4me1, H3K4me2, H3K9me2, and H3K27me2 peptides were incubated with purified recombinant AtLSD1 or buffer, and the reaction mixtures were analyzed by mass spectrometry. In the absence of AtLSD1, the H3K4me1 and H3K4me2 peptides display molecular masses of 2268 and 2282, respectively, as expected for these

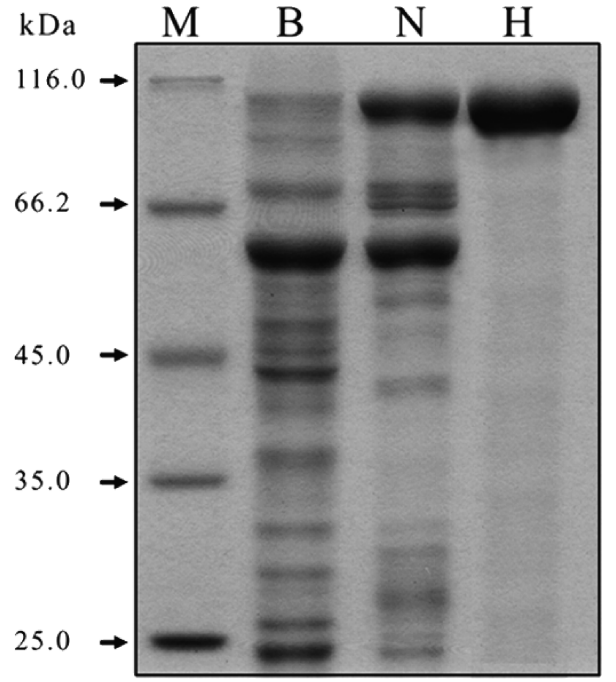

FIGURE 3: Purification of recombinant AtLSD1 expressed in bacteria. Analysis of representative protein samples from each stage of the purification protocol by SDS−PAGE (10% polyacrylamide). Key: B, crude bacterial extract; N, pooled elution fractions from the Ni^{2+}-charged resin; H, pooled elution fractions from the HiTrap heparin HP column; M, molecular mass marker.

Table 1: Kinetic Constants for the Demethylation of H3 Peptides by Recombinant AtLSD1 and HsLSD1

peptide	k_{cat} (min^{-1})[a]	K_m (μM)[a]
AtLSD1		
H3K4me1	0.50 ± 0.06	8.9 ± 0.8
H3K4me2	0.68 ± 0.08	10.7 ± 0.6
H3K4me2 in 10% glycerol[b]	0.34 ± 0.08	12.8 ± 1.0
H3K4me1-S10pho	no activity	no activity
HsLSD1−CoREST		
H3K4me1	6.50 ± 0.60	6.1 ± 0.6

[a] Enzymatic activity of recombinant AtLSD1 and of recombinant HsLSD1 in complex with CoREST (HsLSD1−CoREST) was determined in 50 mM Tris-HCl and 30% glycerol, pH 8.0, using a constant O_2 concentration at the air-saturated level and a peptide concentration either saturating (147 μM for apparent k_{cat} determination) or varying between 2 and 147 μM (for apparent K_m determination). Data are the mean ± SEM of at least three independent experiments. [b] The assay was performed in 50 mM Tris-HCl and 10% glycerol, pH 8.0. Similar results were obtained in the absence of glycerol.

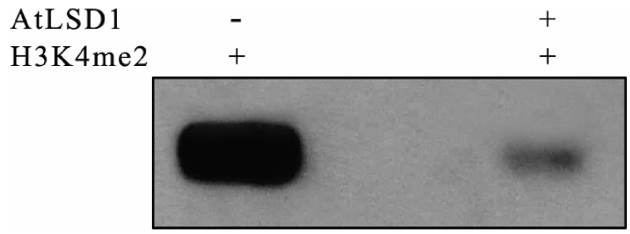

FIGURE 4: Demethylation of H3K4me2 peptide by recombinant AtLSD1. H3K4me2 peptide was incubated for 2 h with recombinant AtLSD1 and analyzed by Western blot using an anti-H3K4me2 methylation-specific antibody.

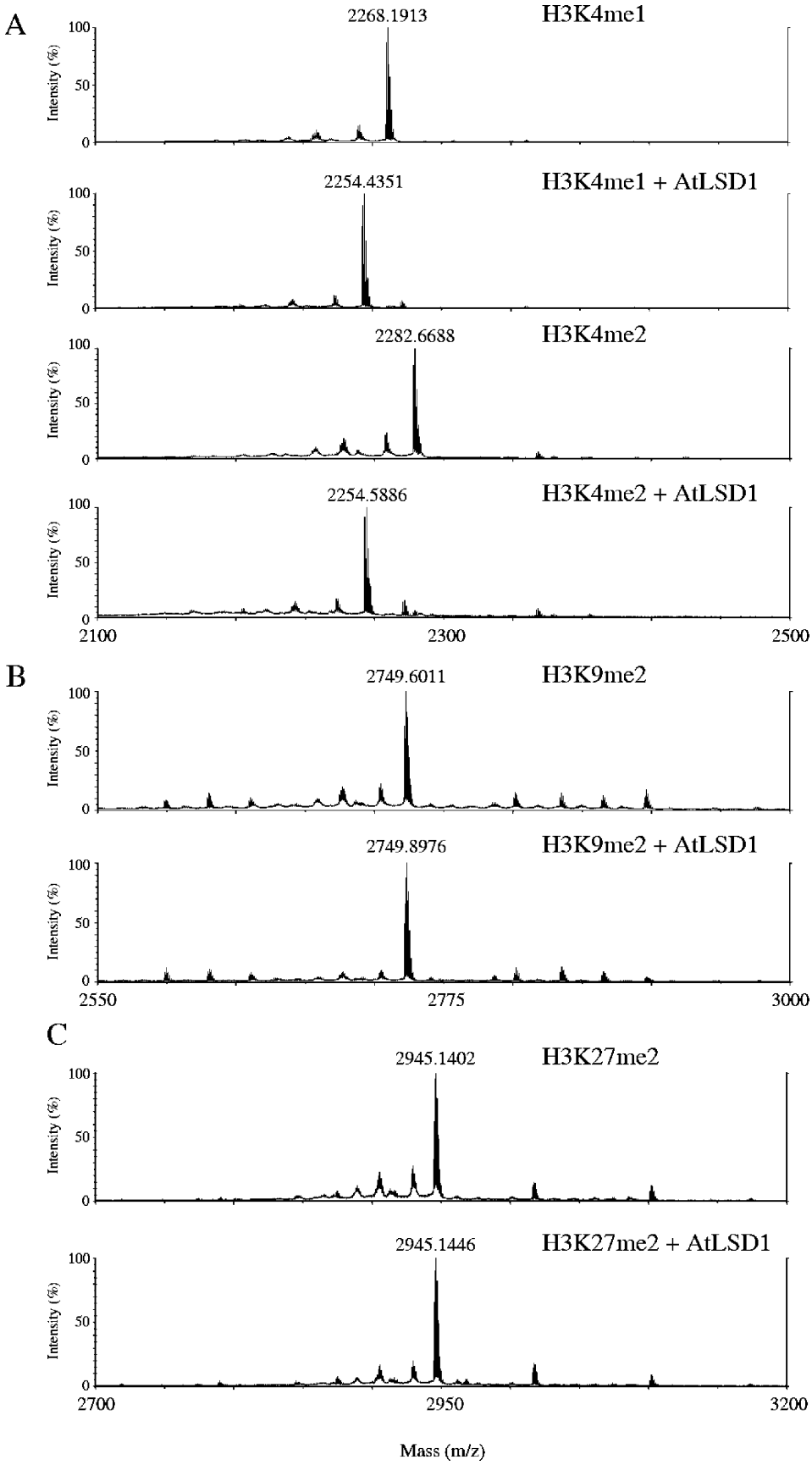

FIGURE 5: Mass spectrometry analysis of methylated H3 peptides after incubation with recombinant AtLSD1. H3K4me1 and H3K4me2 (panel A), H3K9me2 (panel B), and H3K27me2 (panel C) peptides were incubated for 4 h with buffer or purified recombinant AtLSD1, and reaction mixtures were analysed by mass spectrometry.

peptides (Figure 5, panel A). In the presence of AtLSD1 for both peptides a new peak appeared at a molecular mass of 2254, which well corresponds to the molecular mass of the demethylated peptide (Figure 5, panel A). On the contrary,

the peaks corresponding to the H3K9me2 and H3K27me2 peptides were found to be unaffected by incubation with recombinant AtLSD1 (Figure 5, panels B and C).

The activity of the recombinant enzyme with the H3K4me2 and H3K4me1 peptides was shown to be higher at pH 8.0 than at pH 6.0 or at pH 9.0 (data not shown) and to increase at higher glycerol concentrations (50% increase in the presence of 30% glycerol as compared to that in the presence of 0–10% glycerol) (Table 1). Interestingly, k_{cat} values of AtLSD1 were shown to be about 10-fold lower than that of HsLSD1 in free form (*5*) or in complex with CoREST (present study and ref *26*) (Table 1). Misfolding of the recombinant protein can be excluded on the basis of CD spectroscopy analysis, which indicated a high secondary structure content, the α-helix/β sheet percentage being 38−44% as calculated using CONTIN (*51*), K2D (*52*), or SELCON3 (*53*) methods. AtLSD1 catalytic activity resulted strongly inhibited in the presence of 50 mM KCl (50% inhibition) or $MgCl_2$ (75% inhibition), which suggests that electrostatic interactions are an important factor in AtLSD1 catalytic activity, as has been also demonstrated for HsLSD1 (*5*). Furthermore, phosphorylation of the H3Ser10 residue totally abolished the AtLSD1 demethylase activity toward the H3K4me1 peptide, as shown by the lack of any detectable activity of recombinant AtLSD1 toward the H3K4me1-Ser10pho peptide (Table 1).

Comparative Analysis of the Three-Dimensional Structure of AtLSD1. Figure 6 shows the three-dimensional structure of AtLSD1 modeled using the HsLSD1 crystal structure as a template [PDB code 2IW5 (*24*)]. As already predicted on the basis of the amino acid sequence alignment (Figure 1), the most striking difference between the two proteins is the almost complete absence of the Tower domain in AtLSD1. On the other hand, comparative analysis of the active site structures of AtLSD1 and HsLSD1 reveals a high degree of conservation of the residues building up the site, major substitutions in AtLSD1 being only Ser for Met332, Tyr for Trp695, and Tyr for Phe538 (Figure 7). However, none of these residues are involved in direct contacts with the substrate-like pLys4Met peptide inhibitor in HsLSD1 (*26*). In addition, modeling of the complex formed between AtLSD1 and this substrate-like peptide inhibitor, modeled by superimposition of the three-dimensional model of AtLSD1 with the three-dimensional structure of the complex formed by HsLSD1 with the peptide inhibitor [PDB code 2V1D (*26*)], highlights the strict conservation of the complex network of interactions observed between the peptide inhibitor and HsLSD1 (Figure 7). In particular, the acidic patch formed by Asp375, Glu379, and the carbonyl group of Cys360, which in HsLSD1 interacts with the peptide pArg8 residue, is strictly conserved in AtLSD1 (residues Asp367, Glu371, and Cys352). Strict conservation is also observed for residues Asp553 and Asp556 of HsLSD1 which bind the peptide pArg2 residue (Asp446 and Asp449 of AtLSD1). In addition, several hydrogen bonds which stabilize the HsLSD1 complex with the substrate-like peptide inhibitor are also conserved in the modeled AtLSD1 complex: (1) the hydrogen bond between Asn383 (Asn375 in AtLSD1) and the backbone nitrogen atoms of pThr11 and pGly12; (2) the hydrogen bond between His564 (His457 in AtLSD1) and the Oγ atom of pThr6; (3) the hydrogen bonds between the backbone nitrogen of pAla1 and Asn540 side-chain carbonyl group and Ala539 backbone carbonyl group (Asn433 and Ala432 in AtLSD1). Finally, it is also conserved in the HsLSD1 Tyr761 residue (Tyr650 in AtLSD1) which interacts with the pMet4 residue of the substrate-like inhibitor, the latter residue mimicking the dimethylated Lys4 of the histone H3 tail (Figure 7) (*26*).

Analysis of the surface electrostatic potential of AtLSD1 as compared to that of HsLSD1 evidenced a higher negative character of both the active site region and the SWIRM domain (Figure 6). This feature, together with the absence of the HsLSD1 Tower domain, is probably related to the interaction of AtLSD1 with different molecular partners. As a matter of fact, a BLAST search using human CoREST as a bait did not retrieve any protein in the *A. thaliana* genome displaying significant similarity with CoREST.

DISCUSSION

In the present study it was demonstrated that AtLSD1 is a lysine-specific histone demethylase with a substrate specificity similar to that of HsLSD1. In particular, recombinant AtLSD1 is able to specifically demethylate H3K4me2 and H3K4me1 peptides, whereas it shows no activity toward H3K9me2 and H3K27me2 peptides and polyamines. Data presented in this paper represent the first demonstration that also in plants histone methylation is a reversible process. This is an important finding considering that in plants histone modifications are involved in key developmental processes, such as the transition from the vegetative to the reproductive stage (*50*), and will probably contribute to get a better understanding of the underlying mechanism(s). In a recently published study (*32*), the authors failed to detect demethylase activity of their recombinant AtLSD1. In the light of the results described in this paper, it must be concluded that this may be due to instability and/or incorrect folding of the recombinant protein under their experimental conditions. Indeed, we have observed that AtLSD1 catalytic activity resulted greatly enhanced in the presence of increasing amounts of glycerol.

A comparative analysis of the AtLSD1 and the HsLSD1 amino acid sequence and three-dimensional structure showed a high degree of conservation of the residues building up the active site and interacting with the pLys4Met peptide inhibitor. This is in line with the observation that the ionic strength influences the catalytic activity of both the human and the plant enzymes, which suggests that electrostatic interactions are an important factor in the catalytic activity of both enzymes. Similarly, phosphorylation of the H3Ser10 residue, another important epigenetic mark, totally abolishes the demethylase activity toward the H3K4me1 peptide of both AtLSD1 and HsLSD1, probably due to unfavorable electrostatic interactions which make the peptide unable to bind the enzymes in a productive way (*5*). These data suggest that, similarly to the human demethylase, AtLSD1 is able to "read" different epigenetic marks on the histone N-terminal tail, a finding which may have an important biological significance.

A prominent difference between AtLSD1 and HsLSD1 is the lack of the HsLSD1 Tower domain in the AtLSD1. This domain has been shown to be crucial for the histone demethylase activity of HsLSD1 (*22, 23*) and to be involved in HsLSD1−CoREST complex formation (*23, 24*), which

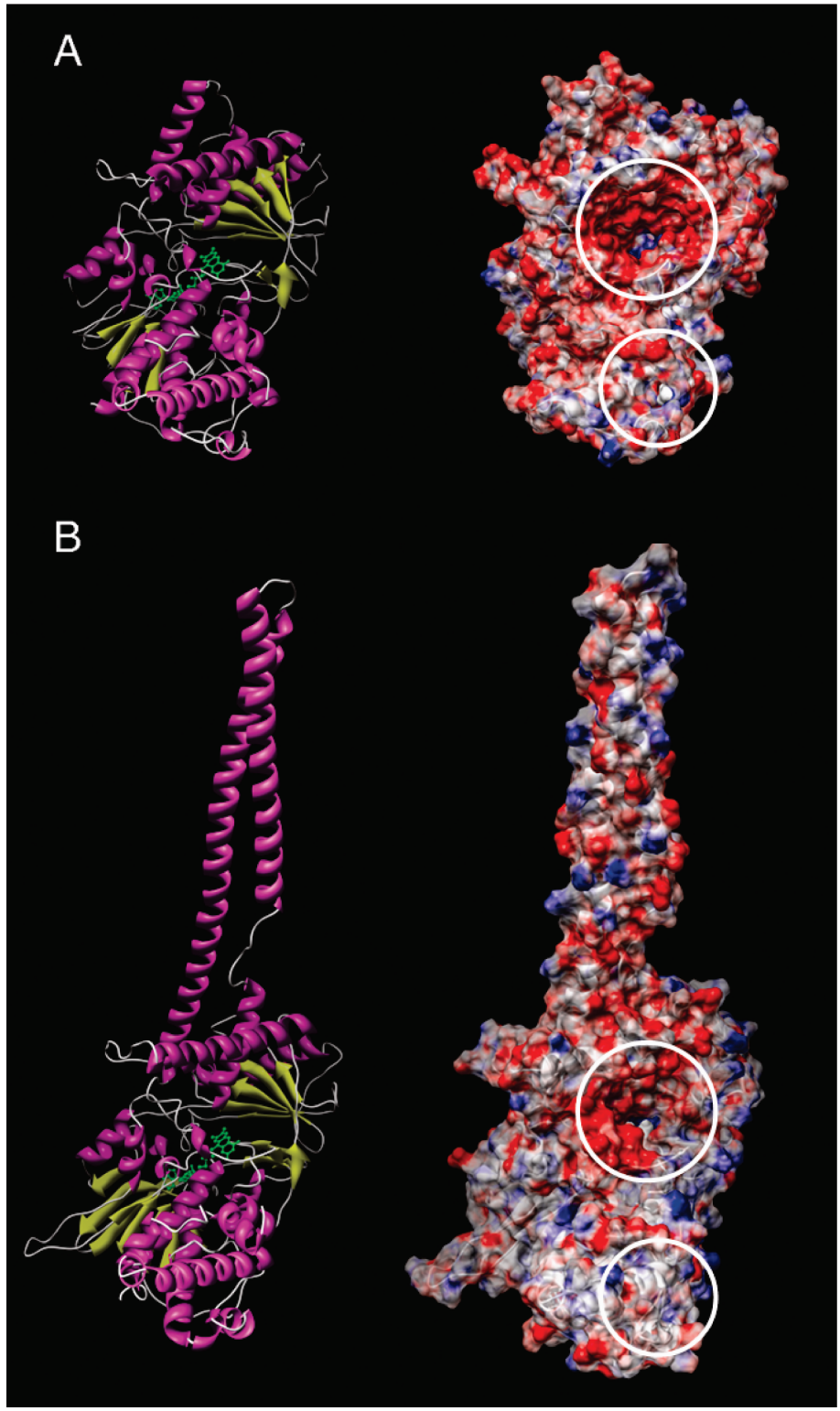

FIGURE 6: Schematic representation of the modeled three-dimensional structure of AtLSD1 (A) and of the crystal structure of HsLSD1 [PDB code 2IW5 (*24*)] (B). The FAD cofactor is shown in green to identify the active site region. Surface electrostatic potential contoured at +10 kT/e (blue) and –10 kT/e (red) is shown on the right panel. White circles highlight differences in the surface electrostatic potential between the two proteins.

in turn has been shown to stimulate the demethylase activity of HsLSD1 toward nucleosomes (*19, 20*). In the case of AtLSD1, despite the lack of the Tower domain, a lysine-specific histone demethylase activity has been demonstrated. However, AtLSD1 and HsLSD1 differ significantly from each other in catalytic efficiency. In particular, AtLSD1 displays a turnover rate 10-fold lower than that of HsLSD1. From this viewpoint it must be noted that a Towerless mutant of HsLSD1 has been shown to have a greatly reduced catalytic activity (approximately 0–10% as compared to the wild-type enzyme) (*22, 23*), indicating that the Tower domain may be involved in the structural organization of the active site. These data suggest that small structural differences in the active site of AtLSD1 due to the lack of the Tower

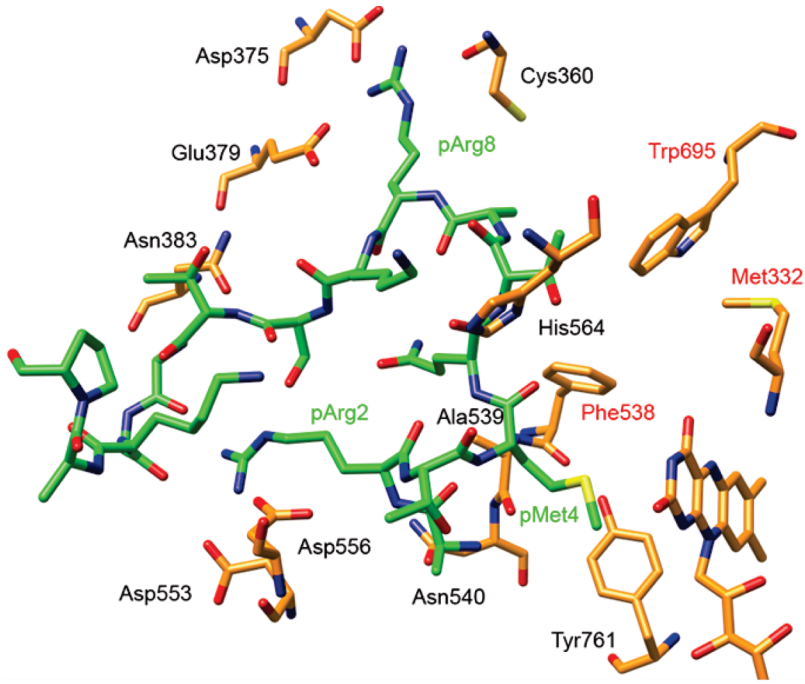

FIGURE 7: Schematic view of the complex formed by HsLSD1 with the substrate-like pLys4Met peptide inhibitor [PDB code 2V1D (*26*)]. HsLSD1 and peptide inhibitor residues contributing to the complex formation (see text) are labeled in black and green, respectively. For reasons of clarity, carbon atoms of HsLSD1 are colored in orange and those of the peptide inhibitor in green. Active site HsLSD1 residues nonconserved in AtLSD1 (substitutions being Met332Ser, Phe538Tyr, and Trp695Tyr) are labeled in red. Note that none of the nonconserved residues interacts with the peptide inhibitor in the HsLSD1 complex.

domain could explain the lower efficiency of this enzyme in respect to the human orthologue. However, it is also possible that AtLSD1 interacts *in vivo* with other proteins, as some recent data indicate (*32*), which may affect its catalytic properties and increase its efficiency. Functional partners of AtLSD1 seem to be different from those of HsLSD1. This is supported not only by the absence in the former protein of the Tower domain but also by a peculiar electrostatic potential distribution of the SWIRM molecular surface. In addition, the sequence similarity search using CoREST as a bait does not retrieve any protein in the *A. thaliana* genome which displays a significant sequence similarity with CoREST, ruling out the possibility that AtLSD1 interacts with CoREST-like macromolecules.

The issue regarding functional roles/partners of proteins belonging to the LSD1 family is further complicated by recently published data (*54*) which demonstrate that HsLSD1 interacts with p53 to repress p53-mediated transcriptional activation and to inhibit the role of p53 in promoting apoptosis through demethylation of residue Lys370, a residue located in the C-terminal region of p53. However, p53 C-terminal tail does not display a significant sequence homology with the histone H3 N-terminal tail (data not shown), suggesting that proteins belonging to the LSD1 family are able to recognize various substrates, most likely through differential molecular interactions.

Very recently it has been reported that in *Arabidopsis AtLSD1*/*AtLSD2* or *AtLSD3* knockout increases H3K4 methylation levels within the *FLC* and the *FWA*, whereas it does not change H3K9 and H3K27 methylation levels (*55, 56*). These data are in agreement with the specific *in vitro* demethylase activity of AtLSD1 toward H3K4 demonstrated in the present work and suggest a similar substrate specificity *in vivo*. However, in another recent report, *AtLSD1* knockout has been shown not to change the H3K4 methylation level within the *FLC* but to reduce that at H3K9 and H3K27 (*32*). The reason for such different results is not known, but it may reside in the fact that knockout of the various *AtLSDs* most probably interferes with the activity of other histone-modifying enzymes, since these have been shown to participate in multiprotein complexes in which they function in a coordinated manner (*57, 58*). This hypothesis could also explain the increase in the acetylation levels of H4 within the FLC in the *AtLSD1* and *AtLSD3* knockout *Arabidopsis* mutants (*32, 33*).

In conclusion, data presented in this paper demonstrate that AtLSD1 is a lysine-specific demethylase with a substrate specificity similar to that of HsLSD1 and an almost identical organization of the active site region. However, significant structural differences are observed at the level of the CoREST-interacting Tower domain of HsLSD1, which, together with the absence of CoREST-like proteins in the *Arabidopsis* genome, indicate that the physiological function of AtLSD1 must be dependent on the interaction with different partners from those of HsLSD1. These observations, together with the above cited report (*54*) pointing to a multifunctional role of HsLSD1 in lysine demethylation, indicate that the *in vivo* functional role of this class of proteins is a very complex one, depending on the interaction with molecular partners which may differ significantly between animal and plant lysine-specific demethylases.

ACKNOWLEDGMENT

The authors thank the *Arabidopsis* Biological Resource Centre and the DNA Stock donor for providing cDNA clone U21563, Prof. Andrea Mattevi and Dr. Claudia Binda (University of Pavia, Italy) for providing purified HsLSD1

in complex with CoREST, Dr. Alessandra Giorgi (University of Rome La Sapienza, Italy) for MALDI-TOF analyses, and Prof. Riccardo Angelini (University Roma Tre, Italy) for critical reading of the manuscript.

REFERENCES

1. Gill, G. (2004) SUMO and ubiquitin in the nucleus: different functions, similar mechanisms. *Genes Dev. 18*, 2046–2059.
2. Cohen-Armon, M., Visochek, L., Katzoff, A., Levitan, D., Susswein, A. J., Klein, R., Valbrun, M., and Schwartz, J. H. (2004) Long-term memory requires ADP-ribosylation. *Science 304*, 1820–1822.
3. Holbert, M. A., and Marmorstein, R. (2005) Structure and activity of enzymes that remove histone modifications. *Curr. Opin. Struct. Biol. 15*, 673–680.
4. Jenuwein, T., and Allis, C. D. (2001) Translating the histone code. *Science 293*, 1074–1080.
5. Forneris, F., Binda, C., Vanoni, M. A., Battaglioli, E., and Mattevi, A. (2005) Human histone demethylase LSD1 reads the histone code. *J. Biol. Chem. 280*, 41360–41365.
6. Zhang, Y., and Reinberg, D. (2001) Transcription regulation by histone methylation: interplay between different covalent modifications of the core histone tails. *Genes Dev. 15*, 2343–2360.
7. Martin, C., and Zhang, Y. (2005) The diverse functions of histone lysine methylation. *Nat. Rev. Mol. Cell Biol. 6*, 838–849.
8. Strahl, B. D., and Allis, C. D. (2000) The language of covalent histone modification. *Nature 403*, 41–45.
9. Margueron, R., Trojer, P., and Reinberg, D. (2005) The key to development: interpreting the histone code? *Curr. Opin. Genet. Dev. 15*, 163–176.
10. Sanders, S. L., Portoso, M., Mata, J., Bahler, J., Allshire, R. C., and Kouzarides, T. (2004) Methylation of histone H4 lysine 20 controls recruitment of Crb2 to sites of DNA damage. *Cell 119*, 603–614.
11. Whetstine, J. R., Nottke, A., Lan, F., Huarte, M., Smolikov, S., Chen, Z., Spooner, E., Li, E., Zhang, G., Colaiacovo, M., and Shi, Y. (2006) Reversal of histone lysine trimethylation by the JMJD2 family of histone demethylases. *Cell 125*, 467–481.
12. Kouzarides, T. (2002) Histone methylation in transcriptional control. *Curr. Opin. Genet. Dev. 12*, 198–209.
13. Cuthbert, G. L., Daujat, S., Snowden, A. W., Erdjument-Bromage, H., Hagiwara, T., Yamada, M., Schneider, R., Gregory, P. D., Tempst, P., Bannister, A. J., and Kouzarides, T. (2004) Histone deimination antagonizes arginine methylation. *Cell 118*, 545–553.
14. Wang, Y., Wysocka, J., Sayegh, J., Lee, Y. H., Perlin, J. R., Leonelli, L., Sonbuchner, L. S., McDonald, C. H., Cook, R. G., Dou, Y., Roeder, R. G., Clarke, S., Stallcup, M. R., Allis, C. D., and Coonrod, S. A. (2004) Human PAD4 regulates histone arginine methylation levels via demethylimination. *Science 306*, 279–283.
15. Shi, Y., Lan, F., Matson, C., Mulligan, P., Whetstine, J. R., Cole, P. A., Casero, R. A., and Shi, Y. (2004) Histone demethylation mediated by the nuclear amine oxidase homolog LSD1. *Cell 119*, 941–953.
16. Tsukada, Y., Fang, J., Erdjument-Bromage, H., Warren, M. E., Borchers, C. H., Tempst, P., and Zhang, Y. (2006) Histone demethylation by a family of JmjC domain-containing proteins. *Nature 439*, 811–816.
17. Yamane, K., Toumazou, C., Tsukada, Y., Erdjument-Bromage, H., Tempst, P., Wong, J., and Zhang, Y. (2006) JHDM2A, a JmjC-containing H3K9 demethylase, facilitates transcription activation by androgen receptor. *Cell 125*, 483–495.
18. Humphrey, G. W., Wang, Y., Russanova, V. R., Hirai, T., Qin, J., Nakatani, Y., and Howard, B. H. (2001) Stable histone deacetylase complexes distinguished by the presence of SANT domain proteins CoREST/kiaa0071 and Mta-L1. *J. Biol. Chem. 276*, 6817–6824.
19. Lee, M. G., Wynder, C., Cooch, N., and Shiekhattar, R. (2005) An essential role for CoREST in nucleosomal histone 3 lysine 4 demethylation. *Nature 437*, 432–435.
20. Shi, Y. J., Matson, C., Lan, F., Iwase, S., Baba, T., and Shi, Y. (2005) Regulation of LSD1 histone demethylase activity by its associated factors. *Mol. Cell 19*, 857–864.
21. Metzger, E., Wissmann, M., Yin, N., Müller, J. M., Schneider, R., Peters, A. H., Günther, T., Buettner, R., and Schüle, R. (2005) LSD1 demethylates repressive histone marks to promote androgen-receptor-dependent transcription. *Nature 437*, 436–439.
22. Stavropoulos, P., Blobel, G., and Hoelz, A. (2006) Crystal structure and mechanism of human lysine-specific demethylase-1. *Nat. Struct. Mol. Biol. 13*, 626–632.
23. Chen, Y., Yang, Y., Wang, F., Wan, K., Yamane, K., Zhang, Y., and Lei, M. (2006) Crystal structure of human histone lysine-specific demethylase 1 (LSD1). *Proc. Natl. Acad. Sci. U.S.A. 103*, 13956–13961.
24. Yang, M., Gocke, C. B., Luo, X., Borek, D., Tomchick, D. R., Machius, M., Otwinowski, Z., and Yu, H. (2006) Structural basis for CoREST-dependent demethylation of nucleosomes by the human LSD1 histone demethylase. *Mol. Cell 23*, 377–387.
25. Yang, M., Cullane, J. C., Szewczuk, L. M., Gocke, C. B., Brautigam, C. A., Tomchick, D. R., Machius, M., Cole, P. A., and Yu, H. (2007) Structural basis of histone demethylation by LSD1 revealed by suicide inactivation. *Nat. Struct. Mol. Biol. 14*, 535–539.
26. Forneris, F., Binda, C., Adamo, A., Battaglioli, E., and Mattevi, A. (2007) Structural basis of LSD1-CoREST selectivity in histone H3 recognition. *J. Biol. Chem. 282*, 20070–20074.
27. Yang, M., Cullane, J. C., Szewczuk, L. M., Jalili, P., Ball, H. L., Machius, M., Cole, P. A., and Yu, H. (2007) Structural basis for the inhibition of the LSD1 histone demethylase by the antidepressant *trans*-2-phenylcyclopropylamine. *Biochemistry 46*, 8058–8065.
28. Forneris, F., Binda, C., Dall'Aglio, A., Fraaije, M. W., Battaglioli, E., and Mattevi, A. (2006) A highly specific mechanism of histone H3-K4 recognition by histone demethylase LSD1. *J. Biol. Chem. 281*, 35289–35295.
29. Jasencakova, Z., Soppe, W. J., Meister, A., Gernand, D., Turner, B. M., and Schubert, I. (2003) Histone modifications in *Arabidopsis*—high methylation of H3 lysine 9 is dispensable for constitutive heterochromatin. *Plant J. 33*, 471–480.
30. Lippman, Z., Gendrel, A. V., Black, M., Vaughn, M. W., Dedhia, N., McCombie, W. R., Lavine, K., Mittal, V., May, B., Kasschau, K. D., Carrington, J. C., Doerge, R. W., Colot, V., and Martienssen, R. (2004) Role of transposable elements in heterochromatin and epigenetic control. *Nature 430*, 471–476.
31. Bastow, R., Mylne, J. S., Lister, C., Lippman, Z., Martienssen, R. A., and Dean, C. (2004) Vernalization requires epigenetic silencing of FLC by histone methylation. *Nature 427*, 164–167.
32. Krichevsky, A., Gutgarts, H., Kozlovsky, S. V., Tzfira, T., Sutton, A., Sternglanz, R., Mandel, G., and Citovsky, V. (2007) C2H2 zinc finger-SET histone methyltransferase is a plant-specific chromatin modifier. *Dev. Biol. 303*, 259–269.
33. He, Y., Michaels, S. D., and Amasino, R. M. (2003) Regulation of flowering time by histone acetylation in *Arabidopsis*. *Science 302*, 1751–1754.
34. Altschul, S. F., Madden, T. L., Schaffer, A. A., Zhang, J., Zhang, Z., Miller, W., and Lipman, D. J. (1997) Gapped BLAST and PSI-BLAST: a new generation of protein database search programs. *Nucleic Acids Res. 25*, 3389–3402.
35. Thompson, J. D., Higgins, D. G., and Gibson, T. J. (1994) CLUSTAL W: improving the sensitivity of progressive multiple sequence alignment through sequence weighting, position-specific gap penalties and weight matrix choice. *Nucleic Acids Res. 22*, 4673–4680.
36. Forneris, F., Binda, C., Vanoni, M. A., Mattevi, A., and Battaglioli, E. (2005) Histone demethylation catalysed by LSD1 is a flavin-dependent oxidative process. *FEBS Lett. 579*, 2203–2207.
37. Deleage, G., and Geourjon, C. (1993) An interactive graphic program for calculating the secondary structure content of proteins from circular dichroism spectrum. *Comput. Appl. Biosci. 2*, 197–199.
38. Holt, A., and Baker, G. B. (1995) Metabolism of agmatine (clonidine-displacing substance) by diamine oxidase and the possible implications for studies of imidazoline receptors. *Prog. Brain Res. 106*, 187–197.
39. Laemmli, U. K. (1970) Cleavage of structural proteins during the assembly of the head of bacteriophage T4. *Nature 277*, 680–685.
40. Gehrig, H. H., Winter, K., Cushman, J., Borland, A., and Taybi, T. (2000) An improved RNA isolation method for succulent plant species rich in polyphenols and polysaccharides. *Plant Mol. Biol. Rep. 18*, 369–376.
41. Petrey, D., Xiang, Z., Tang, C. L., Xie, L., Gimpelev, M., Mitros, T., Soto, C. S., Goldsmith-Fischman, S., Kernytsky, A., Schlessinger, A., Koh, I. Y., Alexov, E., and Honig, B. (2003) Using multiple structure alignments, fast model building, and energetic analysis in fold recognition and homology modeling. *Proteins 53*, 430–435.

42. Laskowski, R. A., MacArthur, M. W., Moss, D. S., and Thornton, J. M. (1993) PROCHECK: a program to check the stereochemical quality of protein structures. *J. Appl. Crystallogr. 26*, 283–291.
43. Rocchia, W., Alexov, E., and Honig, B. (2001) Extending the applicability of the nonlinear Poisson-Boltzmann equation: Multiple dielectric constants and multivalent ions. *J. Phys. Chem. B 105*, 6507–6514.
44. Pettersen, E. F., Goddard, T. D., Huang, C. C., Couch, G. S., Greenblatt, D. M., Meng, E. C., and Ferrin, T. E. (2004) UCSF chimera—A visualization system for exploratory research and analysis. *J. Comput. Chem. 25*, 1605–1612.
45. Brooks, B. R., Bruccoleri, R. E., Olafson, B. D., States, D. J., Swaminathan, S., and Karplus, M. (1983) CHARMM: A Program for Macromolecular Energy, Minimization, and Dynamics Calculations. *J. Comput. Chem. 4*, 187–217.
46. MacKerell, A. D., Jr., Bashford, D., Bellott, M., Jr., Evanseck, J. D., Field, M. J., Fischer, S., Gao, J., Guo, H., Ha, S., Joseph-McCarthy, D., Kuchnir, L., Kuczera, K., Lau, F. T. K., Mattos, C., Michnick, S., Ngo, T., Nguyen, D. T., Prodhom, B., Reiher, W. E., III, Roux, B., Schlenkrich, M., Smith, J. C., Stote, R., Straub, J., Watanabe, M., Wiorkiewicz-Kuczera, J., Yin, D., and Karplus, M. (1998) All-atom empirical potential for molecular modeling and dynamics studies of proteins. *J. Phys. Chem. B 102*, 3586–3616.
47. Tavladoraki, P., Rossi, M. N., Saccuti, G., Perez-Amador, M. A., Polticelli, F., Angelini, R., and Federico, R. (2006) Heterologous expression and biochemical characterization of a polyamine oxidase from *Arabidopsis thaliana* involved in polyamine back-conversion. *Plant Physiol. 141*, 1519–1532.
48. Nicolas, E., Lee, M. G., Hakimi, M. A., Cam, H. P., Grewal, S. I., and Shiekhattar, R. (2006) Fission yeast homologs of human histone H3 lysine 4 demethylase regulate a common set of genes with diverse functions. *J. Biol. Chem. 281*, 35983–35988.
49. Bradley, C., van der Meer, R., Roodi, N., Yan, H., Chandrasekharan, M. B., Sun, Z. W., Mernaugh, R. L., and Parl, F. F. (2007) Carcinogen-induced histone alteration in normal human mammary epithelial cells. *Carcinogenesis 28*, 2184–2192.
50. He, Y., and Amasino, R. M. (2005) Role of chromatin modification in flowering-time control. *Trends Plant Sci. 10*, 30–35.
51. Provencher, S. W. (1982) A constrained regularization method for inverting data represented by linear algebraic or integral-equations. *Comput. Phys. Commun. 27*, 213–227.
52. Andrade, M. A., Chacon, P., Merelo, J. J., and Moran, F. (1993) Evaluation of secondary structure of proteins from UV circular dichroism spectra using an unsupervised learning neural network. *Protein Eng. 6*, 383–390.
53. Sreerama, N., Venyaminov, S. Y., and Woody, R. W. (1999) Estimation of the number of alpha-helical and beta-strand segments in proteins using circular dichroism spectroscopy. *Protein Sci. 8*, 370–380.
54. Huang, J., Sengupta, R., Espejo, A. B., Lee, M. G., Dorsey, J. A., Richter, M., Opravil, S., Shiekhattar, R., Bedford, M. T., Jenuwein, T., and Berger, S. L. (2007) p53 is regulated by the lysine demethylase LSD1. *Nature 449*, 105–108.
55. Jiang, D., Yang, W., He, Y., and Amasino, R. M. (2007) *Arabidopsis* relatives of the human lysine-specific demethylase 1 repress the expression of FWA and FLOWERING LOCUS C and thus promote the floral transition. *Plant Cell 19*, 2975–2987.
56. Liu, F., Quesada, V., Crevillén, P., Bäurle, I., Swiezewski, S., and Dean, C. (2007) The *Arabidopsis* RNA-binding protein FCA requires a lysine-specific demethylase 1 homolog to downregulate FLC. *Mol. Cell 28*, 398–407.
57. Lee, M. G., Wynder, C., Bochar, D. A., Hakimi, M. A., Cooch, N., and Shiekhattar, R. (2006) Functional interplay between histone demethylase and deacetylase enzymes. *Mol. Cell. Biol. 26*, 6395–6402.
58. Wissmann, M., Yin, N., Müller, J. M., Greschik, H., Fodor, B. D., Jenuwein, T., Vogler, C., Schneider, R., Günther, T., Buettner, R., Metzger, E., and Schüle, R. (2007) Cooperative demethylation by JMJD2C and LSD1 promotes androgen receptor-dependent gene expression. *Nat. Cell Biol. 9*, 347–353.

BI701969K